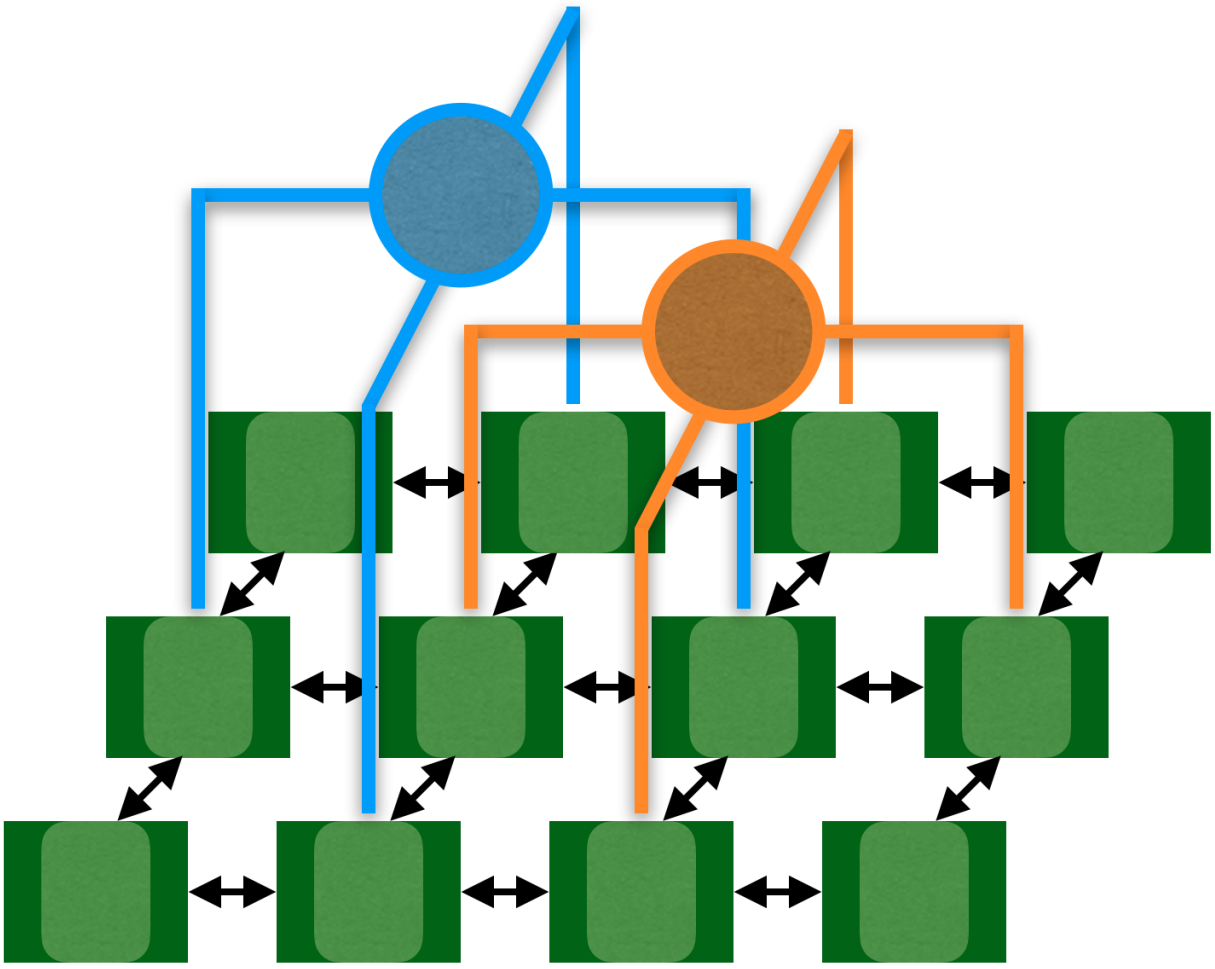

Quantum Optics with Giant Atoms in 2D Structured Environments

Master's Thesis in Microtechnology and Nanoscience

Emil Ingelsten

DEPARTMENT OF MICROTECHNOLOGY AND NANOSCIENCE
CHALMERS UNIVERSITY OF TECHNOLOGY
Gothenburg, Sweden 2023
www.chalmers.se

Master's Thesis MCCX04

Quantum Optics with Giant Atoms in 2D Structured Environments

Emil Ingelsten

CHALMERS
UNIVERSITY OF TECHNOLOGY

Department of Microtechnology and Nanoscience
Chalmers University of Technology
Gothenburg, Sweden 2023

Quantum Optics with Giant Atoms in 2D Structured Environments

Emil Ingelsten

Supervisors: Anton Frisk Kockum and Ariadna Soro Álvarez, Department of Microtechnology and Nanoscience
Examiner: Anton Frisk Kockum, Department of Microtechnology and Nanoscience

Master's Thesis MCCX04
Department of Microtechnlogy and Nanoscience
Chalmers University of Technology
SE-412 96 Gothenburg
Phone number +46 31 772 1000

Cover page: Illustration of a "braided diamonds" configuration of giant atoms, one of the simplest 2D configurations to exhibit decoherence-free interaction.

Typeset in LaTeX
Gothenburg, Sweden 2023

Quantum Optics with Giant Atoms in 2D Structured Environments

Emil Ingelsten

Department of Microtechnology and Nanoscience
Chalmers University of Technology

Abstract

One of the major hurdles in the ongoing efforts to construct a working large-scale quantum computer is achieving rapid interactions between qubits without risking a loss of energy (and thus information) to their surroundings. This loss of energy is known as *decoherence*. In recent years, one possible solution to this problem that has shown promise is the use of so-called *giant atoms*. In certain configurations, these systems have been shown to exhibit *decoherence-free interaction* (DFI) when coupled to one-dimensional environments, such as transmission lines or photonic crystal waveguides. For DFI to be possible, the atoms involved must be *perfectly subradiant* – that is, they must not spontaneously decay into their environments. In this study, we used numerical simulations combined with the methods of *resolvent formalism* to examine under what conditions giant atoms exhibit perfect subradiance and DFI when coupled to two-dimensional (2D) environments. More specifically, structured 2D environments – i.e. resonator lattices – were considered. In such environments, there are finite energy bands and band gaps, which causes effects that are not predicted by the so-called Born-Markov approximation, e.g. *time delay*. Multiple generalisations of previously known setups exhibiting perfect subradiance were found. Furthermore, a number of different configurations exhibiting DFI were discovered, including grid-like ones that in principle could be extended indefinitely.

Keywords: quantum optics, giant atoms, 2D, structured environments, subradiance, decoherence-free interaction, resolvent formalism.

Acknowledgements

First and foremost, I would like to give a massive thank you to my supervisors Anton Frisk Kockum and Ariadna Soro Álvarez. They have been a tremendous resource, and without their support, help and encouragement, this thesis project would not have been possible. I would especially like to give a shout-out to Ariadna for all the hours spent listening to me vent about the various difficulties I faced this spring. Furthermore, I would like to thank the Knut and Alice Wallenberg Foundation for their contributions towards the Wallenberg Centre for Quantum Technology. This institution is to a large extent what makes thesis projects such as this one, as well as a lot of related cutting-edge research in fields like quantum optics and quantum computing, possible here at Chalmers. In addition, I want to thank Alejandro González-Tudela and Alberto del Angel for several interesting discussions of giant atoms and their properties when coupled to structured environments. I would also like to thank David Hambraeus for many interesting discussions this spring. While these were generally about topics of slightly less immediate relevance to the subject matter of the thesis, they were nevertheless very much appreciated. Finally, I would like to thank Erika Magnusson for her valuable feedback, which helped polish this report.

Emil Ingelsten, Gothenburg, June 2023

Contents

1 Introduction **1**
1.1 Atoms, Small and Giant . . . 1
1.2 Aims and Scope . . . 2

2 Theory **3**
2.1 Time Evolution of Quantum States . . . 3
2.1.1 Numerical Methods . . . 4
2.2 Resolvent Formalism . . . 5
2.2.1 Perturbation Theory . . . 9
2.3 Small Atoms in 1D Environments . . . 11
2.3.1 Direct Numerical Time Evolution . . . 13
2.3.2 Time Evolution via Resolvent Formalism . . . 14
2.3.2.1 A Single Small Atom . . . 16
2.3.2.2 Two Small Atoms . . . 18
2.4 Giant Atoms in 1D Environments . . . 21
2.4.1 A Single Giant Atom . . . 22
2.4.2 Multiple Giant Atoms and DFI . . . 24
2.5 Giant Atoms in 2D Environments . . . 26

3 Results **31**
3.1 Efficient Simulation of Giant Atoms . . . 31
3.2 Subradiant Small Atoms in 2D environments . . . 32
3.3 Subradiant Giant Atoms in 2D environments . . . 38
3.4 DFI in 2D structured environments . . . 43

4 Discussion, Conclusions and Outlook **53**

References **55**

A The Residue of an Operator **I**

B Efficient Computation of the Time Evolution Operator **IV**
B.1 Small atoms . . . IV
B.2 Giant atoms . . . VIII
B.2.1 Giant Atoms with Even Coupling Strength . . . VIII
B.2.2 Giant Atoms with Uneven Coupling Strength . . . X
B.3 A Non-Recursive Formula for Λ_k . . . XI

1

Introduction

In the ongoing race to build a large-scale quantum computer, one of the major hurdles is *decoherence*, where the energy (and thus the information) stored in a quantum bit, or qubit, is lost to the environment. One path towards a solution to this problem that has shown promise in recent years is the usage of so-called *giant atoms* [1]. These atom-like systems have been shown to exhibit *decoherence-free interaction* in certain configurations when coupled to one-dimensional (1D) environments [2–5]. In this thesis, we will expand on current knowledge by examining their behaviour when coupled to two-dimensional (2D) environments – specifically structured ones, i.e. resonator lattices – and the conditions for DFI in 2D.

1.1 Atoms, Small and Giant

Many of the most important advancements in materials science, communication technology and computing over the past century can be attributed to achieving a deeper understanding of quantum mechanics and how it applies to different fields. In the past 40 years specifically, there has been explosive growth in a number of fields related to studying how quantum effects like entanglement and superposition can be leveraged more directly in information science and computing, e.g. by making a quantum computer [6].

One of these fields is quantum optics, where interactions between individual photons and atom-like systems (such as superconducting qubits [7]) are studied. Until recently, most of the atom-like systems studied experimentally were small compared to the wavelength of the light they interact with. Natural atoms, for example, have a radius of $\sim 10^{-10}\,\mathrm{m}$ and interact with optical light, which has wavelengths between 10^{-6} and $10^{-7}\,\mathrm{m}$.

However, in an experiment performed at Chalmers University of Technology in 2014 [8], the so-called *giant atom* regime was reached. In this regime, the size of the studied atoms is no longer negligible compared to the wavelength of the photons involved (this is why the atoms in question are referred to as "giant" [1]). Since 2014, further theoretical and experimental inquiries have been made, resulting in the discovery of several interesting phenomena. Perhaps most interestingly, giant atoms can interact *without decohering*, i.e. they can exchange energy (and thus information) via their environment with practically zero risk of losing it. This so-called *decoherence-free interaction* (DFI) makes giant atoms a promising candidate for future applications in quantum simulation and computation, since decoherence is currently a major hurdle in these fields.

1.2 Aims and Scope

Until now, giant atoms have mostly been studied in the context of having them coupled to 1D waveguides. In this thesis, we will expand on current knowledge by examining how giant atoms behave when coupled to (1D and) 2D structured environments – lattices of resonators coupled via nearest-neighbour interactions – in different configurations. These environments have been studied before for small atoms [9], but not for giant atoms to the same extent. The studies that *have* been performed for giant atoms so far have studied single giant atoms [10], whereas we will examine systems consisting of multiple giant atoms. To these ends, we will make use of numerical simulations combined with the complex-analysis methods of *resolvent formalism* [11], with a focus on the former.

An important delimitation for this thesis is the fact that we will only consider square resonator lattices – more complicated lattices such as triangular or hexagonal ones will be left to future studies. Apart from this, it should be noted that the models used in this thesis make use of various approximations. Examples include truncation of Hilbert space to the *single-excitation subspace* and the *rotating wave approximation*. While the approximations and their legitimacy will be discussed, no in-depth analysis of their possible effects on the results will be made.

2

Theory

To follow and understand the contents of this thesis, a fair amount of prior knowledge is needed – primarily relating to how giant atoms are modelled using quantum mechanics. In this section, we first recapitulate some of the basics of quantum mechanics before showing how this can be reformulated in the so-called *resolvent formalism*. We then describe how to use this formalism to model giant atoms in different setups.

2.1 Time Evolution of Quantum States

The time evolution of a non-relativistic quantum state $|\psi(t)\rangle$ follows the Schrödinger equation [12],

$$i\hbar\frac{\mathrm{d}}{\mathrm{d}t}|\psi(t)\rangle = \hat{H}|\psi(t)\rangle\,. \tag{2.1}$$

Here, $\hbar$ is Planck's (reduced) constant and $\hat{H}$ is the Hamiltonian operator, whose eigenvalues correspond to possible system energies. Integrating this first order linear differential equation, we find that an initial state $|\psi(0)\rangle$ evolves according to

$$|\psi(t)\rangle = \hat{U}(t)|\psi(0)\rangle\,, \tag{2.2}$$

where the time evolution operator $\hat{U}(t)$ is given by

$$\hat{U}(t) = \exp\Big(-\frac{i}{\hbar}\int_0^t \hat{H}(t)\,\mathrm{d}t\Big). \tag{2.3}$$

If the Hamiltonian is time-independent, we can move it outside the integral, so that the time-evolution operator reduces to

$$\hat{U}(t) = \exp\Big(-\frac{i}{\hbar}\hat{H}t\Big). \tag{2.4}$$

In general, computing this operator exponential exactly is not straightforward. Many systems – atoms among them – have an infinite number of energy eigenstates, making $\hat{H}$ infinite-dimensional. As it turns out, however, this is not as big of a problem as it might first appear. For processes involving initial states with limited energy (i.e. for almost all intents and purposes), we can safely ignore states with energy significantly higher than that of the initial state. How do we accomplish this in practice? Well, if we choose some basis $\{|k\rangle\}_{k=1}^{n}$ for the subspace $\mathcal{C}$ of states that have low-enough energy to be relevant, we can project all states and operators onto this subspace using the projection operator

$$\mathcal{P}_{\mathcal{C}} = \sum_{k=1}^{n}|k\rangle\langle k|\,. \tag{2.5}$$

This means that any state $|\psi\rangle$ is truncated into

$$|\psi\rangle_{\mathcal{C}} = \mathcal{P}_{\mathcal{C}} |\psi\rangle = \sum_k \psi_k |k\rangle \tag{2.6}$$

with $\psi_k = \langle k|\psi\rangle$ being some complex number for every value of k. Effectively, then, our states are modelled as complex n-dimensional vectors. Similarly, any operator $\hat{A}$ is truncated into

$$\hat{A}_{\mathcal{C}} = \mathcal{P}_{\mathcal{C}} \hat{A} \mathcal{P}_{\mathcal{C}} = \sum_{k,l} A_{kl} |k\rangle\langle l| , \tag{2.7}$$

where

$$A_{kl} = \langle k|\hat{A}|l\rangle \tag{2.8}$$

is a complex number for every combination of values of k and l. In other words, the operator $\hat{A}$ is effectively modelled as an $n \times n$ complex matrix with matrix elements A_{kl}.

In this framework, the time evolution operator (for time-independent $\hat{H}$) is a matrix exponential

$$U(t) = \exp\Big(-\frac{i}{\hbar} H t\Big), \tag{2.9}$$

where H is the $n \times n$ matrix representation of $\hat{H}_{\mathcal{C}}$.

2.1.1 Numerical Methods

When evaluating this matrix exponential numerically it is especially convenient to work in the *energy eigenbasis*, where H is diagonal – specifically, $H_{kl} = E_k \delta_{kl}$ (no sum), where E_k is the energy of the kth energy eigenstate. The reason for this is that the exponential of a diagonal matrix is very easy to compute:

$$\begin{aligned} U(t) = \exp\Big(-\frac{i}{\hbar} H t\Big) = \exp\Big[-\frac{i}{\hbar} \operatorname{diag}(E_1, \ldots, E_n) t\Big] = \\ = \operatorname{diag}\Big[\exp\Big(-\frac{i}{\hbar} E_1 t\Big), \ldots, \exp\Big(-\frac{i}{\hbar} E_n t\Big)\Big]. \end{aligned} \tag{2.10}$$

Unfortunately, while the Hamiltonians of some simple systems – isolated atoms among them – are intuitive to express in their eigenbasis, this is often not at all the case for systems consisting of many different parts all interacting with each other.

One way to get around this is to simply diagonalise H directly by calculating the eigenstates of H and their corresponding eigenenergies and then performing a change of basis into the energy eigenbasis. However, this is in general not significantly faster than current state-of-the-art algorithms for calculating a matrix exponential directly – for example, the algorithm used by the `linalg.expm()` function in the python package SciPy [13] takes $\mathcal{O}(N^3)$ operations [14, 15], just like the fastest diagonalisation algorithms currently in use [16].

Even for systems where there is no easy way to express the total Hamiltonian $\hat{H}$ in its eigenbasis, however, it may well be that $\hat{H}$ can be split into parts that are more well-behaved. In particular, it is quite often the case that it can be split into two parts $\hat{H} = \hat{K} + \hat{V}$ such that the "kinetic" part $\hat{K}$ and the "potential" part $\hat{V}$ are diagonal in bases that are related to one another via a Fourier transform (FT). The canonical example of this is a quantum particle moving in a position-dependent potential. In this

case, the kinetic Hamiltonian $\hat{K} = \frac{\hat{p}^2}{2m}$ is diagonal in the momentum basis and the potential Hamiltonian $\hat{V} = V(\hat{x})$ is diagonal in the position basis.

The time evolution of Hamiltonians exhibiting such a structure can be simulated efficiently by using a so-called *split-operator* approach [17]. These methods are based on the fact that while

$$\hat{U}(t) = \exp\left[-i\frac{\hat{K}+\hat{V}}{\hbar}t\right] \neq \hat{U}_K(t)\hat{U}_V(t) \equiv \exp\left[-i\frac{\hat{K}}{\hbar}t\right]\exp\left[-i\frac{\hat{V}}{\hbar}t\right] \tag{2.11}$$

since $\hat{K}$ and $\hat{V}$ don't commute, it can be shown by performing a series expansion in t that

$$\hat{U}(t) = \hat{U}_V(t)\hat{U}_K(t) + \frac{1}{2}\left[\hat{V},\hat{K}\right]t^2 + \mathcal{O}\left(t^3\right). \tag{2.12}$$

This is related to the *Baker-Campbell-Hausdorff formula* [18], which gives the operator Z satisfying $e^Z = e^X e^Y$ in terms of X, Y and commutators of X and Y. In other words, as long as we use sufficiently small time steps Δt, we can alternate between applying $\hat{U}_K(\Delta t)$ and $\hat{U}_V(\Delta t)$ and still achieve time evolution that is accurate to $\mathcal{O}(\Delta t^2)$. In fact, we can do even better without much additional effort, since it can be shown that the operator

$$\hat{U}_V\left(\frac{\Delta t}{2}\right)\hat{U}_K(\Delta t)\hat{U}_V\left(\frac{\Delta t}{2}\right) \tag{2.13}$$

is $\mathcal{O}(\Delta t^3)$ accurate [17]. Applying many such operators in succession yields a total time-evolution operator that is identical to the one gotten by applying $\hat{U}_K(\Delta t)\hat{U}_V(\Delta t)$ repeatedly, except for the fact that one application of $\hat{U}_V(\frac{\Delta t}{2})$ has been moved from the start of the time evolution to the end.

To go between the eigenbases of $\hat{V}$ and $\hat{K}$, we can use a *fast Fourier transform* (FFT) with computational cost $\mathcal{O}(N \log N)$ for a system with N eigenstates [19]. This means that the time evolution of such a system, with Hamiltonian $\hat{H} = \hat{K} + \hat{V}$, can be evaluated to $\mathcal{O}(\Delta t^3)$ accuracy by repeatedly applying the operator

$$\tilde{U}(\Delta t) \equiv \mathcal{F}^{-1}\hat{U}_K(\Delta t)\mathcal{F}\hat{U}_V(\Delta t), \tag{2.14}$$

sandwiched between an initial $\hat{U}_V(-\Delta t/2)$ and a final $\hat{U}_V(\Delta t/2)$. Here, $\mathcal{F}$ denotes the FFT, and $\mathcal{F}^{-1}$ its inverse, the IFFT. Since all operator exponentials can be computed in their eigenbases, where the computational cost to do so is only $\mathcal{O}(N)$, the total computational cost of this algorithm is $\mathcal{O}(N \log N)$.

2.2 Resolvent Formalism

For a given Hamiltonian H (suppressing hats on operators from now on), the associated time evolution operator is, by construction, the solution of the operator Schrödinger equation

$$i\hbar\frac{\mathrm{d}}{\mathrm{d}t}U(t) = HU(t) \Leftrightarrow \left[i\hbar\frac{\mathrm{d}}{\mathrm{d}t} - H\right]U(t) = 0. \tag{2.15}$$

This means that the so-called retarded and advanced Green's function operators, or *real-space propagators* [11, 20], for the Schrödinger equation are given by

$$K_+(t) = U(t)\Theta(t) \quad \text{and} \quad K_-(t) = -U(t)\Theta(-t), \tag{2.16}$$

respectively, assuming H is time-independent. Here, $\Theta(t)$ is the Heaviside step function, defined so that

$$\Theta(t) = \begin{cases} 0 & \text{for } t < 0 \\ \frac{1}{2} & \text{for } t = 0 \\ 1 & \text{for } t > 0. \end{cases} \tag{2.17}$$

To see that $K_\pm(t)$ indeed are Green's function operators for the Schrödinger equation, we can simply apply the Schrödinger operator onto them and note that they satisfy

$$\left[i\hbar\frac{\mathrm{d}}{\mathrm{d}t} - H\right]K_\pm(t) = i\hbar\delta(t). \tag{2.18}$$

With these definitions, we see that K_+ (K_-) corresponds to time-evolution forwards (backwards) in time, and for all values of t we have

$$U(t) = K_+(t) - K_-(t), \tag{2.19}$$

where K_+ (K_-) is identically zero for $t < 0$ ($t > 0$). As it turns out, it is especially convenient to work with the *Fourier transforms* of $K_\pm$, i.e. the *Fourier-space propagators* $G_\pm$ defined so that

$$K_\pm(t) = -\frac{1}{2\pi i}\int_{\mathbb{R}} \mathrm{d}E\, e^{-iEt/\hbar}G_\pm(E). \tag{2.20}$$

Why is this so convenient? Well, as we will see the Fourier-space propagators are very simple:

$$G_\pm(E) = \lim_{\varepsilon\to 0^+} \frac{1}{E - H \pm i\varepsilon}. \tag{2.21}$$

While deriving this expression from scratch is not trivial, it is quite straightforward to show that it yields the correct expression for $K_\pm$ when inserted into Eq. (2.20). Note that we are here making use of what is arguably a slight abuse of notation but nevertheless ubiquitous in physics: the "reciprocal" of $E - H \pm i\varepsilon$ is to be interpreted as the operator inverse, i.e.

$$\frac{1}{E - H \pm i\varepsilon} \equiv [(E \pm i\varepsilon)\mathbb{1} - H]^{-1}, \tag{2.22}$$

where $\mathbb{1}$ is the identity operator. Let us verify that these expressions for $G_\pm$ indeed agree with Eq. (2.20). For brevity, we will only show that the inverse Fourier transform of G_+ is K_+, but the advanced case (with minus signs) is entirely analogous.

The Fourier integral

$$K_+(t) = -\frac{1}{2\pi i}\int_{\mathbb{R}} \mathrm{d}E\, e^{-iEt/\hbar}G_+(E) = -\frac{1}{2\pi i}\lim_{\varepsilon\to 0^+}\int_{\mathbb{R}} \mathrm{d}E\, \frac{e^{-iEt/\hbar}}{E - H + i\varepsilon} \tag{2.23}$$

can be rewritten as a contour integral

$$K_+(t) = \frac{1}{2\pi i}\lim_{\varepsilon\to 0^+}\int_{\gamma_+(\varepsilon)} \mathrm{d}z\, \frac{e^{-izt/\hbar}}{z - H}, \tag{2.24}$$

where $\gamma_+(\varepsilon) = \{z \in \mathbb{C} : z = E + i\varepsilon\}$ with $E \in \mathbb{R}$ going from ∞ to $-\infty$, see Fig. 2.1. To compute this contour integral, it is convenient to use the residue theorem. For this to be possible, however, we need to extend γ_+ into a closed curve. By Jordan's lemma [21], this extension can be accomplished without changing the value of the integral by integrating

around a half-circle of infinite radius in the upper half-plane (UHP) for $t < 0$ and in the lower half-plane (LHP) for $t > 0$. The residue theorem [22] then gives us that

$$K_+(t) = \frac{1}{2\pi i} \oint_\gamma \mathrm{d}z \, \frac{e^{-izt/\hbar}}{z - H} = \operatorname*{Res}_\gamma \left[\frac{e^{-izt/\hbar}}{z - H} \right], \tag{2.25}$$

with γ enclosing the UHP excluding the real axis for $t < 0$ and enclosing the LHP including the real axis for $t > 0$, see Fig. 2.1. Here, $\mathrm{Res}_\gamma[\cdot]$ denotes the sum of all residues enclosed within γ. Since the poles of the integrand effectively lie at the eigenvalues of the Hamiltonian (see appendix A) and these are all real, the integral is zero for $t < 0$. For $t > 0$ we instead get

$$K_+(t) = \operatorname*{Res}_{z=H} \left[\frac{e^{-izt/\hbar}}{z - H} \right] = e^{-iHt/\hbar} = U(t), \tag{2.26}$$

as desired. For the definition of "the residue at $z = H$", see appendix A.

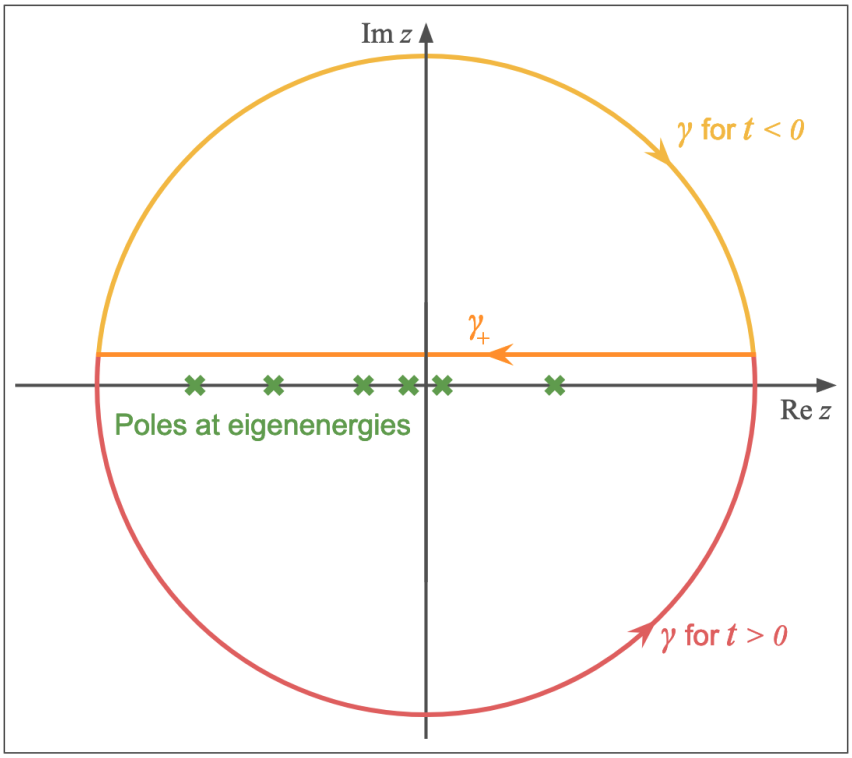

Figure 2.1: The original contour of integration γ_+ from Eq. (2.24) in orange, as well as the extensions to make the closed path γ for positive and negative t in red and yellow, respectively.

The utility of complexifying the Fourier-space propagators in this way leads us to introduce the operator-valued function

$$G(z) \equiv \frac{1}{z - H}, \tag{2.27}$$

where z is allowed to take arbitrary complex values. This function is called the *resolvent* of the Hamiltonian H [11]. In terms of the resolvent, the Fourier-space propagators are given by

$$G_\pm(E) = \lim_{\varepsilon \to 0^+} G(E \pm i\varepsilon), \tag{2.28}$$

which means that the time-evolution operator can be expressed as a contour integral

$$U(t) = \frac{1}{2\pi i} \int_{\gamma_+ + \gamma_-} \mathrm{d}z \, e^{-izt/\hbar} G(z), \tag{2.29}$$

with $\gamma_\pm$ infinitesimally close to the real axis and oriented as in Fig. 2.2 below.

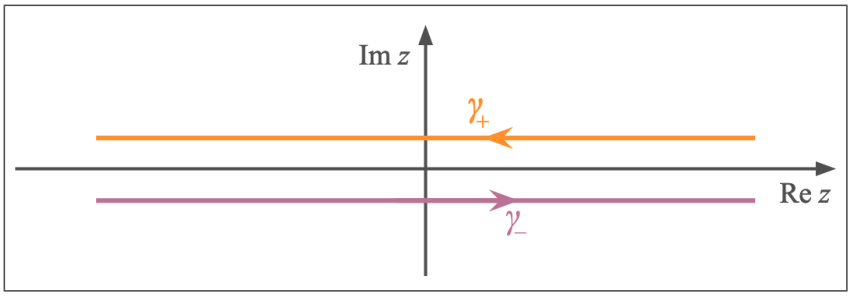

Figure 2.2: The two contours of integration $\gamma_\pm$ from Eq. (2.29).

One slight issue that we have swept under the rug here is what happens when H has a continuous spectrum of eigenvalues somewhere along the real axis. As it turns out [11], if H has such a band between the energies $E_{\min}$ and $E_{\max}$, then $G(z)$ will have a *branch cut* (BC) along the real axis between $z = E_{\min}$ and $z = E_{\max}$. This BC is characterised by the fact that $G(z)$ has different limiting values when approaching the BC from the UHP and the LHP. Unfortunately, the residue theorem cannot be applied as-is when the interior of the integration contour includes a BC. What we would like to do is to somehow include the information contained in the BC while keeping the branch points outside the integration contour.

Since the residue theorem requires the integrated function to be analytic along the path [22], our integration contour cannot cross the branch cut. What we can do, however, is to continue the integrated function analytically on the other side of the branch cut – onto its second *Riemann sheet* (RS). In some situations, notably when dealing with the projection of the resolvent onto a subspace representing some part of the total system, there may be *unstable poles* on the second RS [11], i.e. poles with negative imaginary part. These are effectively the mechanism by which energy can leave the subsystem in question (see e.g. Refs. [5] and [9]). In any case, by extending our contour onto the second Riemann sheet in this way, illustrated in Fig. 2.3, we can apply the residue theorem after all. Note, however, that we still need to take into account the "detour integral" along our new branch cuts, which is likely nonzero.

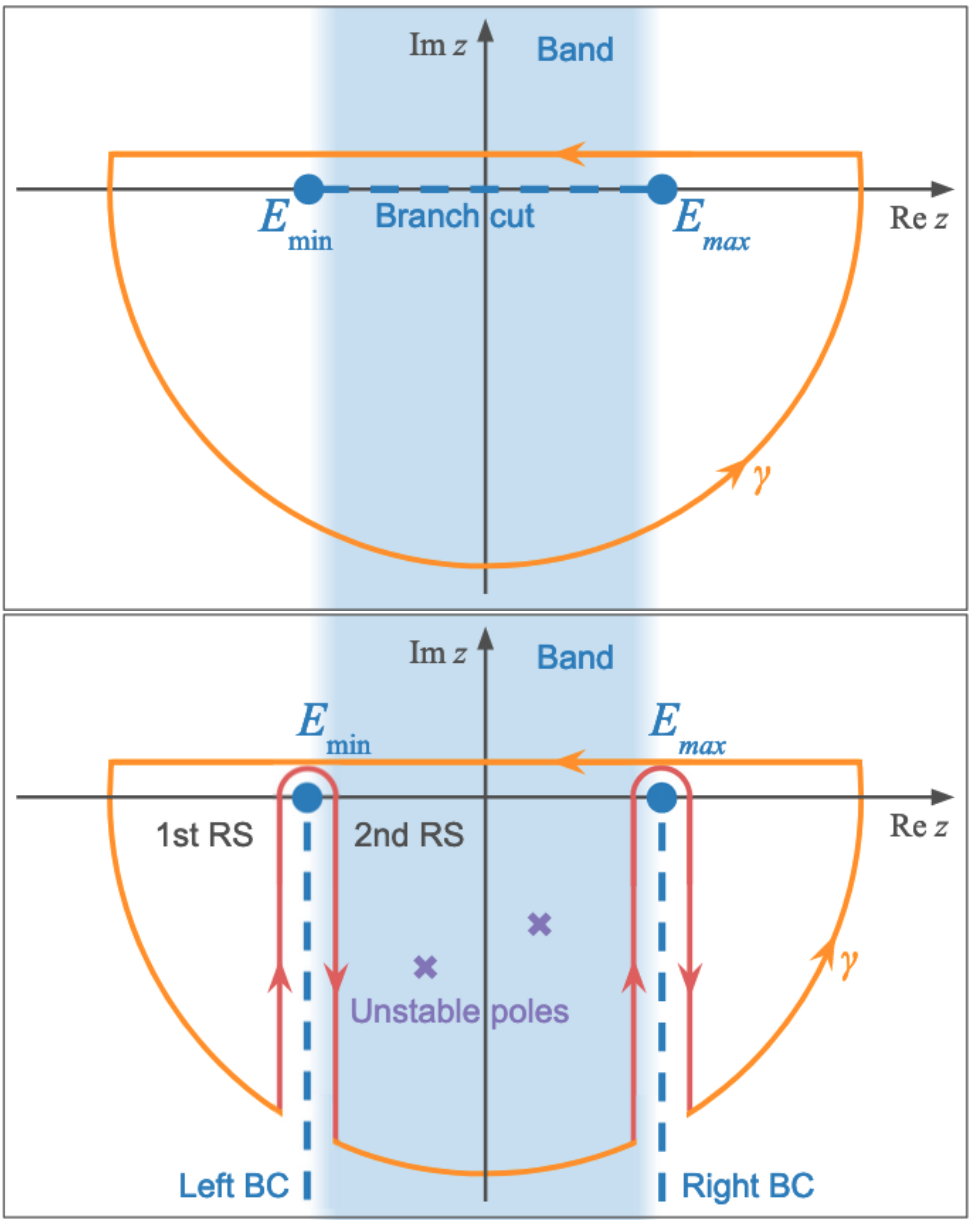

Figure 2.3: Top: the $t > 0$ integration contour γ from Eq. (2.25) in the case where H has a continuous band between the energies $E_{\min}$ and $E_{\max}$. Bottom: the modified integration contour, lying partly on the second Riemann sheet. By the residue theorem, the value of the original contour integral is the sum of the residues at the unstable poles minus the contributions from the detours in red. Figure inspired by Refs. [5] and [9].

2.2.1 Perturbation Theory

Suppose that we want to study a system described by a total Hamiltonian $H = H_0 + V$, where H_0 is diagonal and V is some off-diagonal perturbation, encoding the coupling between the eigenstates of H_0. If we use the operator identity

$$A^{-1} = B^{-1} + B^{-1}(B - A)A^{-1} \tag{2.30}$$

with $A = z - H$ and $B = z - H_0$ we see that since $B - A = H - H_0 = V$, the resolvents are related via

$$G(z) = G_0(z) + G_0(z)VG(z). \tag{2.31}$$

If we use this expression recursively, we see that as long as V is small, $G(z)$ can be expressed as a perturbative expansion in powers of V around $G_0(z)$:

$$G(z) = G_0(z) + G_0(z)VG_0(z) + G_0(z)VG_0(z)VG_0(z) + \cdots . \tag{2.32}$$

This can also be translated into a perturbative expansion for the matrix elements of $G(z)$, namely

$$G_{ij}(z) = \frac{\delta_{ij}}{z - E_i} + \frac{1}{z - E_i}V_{ij}\frac{1}{z - E_j} + \sum_k \frac{1}{z - E_i}V_{ik}\frac{1}{z - E_k}V_{kj}\frac{1}{z - E_j} + \cdots . \tag{2.33}$$

Just like in perturbative Quantum Field Theory [11, 20], this can be represented as an infinite series of Feynman diagrams

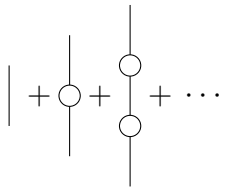

where the lines represent propagation according to G_0 and the circles represent interactions via V.

Now, suppose we are mainly interested in the population of a subspace of H_0 eigenstates, which we can call $\mathcal{S}$, with associated projection and rejection operators P and $Q = \mathbb{1} - P$. By definition, the resolvent satisfies

$$(z - H)G(z) = \mathbb{1}. \tag{2.34}$$

If we apply P from the right, insert $\mathbb{1} = P + Q$ between the two factors on the LHS and P or Q from the left, we get the following two equations:

$$\begin{cases} P(z - H)PG(z)P - PVQG(z)P & = P \\ -QVPG(z)P + Q(z - H)QG(z)P & = 0. \end{cases} \tag{2.35}$$

Here, we have used the fact that $P(z - H_0)Q = 0 = Q(z - H_0)P$, since $z - H_0$ is diagonal. Solving the second equation for $QG(z)P$, we see that

$$QG(z)P = \frac{Q}{z - QHQ}VPG(z)P. \tag{2.36}$$

Inserting this into the first equation yields

$$P\left[z - H - V\frac{Q}{z - QHQ}V\right]PG(z)P = P, \tag{2.37}$$

which means that the projection of the resolvent onto our subspace of interest $\mathcal{S}$ is given by

$$PG(z)P = \frac{P}{z - P\left[H_0 + V + V\frac{Q}{z - QHQ}V\right]P}. \tag{2.38}$$

In other words, the *effective* Hamiltonian as far as time-evolution of states in $\mathcal{S}$ is concerned is given not by PH_0P or PHP, but rather by $P(H_0 + \Sigma(z))P$, with Σ being the *self-energy* or *level-shift* operator [11] defined by

$$\Sigma(z) \equiv V + V\frac{Q}{z - QHQ}V. \tag{2.39}$$

This operator, or rather its projection $P\Sigma(z)P$, lets us take into account all of the effective change in H_0 caused by the perturbation V felt by states in the $\mathcal{S}$ subspace. And this is accomplished without including any superfluous information about the "uninteresting" H_0 eigenstates not contained in $\mathcal{S}$! Inserting Σ into Eq. (2.38) lets us rewrite it as

$$PG(z)P = \frac{P}{z - PH_0P - P\Sigma(z)P}. \tag{2.40}$$

With all this behind us, it is now time to take a look at how this can be applied to studying atoms – both small and "giant" – and their interactions with their environments.

2.3 Small Atoms in 1D Environments

The specific environments we are interested in are *structured* ones, meaning lattices of resonators – in our case with nearest neighbour-coupling. These kinds of environments have many physical manifestations [23]. Examples include photonic crystal waveguides [24] and optical lattices [25, 26] coupled to cold atoms, as well as microwave photonic crystals [27] and superconducting metamaterials [28] coupled to superconducting qubits. The reason they are interesting is the fact that they have non-trivial dispersion relations with bands and band gaps, which gives rise to a whole host of phenomena [23]. A single resonator can for our intents and purposes be modelled as a harmonic oscillator [29]. In other words, its Hamiltonian can be taken to be

$$H_R = \omega_R a^\dagger a, \tag{2.41}$$

where ω_R is the characteristic angular frequency and a ($a^\dagger$) is the annihilation (creation) operator associated with subtracting (adding) photons in the fundamental mode. Note that we are here suppressing a factor of $\hbar$, and will continue to do so from now on by working in units where $\hbar = 1$.

To model a 1D lattice of resonators, then, we need one copy of this Hamiltonian for every resonator as well as an interaction term encoding the fact that every resonator can interact with its nearest neighbours. Assuming every resonator has the same frequency ω_B, and the nearest-neighbour coupling is J, this means that a 1D resonator lattice with N resonators can be modelled [5, 9] using the Hamiltonian

$$H_B = \omega_B \sum_{n=1}^{N} {a^\dagger}_n a_n - J \sum_{\langle m,n\rangle} (a_m^\dagger a_n + a_n^\dagger a_m), \tag{2.42}$$

where $\langle m, n\rangle$ denotes all neighbouring resonators.

If we want to couple some number M of small atoms to our "bath" of resonators, we need a way to model them, as well as the coupling between the atoms and the bath. Since we are mainly interested in the single-excitation regime, we can neglect all energy levels for our atoms except the ground state $|g\rangle$ and the first excited state $|e\rangle$. If we do so, our system can be modelled [29] using the Rabi Hamiltonian

$$H = \sum_{a=1}^{M} \omega_a \sigma_a^\dagger \sigma_a + \sum_{a=1}^{M} g_a\Big(\sigma_a^\dagger + \sigma_a\Big)(a_{n_a}^\dagger + a_{n_a}) + H_B, \tag{2.43}$$

where ω_a is the energy difference between the $|g\rangle$ and $|e\rangle$ states for atom a. Here we have also used the notation $\sigma_a^\dagger$ (σ_a) for the raising (lowering) operator for atom a and

introduced the atom-bath coupling strength g. Note that since we are using small atoms, every atom only couples to the bath through a single resonator – specifically, atom a couples to resonator n_a.

We can, in fact, make one further simplification – namely, the *rotating wave approximation* (RWA), where we only consider interactions preserving the total number of excitations in the system. The effect of this can be understood as neglecting terms oscillating at $\omega_a + \omega_B$ and keeping terms that oscillate at $|\omega_a - \omega_B|$. This is a valid approximation when the detuning $\Delta_a \equiv \omega_a - \omega_B$ of atom a from the resonator frequency ω_B is small and the coupling is weak, i.e. when $\omega_a \sim \omega_B \gg g$. At frequencies in the realm of optical light and microwaves, this is a good approximation [23].

Performing the RWA results in the so-called *Jaynes-Cummings Hamiltonian* [29], which is the model we will be using for the rest of this thesis:

$$H = \sum_{a=1}^{M} \omega_a \sigma_a^\dagger \sigma_a + \sum_{a=1}^{M} g_a \Big(\sigma_a^\dagger a_{n_a} + \sigma_a a_{n_a}^\dagger \Big) + H_B \tag{2.44}$$

Since the diagonal bath term $\omega_B \sum_{n=1}^{N} a_n^\dagger a_n$ does not contribute any interesting dynamics, it is advantageous to move into a reference frame "rotating at ω_B" [5], effectively cancelling all time evolution coming from this term. This yields a modified system Hamiltonian, looking like

$$H = \sum_{a=1}^{M} \Delta_a \sigma_a^\dagger \sigma_a + \sum_{a=1}^{M} g_a \Big(\sigma_a^\dagger a_{n_a} + \sigma_a a_{n_a}^\dagger \Big) + H_B', \tag{2.45}$$

where

$$H_B' = -J \sum_{\langle m,n \rangle} (a_m^\dagger a_n + a_n^\dagger a_m). \tag{2.46}$$

Removing the prime from H_B' and making the further definitions

$$H_A = \sum_{a=1}^{M} \Delta_a \sigma_a^\dagger \sigma_a \tag{2.47}$$

and

$$H_{\text{int}} = \sum_{a=1}^{M} g_a \Big(\sigma_a^\dagger a_{n_a} + \sigma_a a_{n_a}^\dagger \Big), \tag{2.48}$$

we see that our total system Hamiltonian is given by

$$H = H_A + H_B + H_{\text{int}}, \tag{2.49}$$

or, if we want to write out all the terms explicitly,

$$H = \sum_{a=1}^{M} \Delta_a \sigma_a^\dagger \sigma_a - J \sum_{\langle m,n \rangle} (a_m^\dagger a_n + a_n^\dagger a_m) + \sum_{a=1}^{M} g_a \Big(\sigma_a^\dagger a_{n_a} + \sigma_a a_{n_a}^\dagger \Big). \tag{2.50}$$

Here, H_A is only related to the atoms, H_B is only related to the bath, and all interactions between atoms and bath are encoded in H_{int}.

2.3.1 Direct Numerical Time Evolution

Since we are using the RWA, we can safely truncate our state space to the *single-excitation subspace*. This subspace consists of all states with one atom excited, which we can label $\{|a\rangle\}_{a=1}^{M}$, plus all the states where one of the resonators is excited, which we can label $\{|n\rangle\}_{n=0}^{N-1}$. While the bath Hamiltonian

$$H_B = -J \sum_{\langle m,n \rangle} (a_m^\dagger a_n + a_n^\dagger a_m) \tag{2.51}$$

is not diagonal in the position basis, it *is* diagonal in the momentum basis [5], consisting of the momentum eigenstates

$$|k\rangle \equiv \frac{1}{\sqrt{N}} \sum_{n=0}^{N-1} e^{-ikn} |n\rangle , \tag{2.52}$$

with $k \in \left\{-\pi, \ldots, \pi - \frac{2\pi}{N}\right\}$. To show this, we first note that this definition of the $|k\rangle$ states implies that the momentum space creation operator must look like

$$a_k^\dagger = \frac{1}{\sqrt{N}} \sum_{n=0}^{N-1} e^{-ikn} a_n^\dagger, \tag{2.53}$$

with the corresponding annihilation operator being the Hermitian conjugate of this expression. Performing an inverse discrete Fourier transform, we find that

$$a_n^\dagger = \frac{1}{\sqrt{N}} \sum_{k} e^{ikn} a_k^\dagger, \tag{2.54}$$

with the sum going over all $k \in \left\{-\pi, \ldots, \pi - \frac{2\pi}{N}\right\}$. Inserting this into Eq. (2.51) yields

$$\begin{aligned} H_B &= -\frac{J}{N} \sum_{\langle m,n \rangle} \sum_{k,k'} (e^{i(km-k'n)} a_k^\dagger a_{k'} + e^{-i(km-k'n)} a_{k'}^\dagger a_k) \\ &= \{\text{net zero contribution from } k \neq k',\ m-n=1\} = \\ &= -J \sum_{k} (e^{ik} + e^{-ik}) a_k^\dagger a_k \\ &= \sum_{k} \omega(k) a_k^\dagger a_k, \end{aligned} \tag{2.55}$$

with $\omega(k) \equiv -2J \cos k$. As we can see, H_B is indeed diagonal in this basis.

Note that the change of basis performed here implicitly imposes periodic boundary conditions, since the discrete Fourier transform is based on splitting position-space data up into a sum of periodic signals with different frequencies. In the physical systems we are interested in modelling, this is strictly speaking not the correct choice of boundary conditions, since energy cannot simply jump from one edge of the lattice to the other. However, this is not a problem as long as we keep our simulations short enough that no emissions from the atoms we are studying have the time to reach the atom again after travelling the length of the lattice, wrapping around to the other side after hitting the edge.

Taking a step back, this means that H_A and H_B are diagonal in bases related by a Fourier transform, so we can use split-operator methods as-is to efficiently simulate the

time evolution generated by the Hamiltonian $H_A + H_B$. Unfortunately, that is not quite our full Hamiltonian – our Hamiltonian also contains an interaction term H_{int} which is off-diagonal in both bases. As it turns out, however, this is not as big of a problem as it might appear. It can be shown [5, 9] (see also the first section of appendix B for a derivation) that all of the nonzero matrix elements in

$$U_V(\Delta t) = \exp[-i(H_A + H_{\text{int}})\Delta t] \tag{2.56}$$

are simply copies of the matrix elements of

$$U_a(\Delta t) = \exp[-iH_a\Delta t], \tag{2.57}$$

for $a \in \{1, \ldots, M\}$, where

$$H_a = \begin{bmatrix} \Delta_a & g_a \\ g_a & 0 \end{bmatrix}, \tag{2.58}$$

as long as no two atoms couple to the same resonator. Thus, instead of computing an $(M+N) \times (M+N)$ matrix exponential, it is sufficient to compute M different 2×2 matrix exponentials – or fewer, if some of the atoms have identical values for Δ and g.

Having computed $U_a(\Delta t)$ for every atom, one can reconstruct the full time-evolution operator matrix $U_V(\Delta t)$ based on knowledge of which atom couples to which coupling point. As it turns out, however, this is unnecessary. Instead of recreating $U_V(\Delta t)$ and performing an $\mathcal{O}[(M+N)^2]$ matrix-vector multiplication in each time step, we can apply the map encoded by $U_V(\Delta t)$ manually [5]. Since most resonators are unaffected by this map as they are not coupled to any atom, this reduces the complexity of evolving our system a single time step to being linear in M and N.

All in all, a single time step forward from time index `ti` to `ti+1` can be performed using the following algorithm (using `Python` syntax):

```
psi[ti+1,:] = psi[ti,:]
for a in range(M):
    psi[ti+1,a] = U_eff[a][0,0] * psi[ti,a] + U_eff[a][0,1] * psi[ti,M+cpLoc[a]]
    psi[ti+1,a] = U_eff[a][1,0] * psi[ti,a] + U_eff[a][1,1] * psi[ti,M+cpLoc[a]]

psi_bath_k = FFT(psi[ti+1,M:])
psi_bath_k = U_K * psi_bath_k
psi[ti+1,M:] = IFFT(psi_bath_k)
```

Here, `psi[ti,:]` is a complex vector of length $M+N$ containing the system wave function at time $t = \texttt{ti} \cdot \Delta t$, with the first M elements corresponding to the atoms and the following N elements corresponding to the resonators. As for the other variables, `U_eff[a]` is the 2×2 matrix $U_a(\Delta t)$ defined in Eq. (2.57), `cpLoc[a]` is the index for the resonator coupled to atom a and `U_K` is a complex vector of length N encoding the diagonal matrix $U_K(\Delta t) = \exp(-iH_B\Delta t)$.

2.3.2 Time Evolution via Resolvent Formalism

Rewriting Eq. (2.50) entirely in the basis where H_A and H_B are both diagonal, the Hamiltonian describing a system of M small atoms coupled to a 1D resonator lattice of

length N is

$$H = \sum_{a=1}^{M} \Delta_a \sigma_a^\dagger \sigma_a + \sum_k \omega(k) a_k^\dagger a_k + \sum_{a=1}^{M} \frac{g_a}{\sqrt{N}} \sum_k \left(e^{-ikn_a} \sigma_a^\dagger a_k + e^{ikn_a} \sigma_a a_k^\dagger \right), \tag{2.59}$$

where the three terms correspond to H_A, H_B and H_{int}, respectively.

Since we are mainly interested in how the atoms interact with each other, let us choose the *subspace of interest* $\mathcal{S}$ discussed in section 2.2.1 as the subspace of states where one of the atoms is excited, i.e. $\{|a\rangle\}_{a=1}^{M}$. Referring to the projection and rejection operators for $\mathcal{S}$ as P and Q like before, we can see that all of the information about how excitations move between the atoms is contained in the operator $C(t) = PU(t)P$. All the matrix elements $C_{ab}(t) \equiv \langle a|C(t)|b\rangle = \langle a|U(t)|b\rangle$ of this operator correspond to the probabilities of measuring an excitation in atom a after time t given that atom b is excited at $t = 0$. By Eq. (2.29), this operator can be written in terms of the resolvent, $G(z) = (z - H)^{-1}$, in the following way:

$$C(t) = \frac{1}{2\pi i} \int_{\gamma_+ + \gamma_-} \mathrm{d}z \, e^{-izt} PG(z)P, \tag{2.60}$$

with $\gamma_\pm$ defined like before.

Restricting to the case where $t > 0$ and closing the contour of integration as discussed in section 2.2, we can rewrite this as

$$\begin{aligned} C(t) &= \frac{1}{2\pi i} \oint_\gamma \mathrm{d}z \, e^{-izt} PG(z)P = \{\text{equation (2.40)}\} = \\ &= \frac{1}{2\pi i} \oint_\gamma \mathrm{d}z \, e^{-izt} \frac{P}{z - PH_0P - P\Sigma(z)P} \end{aligned} \tag{2.61}$$

with γ like in Fig. 2.4.

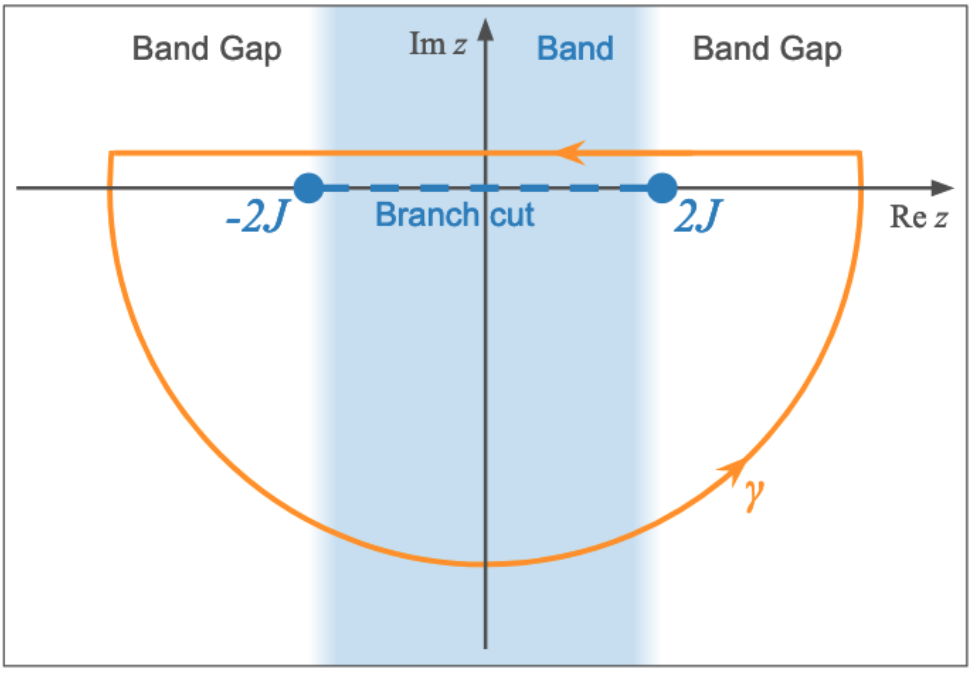

Figure 2.4: The closed path γ we integrate along to find $C(t)$.

2.3.2.1 A Single Small Atom

If $M = 1$, $C(t)$ has only a single matrix element, namely

$$\begin{aligned} C_{11}(t) &= \frac{1}{2\pi i} \oint_\gamma \mathrm{d}z \, \frac{e^{-izt}}{z - \Delta_1 - \Sigma_{11}(z)} = \\ &= \frac{1}{2\pi i} \oint_{\gamma+\tilde{\gamma}} \mathrm{d}z \, \frac{e^{-izt}}{z - \Delta_1 - \Sigma_{11}(z)} - \frac{1}{2\pi i} \int_{\tilde{\gamma}} \mathrm{d}z \, \frac{e^{-izt}}{z - \Delta_1 - \Sigma_{11}(z)} = \\ &= \{\{z_p\} \text{ are the poles of the integrand}\} \\ &= \sum_p \operatorname*{Res}_{z=z_p} \left[\frac{e^{-izt}}{z - \Delta_1 - \Sigma_{11}(z)} \right] - \frac{1}{2\pi i} \int_{\tilde{\gamma}} \mathrm{d}z \, \frac{e^{-izt}}{z - \Delta_1 - \Sigma_{11}(z)} = \\ &= \sum_p R_p e^{-iz_p t} - \frac{1}{2\pi i} \int_{\tilde{\gamma}} \mathrm{d}z \, \frac{e^{-izt}}{z - \Delta_1 - \Sigma_{11}(z)}, \end{aligned} \tag{2.62}$$

where R_p is the residue of $[z - \Delta_1 - \Sigma_{11}(z)]^{-1}$ at $z = z_p$, the detour $\tilde{\gamma}$ looks like in Fig. 2.5 and

$$\begin{aligned} \Sigma_{11}(z) &= \langle 1|\Sigma(z)|1\rangle = \{\text{equation (2.39), } QHQ = H_B\} = \\ &= \cancelto{0}{\langle 1|H_{\text{int}}|1\rangle} + \sum_k \frac{\langle 1|H_{\text{int}}|k\rangle \, \langle k|H_{\text{int}}|1\rangle}{z - \omega(k)} = \\ &= \frac{g_1^2}{N} \sum_k \frac{1}{z - \omega(k)}. \end{aligned} \tag{2.63}$$

To make things easier for ourselves, let us consider the (momentum space) continuum limit $N \to \infty$. This is a good approximation as long as our bath is large in comparison to our atoms, which is the regime we are mostly interested in, since a large bath size limits the effects of our physically hard-to-realise periodic boundary conditions. In this limit, we have for arbitrary functions $f(k)$ that

$$\frac{1}{N} \sum_k f(k) = \frac{1}{2\pi} \sum_k \frac{2\pi}{N} f(k) \to \frac{1}{2\pi} \int_{-\pi}^{\pi} \mathrm{d}k \, f(k), \tag{2.64}$$

since $\Delta k = \frac{2\pi}{N} \to \mathrm{d}k$, and the range of k which is summed over goes to the interval $[-\pi, \pi]$. This means that in the continuum limit,

$$\Sigma_{11}(z) = \frac{g_1^2}{2\pi} \int_{-\pi}^{\pi} \mathrm{d}k \, \frac{1}{z - \omega(k)} = \frac{g_1^2}{2\pi} \int_{-\pi}^{\pi} \mathrm{d}k \, \frac{1}{z + 2J \cos k}. \tag{2.65}$$

It can be shown using complex analysis methods [5, 9] that this evaluates to

$$\Sigma_{11}(z) = \pm \frac{g_1^2}{\sqrt{z^2 - 4J^2}} \tag{2.66}$$

for $\operatorname{Re} z \gtrless 0$.

If $\Sigma_{11}(z)$ were zero, the projected resolvent would only have one pole, namely at $z = \Delta_1$. Since in reality $\Sigma_{11}(z) \sim g_1^2$, the presence of the self-energy only perturbs the pole slightly from its unperturbed location in the weak coupling regime where $g_1 \ll J$. This enables us to make use of the approximation

$$z_p \approx \Delta_1 + \Sigma_{11}(\Delta_1) \tag{2.67}$$

for this pole. Neglecting all the other poles, as well as the contribution from the detour integral along $\tilde{\gamma}$, we find that

$$C_{11}(t) \approx e^{-i(\Delta_1+\Sigma_{11}(\Delta_1))t}, \tag{2.68}$$

so that

$$|C_{11}(t)|^2 \approx e^{2\,\mathrm{Im}[\Sigma_{11}(\Delta_1)]t}, \tag{2.69}$$

which corresponds to exponential decay with decay rate

$$\Gamma(\Delta_1) = -2\,\mathrm{Im}[\Sigma_{11}(\Delta_1)] = \{|\Delta_1| < 2J\} = \frac{2g_1^2}{\sqrt{4J^2-\Delta_1^2}}, \tag{2.70}$$

in accordance with Fermi's golden rule (see e.g. Ref. [20] for a more thorough description of Fermi's golden rule). This is known as the Wigner-Weisskopf approach, which can be shown to be a type of *Born-Markov approximation* [9]. Roughly speaking, the Born-Markov approximation entails the assumption that the future time evolution of the system is only dependent on the current state and not on past states [1]. This approximation is accurate when our structured environment behaves almost like a continuous waveguide, i.e. far from the band edges. This can for example be seen in Refs. [9] and [5].

Note that outside the band, i.e. for $|\Delta_1| > 2J$, the self-energy is real, which means that the Wigner-Weisskopf approximation predicts no decay. Intuitively, this is because of the fact that the decay of the atom results in an energy Δ_1 being discharged into the bath. While the main recipients of such an energy discharge would ordinarily be the bath modes with energy Δ_1, there are no such modes for $|\Delta_1| > 2J$.

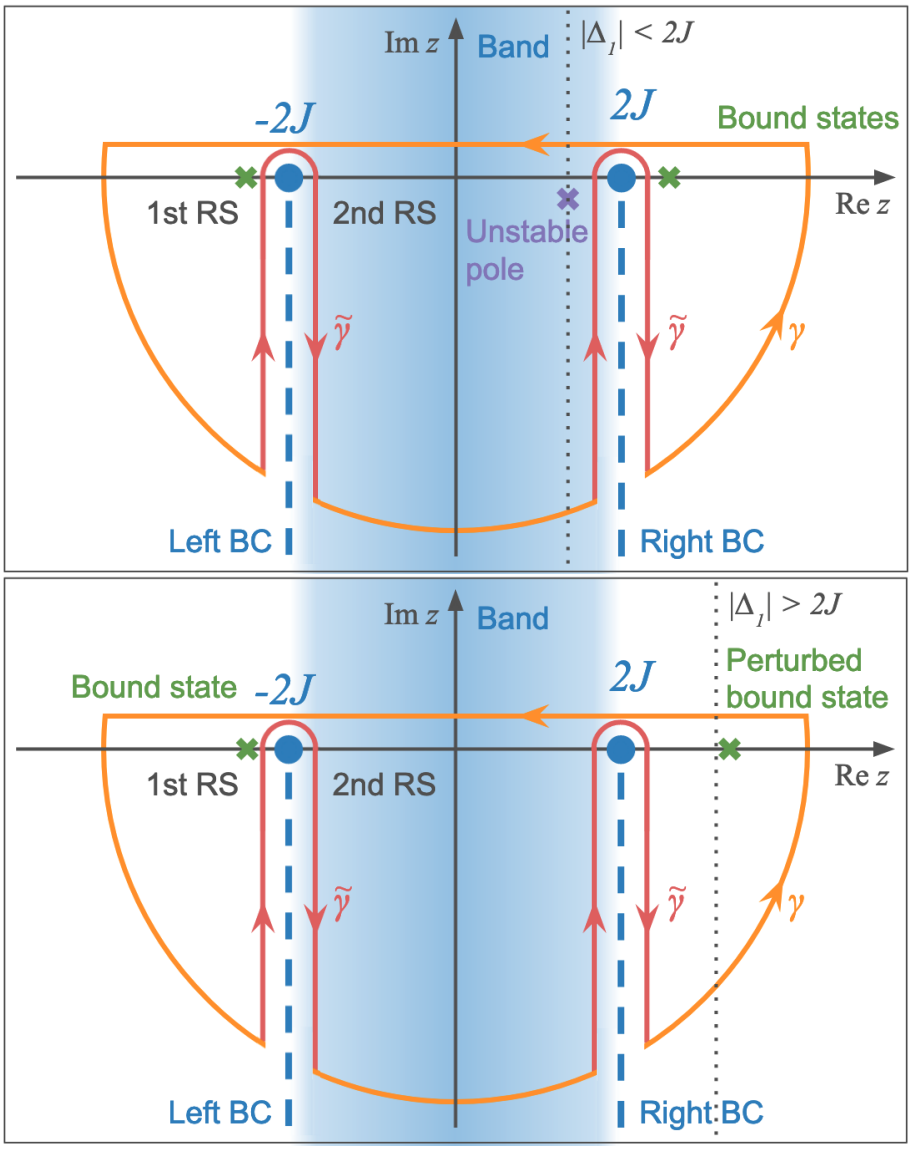

Figure 2.5: The modified path $\gamma + \tilde{\gamma}$ avoiding the branch points and including a portion of the second Riemann sheet. Top: Δ_1 is within the band, resulting in an unstable pole close to $z = \Delta_1$ and exponential decay. Bottom: Δ_1 is outside of the band, resulting in a real pole close to $z = \Delta_1$, corresponding to an atom-photon bound state [5, 9] and (practically) no decay. Figure inspired by Refs. [5] and [9].

2.3.2.2 Two Small Atoms

To get a better sense of how this works out in general, let us consider the case where $M = 2$ in more detail. In this case, $\mathcal{S}$ contains two states $|1\rangle$ and $|2\rangle$ (corresponding to the first and second atom being excited, respectively). This means that $C(t) = \sum_{a,b} |a\rangle\langle b|\, C_{ab}(t)$ is effectively a 2×2 matrix

$$\begin{bmatrix} C_{11}(t) & C_{12}(t) \\ C_{21}(t) & C_{22}(t) \end{bmatrix} = \frac{1}{2\pi i} \oint_\gamma \mathrm{d}z\, e^{-izt} \begin{bmatrix} z - \Delta_1 - \Sigma_{11}(z) & -\Sigma_{12}(z) \\ -\Sigma_{21}(z) & z - \Delta_2 - \Sigma_{22}(z) \end{bmatrix}^{-1}, \tag{2.71}$$

where

$$\begin{aligned}\Sigma_{ab}(z) &= \langle a|\Sigma(z)|b\rangle = \{\text{equation (2.39), } QHQ = H_B\} = \\ &= \cancelto{0}{\langle a|H_{\text{int}}|b\rangle} + \sum_k \frac{\langle a|H_{\text{int}}|k\rangle\ \langle k|H_{\text{int}}|b\rangle}{z-\omega(k)} = \\ &= \frac{g_a g_b}{N}\sum_k \frac{e^{-ik(n_a-n_b)}}{z-\omega(k)}\end{aligned} \tag{2.72}$$

are the matrix elements of the self-energy operator. Again taking the continuum limit $N \to \infty$,

$$\Sigma_{ab}(z) = \frac{g_a g_b}{2\pi}\int_{-\pi}^{\pi} \mathrm{d}k\, \frac{e^{-ik(n_a-n_b)}}{z-\omega(k)} = \frac{g_a g_b}{2\pi}\int_{-\pi}^{\pi} \mathrm{d}k\, \frac{e^{-ik(n_a-n_b)}}{z+2J\cos k}. \tag{2.73}$$

But this integral is over a symmetric interval! This means that only the even part of the integrand contributes, so

$$\begin{aligned}\Sigma_{ab}(z) = \Sigma_{ba}(z) &= \frac{g_a g_b}{2\pi}\int_{-\pi}^{\pi} \mathrm{d}k\, \frac{\cos[k(n_a-n_b)]}{z+2J\cos k} = \\ &= \frac{g_a g_b}{2\pi}\int_{-\pi}^{\pi} \mathrm{d}k\, \frac{e^{ik|n_a-n_b|}}{z+2J\cos k}.\end{aligned} \tag{2.74}$$

Similarly to the single atom case, it can be shown using complex analysis methods [5, 9] that this evaluates to

$$\Sigma_{ab}(z) = \pm\frac{g_a g_b}{\sqrt{z^2-4J^2}} w_{\pm}^{|n_a-n_b|} \tag{2.75}$$

for $\operatorname{Re} z \gtrless 0$, where

$$w_{\pm}(z) = -\frac{z}{2J} \pm \sqrt{\frac{z^2}{4J^2}-1}, \tag{2.76}$$

with the square root function defined to have a branch cut along the negative real axis.

Now, let us take a step back and look at Eq. (2.71) again. On the right-hand side, there is a matrix inverse that needs to be calculated. By the standard 2×2 matrix inverse formula,

$$M = \begin{bmatrix} a & b \\ c & d\end{bmatrix} \Rightarrow M^{-1} = \frac{1}{ad-bc}\begin{bmatrix} d & -b \\ -c & a\end{bmatrix}, \tag{2.77}$$

we find (suppressing the z dependence of the resolvent and the self-energy) that

$$\begin{aligned}(PGP)^{-1} &= \begin{bmatrix} z-\Delta_1-\Sigma_{11} & -\Sigma_{\text{int}} \\ -\Sigma_{\text{int}} & z-\Delta_2-\Sigma_{22}\end{bmatrix}^{-1} = \\ &= \frac{1}{(z-\Delta_1-\Sigma_{11})(z-\Delta_2-\Sigma_{22})-\Sigma_{\text{int}}^2}\begin{bmatrix} z-\Delta_2-\Sigma_{22} & \Sigma_{\text{int}} \\ \Sigma_{\text{int}} & z-\Delta_1-\Sigma_{11}\end{bmatrix},\end{aligned} \tag{2.78}$$

where $\Sigma_{\text{int}} \equiv \Sigma_{12} = \Sigma_{21}$. Thus, the probability of atom 1 keeping an initial excitation after time t is given by the modulus squared of

$$C_{11}(t) = \frac{1}{2\pi i}\oint_\gamma \mathrm{d}z\, \frac{e^{-izt}}{z-\Delta_1-\tilde{\Sigma}_{11}(z)}, \tag{2.79}$$

where

$$\tilde{\Sigma}_{11}(z) = \Sigma_{11}(z) + \frac{\Sigma_{\text{int}}^2(z)}{z-\Delta_2-\Sigma_{22}(z)}, \tag{2.80}$$

and the same holds for atom 2 if we exchange $1 \leftrightarrow 2$ in these expressions. Similarly, the probability of an excitation moving from one of the atoms to the other one after time t is given by the modulus squared of

$$C_{\text{int}}(t) = -\frac{1}{2\pi i}\oint_\gamma \mathrm{d}z\, \frac{e^{-izt}}{\tilde{\Sigma}_{\text{int}}(z)}, \tag{2.81}$$

with

$$\tilde{\Sigma}_{\text{int}}(z) = \Sigma_{\text{int}}(z) - \frac{[z-\Delta_1-\Sigma_{11}(z)][z-\Delta_2-\Sigma_{22}(z)]}{\Sigma_{\text{int}}(z)}. \tag{2.82}$$

Like for the single atom case, these integrals can be evaluated using the residue theorem with the same modified contour $\gamma + \tilde{\gamma}$ as before, visible in Fig. 2.5. Getting exact results is most easily achieved by both finding the exact locations of the poles and evaluating the detour integrals numerically – see e.g. the methodology in Refs. [5] and [9].

Restricting ourselves to the case where the two atoms are identical, one can show [9] that the two eigenstates of the projected resolvent $PG(z)P$ are

$$|\pm\rangle \equiv \frac{|1\rangle \pm |2\rangle}{\sqrt{2}}, \tag{2.83}$$

and the time evolution of these states is given by

$$C_\pm(t) \equiv \langle\pm|C(t)|\pm\rangle = \frac{1}{2\pi i}\oint_\gamma \mathrm{d}z\, \frac{e^{-izt}}{z-\Delta-\Sigma_\pm(z)}, \tag{2.84}$$

where $\Sigma_\pm(z) \equiv \langle\pm|\Sigma(z)|\pm\rangle$. As is easy to show by evaluating $PGP\,|\pm\rangle$, these eigenstate self-energies are given by

$$\Sigma_\pm(z) = \Sigma_{11}(z) \pm \Sigma_{\text{int}}(z) = \zeta\frac{g_1^2}{\sqrt{z^2-4J^2}}\Big(1 \pm w_\zeta^{\Delta x_{12}}\Big), \tag{2.85}$$

where $\zeta \equiv \text{sgn}[\text{Re}\, z]$ and $\Delta x_{12} \equiv |n_1 - n_2|$. Interestingly, for certain values of $\Delta \equiv \Delta_1 = \Delta_2$ these eigenstates can exhibit perfect subradiance (no decay) and perfect superradiance (decay with twice the single-atom decay rate Γ) [9, 30]. In general, sub- and superradiance refer to any decay that is slower or quicker (respectively) than the decay predicted by Fermi's golden rule. Since we are mostly interested in perfect subradiance, however, we will for convenience use the term subradiant to mean specifically perfectly subradiant, unless otherwise noted.

The fact that the $\pm$ eigenstates can exhibit perfect sub-/superradiance can be seen clearly in the Wigner-Weisskopf approximation, where the eigenstate decay rate is simply

$$\Gamma_\pm(\Delta) = \Gamma(\Delta)(1 \pm \cos[k(\Delta)\Delta x_{12}]), \tag{2.86}$$

with $k(\Delta) = \arccos\!\Big(-\frac{\Delta}{2J}\Big)$ being the wavenumber for the bath mode with energy $\omega(k) = -2J\cos k = \Delta$. This can be derived by noting that for $z = \Delta$ within the band, $w_\zeta = e^{i\zeta k(\Delta)}$. Using this expression, we expect to get subradiance for the $|\pm\rangle$ state whenever

$$\cos[k(\Delta)\Delta x_{12}] = \mp 1, \tag{2.87}$$

and superradiance whenever

$$\cos[k(\Delta)\Delta x_{12}] = \pm 1. \tag{2.88}$$

In the middle of the band, i.e. at $\Delta = 0 \Rightarrow k(\Delta) = \frac{\pi}{2}$, this translates into the following:

$$\begin{cases} |+\rangle \text{ subradiant, } |-\rangle \text{ superradiant} & \text{for } \Delta x_{12} \equiv 2 \mod 4 \\ |-\rangle \text{ subradiant, } |+\rangle \text{ superradiant} & \text{for } \Delta x_{12} \equiv 0 \mod 4 \end{cases} \tag{2.89}$$

It should be noted that this behaviour is very much analogous to that of small atoms coupled to a continuous waveguide, where sub- and superradiance just like in our setup is achieved when the phase shift between emissions from two atoms is equal to $\pi \mod 2\pi$ and $0 \mod 2\pi$, respectively [31]. A more detailed analysis beyond the Wigner-Weisskopf approximation [5, 9] shows that these results really do hold almost exactly at $\Delta = 0$. The only major asterisk to this is the effect of *time delay*, which occurs because of non-negligible travel times for excitations between coupling points.

The subradiance and superradiance effects can be thought of as being caused by perfect destructive or constructive interference between the emissions from the two atoms. In the Wigner-Weisskopf approximation, these interference effects are effectively assumed to establish themselves instantaneously. In reality, however [5, 9], the emissions from the two atoms travel through the bath at the group velocity

$$v_g = \left.\frac{\mathrm{d}\omega}{\mathrm{d}k}\right|_{k=k(\Delta)} = 2J \sin k(\Delta) = \sqrt{4J^2 - \Delta^2} = \{\Delta = 0\} = 2J, \tag{2.90}$$

which results in a time delay before the interference is established. At $\Delta = 0$, where the Wigner-Weisskopf approximation is maximally accurate and the behaviour of the bath is most like a continuous waveguide, this leads [9] to an initial partial decay

$$|C_\pm(t)|^2 \sim e^{-\Gamma(0)t} = e^{-g_1^2 t/J} \tag{2.91}$$

for $t < \tau$, where

$$\tau = \frac{\Delta x_{12}}{v_g} \tag{2.92}$$

is the time it takes for the emissions to propagate between the two atoms.

Something that should be mentioned here is that in the subradiant case, while all emissions away from the two atoms do cancel, the interference effects also result in localised photonic excitations *between* the two atoms [9]. Specifically, these excitations take the form of a standing wave with practically zero population in the resonators where the interference is destructive and a population on the order of g^2/J^2 in the resonators with constructive interference. As we shall see in the results chapter, this phenomenon also exists in 2D. It should be noted that apart from the steady state standing wave, there will also be small transient oscillations coming from excitations moving between coupling points, getting reabsorbed by an atom and then re-emitted. These extra oscillations gradually dissipate, partly as external emissions to the environment and partly by contributing their population to the standing wave.

Having put in all this legwork for small atoms, let us now see what happens when we allow the atoms to couple to our resonator lattice at multiple points.

2.4 Giant Atoms in 1D Environments

At first glance, the jump from small to giant atoms doesn't seem to be that great, since the only change to the Hamiltonian lies in the fact that we now allow for multiple coupling

points per atom. As we shall see, however, there are several important differences between the behaviour of small and giant atoms. Since this change only affects H_{int}, H_A and H_B are unchanged from the small atom case, and our total Hamiltonian for the giant atom case looks like

$$H = \sum_{a=1}^{M} \Delta_a \sigma_a^\dagger \sigma_a + \sum_k \omega(k) a_k^\dagger a_k + \sum_{a=1}^{M} \sum_{p=1}^{N_c^{(a)}} \frac{g_{ap}}{\sqrt{N}} \sum_k \left(e^{-ikn_{ap}} \sigma_a^\dagger a_k + e^{ikn_{ap}} \sigma_a a_k^\dagger \right), \tag{2.93}$$

$$H_A = \sum_{a=1}^{M} \omega_a \sigma_a^\dagger \sigma_a \quad H_B = \sum_{\vec{k}} \left[\omega_B + \omega\left(\vec{k}\right) \right] a_{\vec{k}}^\dagger a_{\vec{k}} \tag{2.94}$$

just like before corresponding to H_A, H_B and H_{int}, in that order. Here, atom a couples to $N_c^{(a)}$ different resonators, located at positions $\{n_{ap}\}_{p=1}^{N_c^{(a)}}$. The coupling strength for the interaction between atom a and the resonator at position n_{ap} is g_{ap}.

This more complicated coupling structure of H_{int} means that the algorithm used to quickly calculate the position space time evolution operator $U_V(\Delta t)$ by evaluating

$$U_a(\Delta t) = \exp[-iH_a \Delta t] \quad \text{with} \quad H_a = \begin{bmatrix} \Delta_a & g_a \\ g_a & 0 \end{bmatrix} \tag{2.95}$$

no longer works. As we show in appendix B, it is possible to generalise this method so that it works for giant atoms too, but since this is an original result of this thesis, it will be discussed under **Results** below instead of here.

2.4.1 A Single Giant Atom

As for time evolution via resolvent formalism, Eq. (2.61) still holds for giant atoms. In other words, if P is the projector onto a subspace of interest $\mathcal{S}$, then the time evolution for every state in $\mathcal{S}$ is given by

$$\begin{aligned} C(t) &= \frac{1}{2\pi i} \oint_\gamma \mathrm{d}z \, e^{-izt} PG(z)P = \\ &= \frac{1}{2\pi i} \oint_\gamma \mathrm{d}z \, e^{-izt} \frac{P}{z - PH_0P - P\Sigma(z)P} \end{aligned} \tag{2.96}$$

with γ like in Fig. 2.4.

To get a sense of the behaviour of giant atoms, let us consider the simplest case of a single giant atom with two coupling points, i.e. $M = 1$ and $N_c^{(1)} = 2$. Like for small atoms, $C(t)$ only has a single matrix element in this case:

$$\begin{aligned} C_{11}(t) &= \frac{1}{2\pi i} \oint_\gamma \mathrm{d}z \, \frac{e^{-izt}}{z - \Delta_1 - \Sigma_{11}(z)} = \cdots = \\ &= \sum_p R_p e^{-iz_p t} - \frac{1}{2\pi i} \oint_{\tilde{\gamma}} \mathrm{d}z \, \frac{e^{-izt}}{z - \Delta_1 - \Sigma_{11}(z)}, \end{aligned} \tag{2.97}$$

where R_p is the residue of the projected resolvent $[z - \Delta_1 - \Sigma_{11}(z)]^{-1}$ at the pole $z = z_p$ and the detour $\tilde{\gamma}$ still looks like in Fig. 2.5. As for the self-energy, however, we get a

slightly different expression:

$$\begin{aligned}\Sigma_{11}(z) &= \langle 1|\Sigma(z)|1\rangle = \{\text{equation (2.39), } QHQ = H_B\} = \\ &= \cancelto{0}{\langle 1|H_{\text{int}}|1\rangle} + \sum_k \frac{\langle 1|H_{\text{int}}|k\rangle\ \langle k|H_{\text{int}}|1\rangle}{z-\omega(k)} = \\ &= \frac{1}{N}\sum_k \frac{1}{z-\omega(k)}\Big(g_{11}e^{-ikn_{11}} + g_{12}e^{-ikn_{12}}\Big)\Big(g_{11}e^{ikn_{11}} + g_{12}e^{ikn_{12}}\Big) = \\ &= \frac{1}{N}\sum_k \frac{g_{11}^2 + g_{12}^2 + 2g_{11}g_{12}\cos(k\Delta x_1)}{z+2J\cos k} \xrightarrow{N\to\infty} \\ &\xrightarrow{N\to\infty} \frac{1}{2\pi}\int_{-\pi}^{\pi} \mathrm{d}k\, \frac{g_{11}^2 + g_{12}^2 + 2g_{11}g_{12}\cos(k\Delta x_1)}{z+2J\cos k}\end{aligned} \tag{2.98}$$

with $\Delta x_1 \equiv |n_{12} - n_{11}|$. Comparing this expression with the ones we had for small atoms, we see that this integral must evaluate to

$$\Sigma_{11}(z) = \zeta\frac{1}{\sqrt{z^2-4J^2}}\Big[g_{11}^2 + g_{12}^2 + 2g_{11}g_{12}w_\zeta^{\Delta x_1}\Big], \tag{2.99}$$

with $\zeta = \operatorname{sgn}[\operatorname{Re} z]$ like before. Like for small atoms, the Wigner-Weisskopf approximation gives us that the decay rate of a giant atom in the weak coupling regime is given approximately by

$$\begin{aligned}\Gamma_{\text{GA}}(\Delta_1) &= -2\operatorname{Im}[\Sigma_{11}(\Delta_1)] = \{\Delta_1 < 2J\} = \\ &= \frac{2}{\sqrt{4J^2-\Delta_1^2}}\Big(g_{11}^2 + g_{12}^2 + 2g_{11}g_{12}\cos[k(\Delta_1)\Delta x_1]\Big),\end{aligned} \tag{2.100}$$

where $k(\Delta_1) = \arccos\Big(-\frac{\Delta}{2J}\Big)$, just like for small atoms. This expression is very reminiscent of the expression we had for the symmetric eigenstate $|+\rangle$ with two small atoms. In fact, we see that we get a kind of superradiance with "effective coupling strength" $g_{11} + g_{12}$ (decay rate proportional to this expression squared) for $\cos[k(\Delta_1)\Delta x_1] = 1$. The lowest possible decay rate, or best possible subradiance, is achieved at $\cos[k(\Delta_1)\Delta x_1] = -1$, where the effective coupling strength is $|g_{11} - g_{12}|$. This expression is only zero if $g_{11} = g_{12}$, so this is the only situation where perfect subradiance can be achieved. Setting $g_1 \equiv g_{11} = g_{12}$, we see that

$$\begin{aligned}\Gamma_{\text{GA}}(\Delta_1) &= \frac{4g_1^2}{\sqrt{4J^2-\Delta_1^2}}(1+\cos[k(\Delta_1)\Delta x_1]) = \\ &= 2\Gamma(\Delta_1)(1+\cos[k(\Delta_1)\Delta x_1]),\end{aligned} \tag{2.101}$$

where $\Gamma(\Delta_1)$ is the decay rate of a single small atom with detuning Δ_1. This is almost exactly the same expression that we had for the $|+\rangle$ eigenstate with two identical small atoms in Eq. (2.86)! The only difference is an overall factor of 2. Since the small atom decay rate $\Gamma(\Delta_1)$ is proportional to g^2, we can interpret this additional factor of 2 for the giant atom as an effective coupling strength which is greater by a factor of $\sqrt{2}$ compared to that of the $|+\rangle$ state of two small atoms.

In the middle of the band ($\Delta_1 = 0$), we find that a single giant atom with even coupling, i.e. $g_{11} = g_{12}$, exhibits

$$\begin{cases}\text{subradiance for } \Delta x_1 \equiv 2 \mod 4 \\ \text{superradiance for } \Delta x_1 \equiv 0 \mod 4.\end{cases} \tag{2.102}$$

Just like for two small atoms in a subradiant state, the interference causing the subradiance of a giant atom also builds up a standing wave of localised excitations between its coupling points.

Of course, this is all under the assumption that the Wigner-Weisskopf approximation is accurate. More careful studies [5, 9] suggest that these results indeed do hold, insofar as it is only possible to have subradiance when it is predicted by the Wigner-Weisskopf approach. However, while the approximation is very good at $\Delta_1 \approx 0$, the neglected effects of the residues at the (real) bound state poles and the detour integrals along $\tilde{\gamma}$ get more and more pronounced the closer one gets to the band edge. This results in the approximation breaking down close to the band edges at $|\Delta_1| \to 2J$. Thus, even where the Wigner-Weisskopf approximation predicts perfect subradiance, the observed subradiance is imperfect – though at $\Delta = 0$, it is near-perfect [5, 9].

2.4.2 Multiple Giant Atoms and DFI

Let us now see how subradiant giant atoms can be leveraged to achieve DFI – *decoherence-free interaction*. For simplicity, let us consider the case $M = 2$, like we did for small atoms.

In the general case, we find, just like for two small atoms, that the matrix representation of $C(t)$ is

$$\begin{bmatrix} C_{11}(t) & C_{12}(t) \\ C_{21}(t) & C_{22}(t) \end{bmatrix} = \frac{1}{2\pi i} \oint_\gamma \mathrm{d}z\, e^{-izt} \begin{bmatrix} z - \Delta_1 - \Sigma_{11}(z) & -\Sigma_{12}(z) \\ -\Sigma_{21}(z) & z - \Delta_2 - \Sigma_{22}(z) \end{bmatrix}^{-1}, \tag{2.103}$$

where

$$\begin{aligned} \Sigma_{ab}(z) &= \langle a|\Sigma(z)|b\rangle = \{\text{equation (2.39), } QHQ = H_B\} = \\ &= \cancelto{0}{\langle a|H_{\mathrm{int}}|b\rangle} + \sum_k \frac{\langle a|H_{\mathrm{int}}|k\rangle\ \langle k|H_{\mathrm{int}}|b\rangle}{z - \omega(k)} = \\ &= \frac{1}{N} \sum_k \frac{1}{z + 2J\cos k} \left(\sum_{p=1}^{N_c^{(a)}} g_{ap} e^{-ikn_{ap}} \right) \left(\sum_{q=1}^{N_c^{(b)}} g_{bq} e^{ikn_{bq}} \right) \xrightarrow{N\to\infty} \\ &\xrightarrow{N\to\infty} \frac{1}{2\pi} \int_{-\pi}^{\pi} \mathrm{d}k\, \frac{1}{z + 2J\cos k} \left(\sum_{p=1}^{N_c^{(a)}} g_{ap} e^{-ikn_{ap}} \right) \left(\sum_{q=1}^{N_c^{(b)}} g_{bq} e^{ikn_{bq}} \right) = \\ &= \frac{1}{2\pi} \int_{-\pi}^{\pi} \mathrm{d}k \sum_{p,q} \frac{g_{ap} g_{bq} e^{-ik\Delta x_{pq}^{(ab)}}}{z + 2J\cos k} = \\ &= \zeta \frac{1}{\sqrt{z^2 - 4J^2}} \sum_{p,q} g_{ap} g_{bq} w_\zeta^{\Delta x_{pq}^{(ab)}} \end{aligned} \tag{2.104}$$

with $\Delta x_{pq}^{(ab)} = |n_{ap} - n_{bq}|$ are the matrix elements of the self-energy operator. Just like for small atoms, only the even part of the integrand contributes, because the integral is over an interval which is symmetric around zero. In other words, we still have $\Sigma_{12} = \Sigma_{21} \equiv \Sigma_{\mathrm{int}}$. Now, let us restrict ourselves further, specifically to the case $N_c^{(1)} = N_c^{(2)} = 2$. We already know how Σ_{11} and Σ_{22} look from our examination of a single giant atom with two coupling points. On the other hand, the interaction self energy is given by

$$\Sigma_{\mathrm{int}}(z) = \zeta \frac{1}{\sqrt{z^2 - 4J^2}} \left[g_{11} g_{21} w_\zeta^{\Delta x_{11}} + g_{11} g_{22} w_\zeta^{\Delta x_{12}} + g_{12} g_{21} w_\zeta^{\Delta x_{21}} + g_{12} g_{22} w_\zeta^{\Delta x_{22}} \right], \tag{2.105}$$

where we have suppressed the (12) superscript on $\Delta x_{pq}^{(12)}$.

If we want decoherence-free interaction between the two giant atoms, a good starting point is to pick their coupling points and coupling strengths so that the atoms by themselves are subradiant [5]. As we showed earlier, this requires that each giant atom a couples to each of its coupled resonators with the same strength g_a. If this holds for both atoms, the expression for the interaction self-energy reduces to

$$\Sigma_{\text{int}}(z) = \zeta \frac{g_1 g_2}{\sqrt{z^2 - 4J^2}} \left[w_\zeta^{\Delta x_{11}} + w_\zeta^{\Delta x_{12}} + w_\zeta^{\Delta x_{21}} + w_\zeta^{\Delta x_{22}} \right], \tag{2.106}$$

Furthermore, subradiance of atom a requires that the distance between the coupling points of atom a is

$$\Delta x^{(a)} = \frac{\pi + 2\pi n_a}{k(\Delta_a)} \tag{2.107}$$

for some non-negative integer n_a. It should be noted that this is not a priori well-defined at the band edges, where $k(\Delta) = 0$. One can get around this by noting that $k = 2\pi$ is equivalent to $k = 0$. Either way, however, it is not a problem, since the Wigner-Weisskopf approximation breaks down at the band edges, which means that we would not want to use this expression in those situations in the first place. Under the assumption that both atoms have the same detuning $\Delta \equiv \Delta_1 = \Delta_2$ from the middle of the band, it can be shown [2, 4, 5] that the collective decay rate

$$\Gamma_{\text{coll}}(\Delta) \equiv -2\,\text{Im}[\Sigma_{\text{int}}(\Delta)] \tag{2.108}$$

is zero as long as the two atoms are subradiant by themselves. This takes care of the *decoherence-free* part of DFI. As for the *interaction* part, it can be shown [5] that of the three possible topologies shown in Fig. 2.6 below, only the braided configuration allows for interaction when the two atoms involved are subradiant.

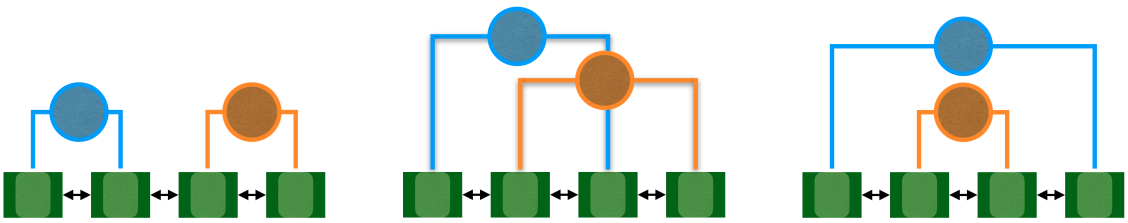

Figure 2.6: The three possible topologies for two giant atoms with two coupling points each. From left to right: separated, braided and nested.

Even for braided giant atoms, however, interaction is not always possible. For interaction to be possible at all, it is necessary that

$$\Delta x_{11} \neq \frac{\pi n}{k(\Delta)} \tag{2.109}$$

for any integer n (labelling the coupling points of both atoms from left to right). Maximal interaction strength is achieved at

$$\Delta x_{11} = \frac{\pi\left(n + \frac{1}{2}\right)}{k(\Delta)}, \tag{2.110}$$

or more precisely at the integer values that are as close as possible to this expression for integer n.

These restrictions on when DFI is achievable can be understood from our earlier discussion of interference effects. In order for a system consisting of two giant atoms to be decoherence-free, the emissions from both atoms must interfere destructively at any point to the left and right of the system. If the two atoms are each subradiant in their own right, this holds. In order for interaction between the atoms to be possible, the emissions from one atom must interfere constructively *at one of the coupling points* of the other atom. In other words, a given subradiant giant atom can couple to another atom precisely at the points between its coupling points where there are localised photonic excitations.

Taken together, equations (2.107) and (2.110) suggest that if we want the first "interaction point" of atom 1 with maximal interaction strength to lie at distance Δx_{11} from the first coupling point of the atom, then the distance between the coupling points of atom 1 must be

$$\Delta x^{(1)} = 2\Delta x_{11}\frac{\pi + 2\pi n_1}{\pi} = 2\Delta x_{11}(1 + 2n_1) \tag{2.111}$$

for some integer n_1. Note that by (2.110), the wavenumber of the emissions must be

$$k = \frac{\pi}{2\Delta x_{11}}, \tag{2.112}$$

which means that the detuning of the atom must be

$$\Delta^{(1)}_{\mathrm{DFI}} = \pm 2J\cos\Big(\frac{\pi}{2\Delta x_{11}}\Big). \tag{2.113}$$

Of course, this is all based on the Wigner-Weisskopf approximation with detunings Δ inside of the band.

As it turns out, it is also possible to achieve DFI between atoms with detunings Δ outside of the band (i.e. for $|\Delta| > 2J$) – in fact, this is possible for both small [9, 32, 33] and giant atoms [5, 34, 35]. This can be understood as resulting from the overlap of the photonic bound states exhibited by the atoms (any atom will be subradiant when detuned from the band, since there is no bath mode with energy $\omega(k) = \Delta$). The main disadvantage of using such bound states for DFI is that they are mostly localised very close to the atoms – their population (and thus interaction strength) decays exponentially with distance from the coupling point(s) of the atom. This means that while it may be a viable method for DFI between nearby atoms, it is unviable to use it for DFI between more distant atoms. On the other hand, DFI with $|\Delta| > 2J$ does not exhibit any initial decay from time delay, which is a significant issue for the interference based DFI with $|\Delta| < 2J$.

Now, let us see how this generalises to 2D lattices.

2.5 Giant Atoms in 2D Environments

The Hamiltonian for M giant atoms coupled to a square 2D resonator lattice is almost the same as the Hamiltonian for the 1D case in Eq. (2.93). In fact, H_A is completely identical, since we haven't changed anything about the atoms themselves. One thing that

is slightly different, though, is the process for diagonalising the bath Hamiltonian H_B. To see this, let us write the H_B entirely in the position basis to start with:

$$H_B = -J \sum_{\langle \vec{m},\vec{n} \rangle} (a^\dagger_{\vec{m}} a_{\vec{n}} + a^\dagger_{\vec{n}} a_{\vec{m}}), \tag{2.114}$$

where $\vec{n} = (n_1, n_2)$ are the coordinates of one of the resonators in the lattice, and $a^{(\dagger)}_{\vec{n}}$ is the annihilation (creation) operator for this resonator. This can still be diagonalised using a Fourier transform, but since our lattice is now 2D, the Fourier transform must be 2D as well [9]. We thus define the Fourier-space creation operator $a^\dagger_{\vec{k}}$ for mode $\vec{k}$ via

$$a^\dagger_{\vec{n}} = \frac{1}{N} \sum_{\vec{k}} e^{i\vec{k}\cdot\vec{n}} a^\dagger_{\vec{k}}, \tag{2.115}$$

where $\vec{k} = (k_1, k_2)$ and the sum goes over all $\vec{k}$ with $k_{1,2} \in \left\{-\pi, \ldots, \pi - \frac{2\pi}{N}\right\}$, similarly to the 1D case. Inserting this expression into Eq. (2.114) and simplifying yields [9] the diagonalised bath Hamiltonian

$$H_B = \sum_{\vec{k}} \omega\left(\vec{k}\right) a^\dagger_{\vec{k}} a_{\vec{k}} \tag{2.116}$$

with

$$\omega\left(\vec{k}\right) = -2J(\cos k_1 + \cos k_2). \tag{2.117}$$

Note that this means that the band now extends from $-4J$ to $4J$ instead of from $-2J$ to $2J$ like in 1D. We also find that the interaction Hamiltonian looks like

$$H_{\text{int}} = \sum_{a=1}^{M} \sum_{p=1}^{N_c^{(a)}} \frac{g_{ap}}{N} \sum_{\vec{k}} \left(e^{-i\vec{k}\cdot\vec{n}_{ap}} \sigma^\dagger_a a_{\vec{k}} + e^{i\vec{k}\cdot\vec{n}_{ap}} \sigma_a a^\dagger_{\vec{k}} \right) \tag{2.118}$$

in this basis. Here, atom a couples to the resonator at $\vec{n}_{ap}$ with coupling strength g_{ap}, with the total number of coupling points being $N_c^{(a)}$ like in the 1D case.

For a single giant atom, it is still the case that all the information about the time evolution of the subspace $\mathcal{S} = \{|1\rangle\}$ is given by

$$C_{11}(t) = \frac{1}{2\pi i} \oint_\gamma \mathrm{d}z \, \frac{e^{-izt}}{z - \Delta_1 - \Sigma_{11}(z)}. \tag{2.119}$$

Now, however, we have

$$\begin{aligned}
\Sigma_{11}(z) &= \cancelto{0}{\langle 1|H_{\text{int}}|1\rangle} + \sum_{\vec{k}} \frac{\left\langle 1\middle|H_{\text{int}}\middle|\vec{k}\right\rangle \left\langle \vec{k}\middle|H_{\text{int}}\middle|1\right\rangle}{z - \omega\left(\vec{k}\right)} = \\
&= \frac{1}{N^2} \sum_{\vec{k}} \frac{1}{z + 2J(\cos k_1 + \cos k_2)} \left(\sum_{p=1}^{N_c^{(1)}} g_{1p} e^{-i\vec{k}\cdot\vec{n}_{1p}} \right) \left(\sum_{q=1}^{N_c^{(1)}} g_{1q} e^{i\vec{k}\cdot\vec{n}_{1q}} \right) \xrightarrow{N\to\infty} \\
&\xrightarrow{N\to\infty} \int_{-\pi}^{\pi} \frac{\mathrm{d}k_1}{2\pi} \int_{-\pi}^{\pi} \frac{\mathrm{d}k_2}{2\pi} \frac{\left(\sum_{p=1}^{N_c^{(1)}} g_{1p} e^{-i\vec{k}\cdot\vec{n}_{1p}}\right)\left(\sum_{q=1}^{N_c^{(1)}} g_{1q} e^{i\vec{k}\cdot\vec{n}_{1q}}\right)}{z + 2J(\cos k_1 + \cos k_2)} = \\
&= \int_{-\pi}^{\pi} \frac{\mathrm{d}k_1}{2\pi} \int_{-\pi}^{\pi} \frac{\mathrm{d}k_2}{2\pi} \frac{\sum_{p=1}^{N_c^{(1)}} g_{1p}^2 + 2\sum_{p<q} g_{1p} g_{1q} \cos\left(\vec{k}\cdot\Delta\vec{x}_{pq}\right)}{z + 2J(\cos k_1 + \cos k_2)},
\end{aligned} \tag{2.120}$$

with $\Delta\vec{x}_{pq} \equiv \vec{n}_{1q} - \vec{n}_{1p}$.

Unfortunately, this double integral is far from trivial to compute. In fact, it can be shown [9, 36] that for arbitrary coupling points, it reduces to a linear combination of the complete elliptic integrals of the first and second kind, respectively defined by

$$K(m) = \int_0^{\frac{\pi}{2}} \frac{\mathrm{d}\varphi}{\sqrt{1 - m\sin^2\varphi}}, \text{ and } E(m) = \int_0^{\frac{\pi}{2}} \mathrm{d}\varphi \sqrt{1 - m\sin^2\varphi}, \tag{2.121}$$

in our case evaluated at $m = 16J^2/z^2$. For example, for a small atom (which we can get by setting $N_c^{(1)} = 1$ in our expression for Σ_{11} above), the self-energy [9] is

$$\Sigma_{11}(z) = \frac{2g_{11}^2}{\pi z} K\left(\frac{16J^2}{z^2}\right). \tag{2.122}$$

It should be noted that there are alternative conventions for exactly how the functions $K(m)$ and $E(m)$ are defined – the definitions given above are the ones used in Ref. [9]. Famously, the values of these integrals in general cannot be expressed in terms of elementary functions.

As it turns out, the expressions for the self-energy matrix elements in the 2D case have an additional branch point compared to the 1D case, positioned right in the middle of the band, at $z = 0$. This can be seen in Fig. 2.7, where we have also marked the modified integration path $\gamma + \tilde{\gamma}$ that can be used if one wants to calculate $C(t)$ using the residue theorem. Note that we now have *three* different Riemann sheets because of the extra branch point.

This extra branch point also means that the Wigner-Weisskopf approximation is no longer accurate in the middle of the band – in fact, it breaks down completely at the branch point $\Delta_1 = 0$, since $\Sigma_{11}(0)$ diverges. Furthermore, while expressions for the interaction self-energy between two arbitrarily positioned coupling points p and q in terms of $K(m)$ and $E(m)$ can be found analytically, doing so for larger displacements Δx_{pq} is quite involved. This is because of the fact that the expressions given in Refs. [9, 36] are recursive, with only a few simple cases (such as $\Delta\vec{x}_{pq} \in \{[0,0],[0,1],[1,1]\}$) being known to begin with. For these reasons, we will leave a detailed analysis of multiple giant atoms via resolvent formalism to future studies, and focus on numerical simulations.

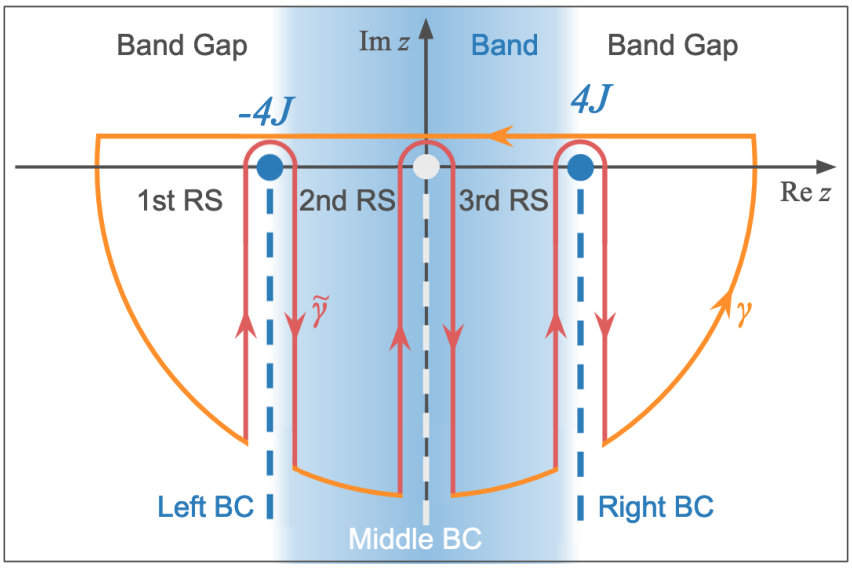

Figure 2.7: The modified path $\gamma + \tilde{\gamma}$ avoiding the branch points and including a portion of the second and third Riemann sheets that can be used to calculate $C(t)$ for 2D lattices. Figure inspired by Ref. [9].

We can, however, still say some things about how we expect the 2D lattice to behave, based on analogies with the 1D case. For an atom with detuning $|\Delta| < 4J$, we still expect any emissions released into the bath to propagate at the group velocity

$$\vec{v}_g = \vec{\nabla}\omega\left(\vec{k}\right)\Big|_{\omega\left(\vec{k}\right)=\Delta} = 2J \begin{bmatrix} \sin k_1 \\ \sin k_2 \end{bmatrix} \Big|_{\omega\left(\vec{k}\right)=\Delta}. \tag{2.123}$$

Since $\vec{k}$ now has two degrees of freedom but we still only have one constraint, we have a free parameter. Let us set $k_1 = k$. Then, our constraint $\omega\left(\vec{k}\right) = \Delta$ gives us that k_2 must satisfy

$$\cos k_2 = -\left(\frac{\Delta}{2J} + \cos k\right) \Rightarrow k_2 = \pm \arccos\left[-\left(\frac{\Delta}{2J} + \cos k\right)\right]. \tag{2.124}$$

Inserting this into Eq. (2.123) and simplifying yields

$$\vec{v}_g = 2J \begin{bmatrix} \sin k \\ \pm\sqrt{1 - \left(\frac{\Delta}{2J} + \cos k\right)^2} \end{bmatrix} \tag{2.125}$$

for arbitrary $k \in (-\pi, \pi]$. Since subradiance (and DFI) in 1D requires that emissions perfectly cancel on the outside of all coupling points (for all k), we expect that it should be non-trivial to engineer subradiance for arbitrary Δ. Something interesting happens at $\Delta = 0$, however. At this value of Δ, the bath group velocity reduces to

$$\vec{v}_g = 2J \sin k \begin{bmatrix} 1 \\ \pm 1 \end{bmatrix}. \tag{2.126}$$

In other words, if our intuition from 1D is still applicable in 2D, this should imply that emissions are only able to propagate along the two main diagonals away from a coupling point. Thus, at $\Delta = 0$ we expect our 2D lattice to effectively work like two orthogonal 1D lattices crossing over each other at the coupling point. As shown in Ref. [9], this seems

to hold – at least to the extent that intuition from 1D lattices can be exploited to craft subradiant states for systems consisting of multiple small atoms. Just like we saw in the 1D case, these states can be mapped to subradiant giant atoms by exchanging each small atom for a coupling point of the giant atom [10].

Let us now see how this works in practice, and what happens when multiple giant atoms are coupled to a 2D resonator lattice.

3

Results

The main results of this thesis when it comes to (perfect) subradiance are that we find a number of more general configurations of small atoms in 2D that have subradiant symmetric or antisymmetric eigenstates, apart from the ones described in Ref. [9]. The configurations with subradiant symmetric eigenstates $|+\rangle$ correspond to subradiant giant atoms if the small atoms are mapped to coupling points, just like in 1D.

As for decoherence-free interaction, it is exhibited by a pair of subradiant giant atoms when each atom has at least one coupling point placed on an "interaction point" of the other. These interaction points correspond to peaks of the standing wave bound state (or *bound state in the continuum*, BIC) generated between the coupling points of an atom. This mirrors the situation in 1D, since it is again only the braided topology which allows for DFI.

Before heading into a more detailed description of these results, let us briefly describe the numerical methods we are using for simulations.

3.1 Efficient Simulation of Giant Atoms

As we show in appendix B, the method described in section 2.3.1 for simulating the time-evolution of small atoms can be generalised to work for giant atoms. In this generalised method, given below for the two-dimensional case, a single time step forward from time index `ti` to `ti+1` can be performed using the following algorithm (again using `Python` syntax):

```
# Evolve using U_eff in real space
psi[ti+1,:] = psi[ti,:]
for a in range(M):
    psiInt = 0
    for cpLoc in cpLocs[a]:
        psiInt += psi[ti,M+cpLoc]

    psi[ti+1,a] = U_eff[a][0,0] * psi[ti,a] + U_eff[a][0,1]/np.sqrt(nCpts[a]) *
    ↪  psiInt
    for cpLoc in cpLocs[a]:
        psi[ti+1,M+cpLoc] += U_eff[a][0,1]/np.sqrt(nCpts[a]) * psi[ti,a] +
        ↪  (U_eff[a][1,1] - 1.)/nCpts[a] * psiInt
```

```
# Go into k-space
psi_bath_k = FFT(np.reshape(psi[ti+1,M:],(N,N)))

# Apply time evolution operator for H_B
psi_bath_k = U_K * psi_bath_k

# Go back into real space
psi[ti+1,M:] = IFFT(psi_bath_k).flatten()
```

Note that since we will mostly be studying configurations where each giant atom couples equally strongly at all coupling points, this is the case described here. For more details on the even more general case where every coupling point has a distinct coupling strength, see appendix B. It should also be noted the algorithm works largely the same regardless of the dimensionality of the bath, except for the fact that the Fourier transforms need to be adapted somewhat. Since the bath is 2D in the case given above, the forward and inverse Fourier transforms denoted by `(I)FFT` are 2D as well.

Analogously to the 1D small atoms case, `psi[ti,:]` is a complex vector of length $M+N^2$ containing the system wave function at time $t = \texttt{ti} \cdot \Delta t$, with the first M elements corresponding to the atoms and the following N^2 elements corresponding to the resonators. The complex number `psiInt` is the sum of the elements of `psi[ti,:]` at the $N_c^{(a)} = \texttt{nCpts[a]}$ different coupling points of atom `a`. Furthermore, `U_eff[a]` is the 2×2 matrix $U_a(\Delta t) \equiv \exp(-iH_a\Delta t)$ with

$$H_a = \begin{bmatrix} \Delta_a & G_a \\ G_a & 0 \end{bmatrix}, \tag{3.1}$$

where G_a is the effective coupling strength, in this case given by $\sqrt{N_c^{(a)}}g_a$. As for the other variables, `cpLocs[a]` are the indices for the resonators coupled to atom a and `U_K` is a complex matrix of size $N \times N$ encoding the non-zero elements of the diagonal matrix $U_K(\Delta t) = \exp(-iH_B\Delta t)$.

Because of rounding errors and numerical errors in the computation of $U_{\text{eff}}^{(a)}(\Delta t)$, the time evolution generated by this algorithm will not in general be perfectly unitary. This is a problem for simulations with many time steps, since a lack of unitarity leads to a gradual change in the normalisation of `psi[ti,:]` away from its original value of 1, which can lead to misleading results for e.g. the total remaining population in the atoms. Thus, for accurate results it is necessary to force unitarity at the expense of a slight increase in computational time by adding the following line to the algorithm above:

```
psi[ti+1,:] /= np.sqrt(np.sum(psi[ti+1,:].real**2 + psi[ti+1,:].imag**2))
```

3.2 Subradiant Small Atoms in 2D environments

As shown in Ref. [9], four small atoms with equal coupling strength g placed at $[2n, 0]$, $[0, 2n]$, $[-2n, 0]$ and $[0, -2n]$, i.e. in a diamond with "radius" $2n$, will have a subradiant

antisymmetric eigenstate $|-\rangle = \frac{1}{2}(|1\rangle - |2\rangle + |3\rangle - |4\rangle)$ if all the atoms have detuning $\Delta = 0$. In this specific configuration, the divergence at $z = 0$ for the self-energy $\Sigma_-(z)$ cancels out [9], which means that the projected resolvent $PG(z)P$ has a regular pole at $z = 0$ instead of a branch point. In fact, it can be shown [9] that this pole is the only net contributor to $C_-(t)$ at $t \to \infty$, which means that

$$\lim_{t\to\infty} C_-(t) \equiv C_-^{(\infty)} = \lim_{t\to\infty} \operatorname*{Res}_{z=0} \left[\frac{e^{-izt}}{z - \Delta - \Sigma_-(z)} \right] = \frac{1}{1 + S(g,n)}, \tag{3.2}$$

where

$$S(g,n) \equiv -\left. \partial_z \Sigma_-(z) \right|_{z=0} \tag{3.3}$$

As it turns out [9], the derivative of the self-energy at $z = 0$ is given by

$$S(g,n) = \frac{g^2}{4J^2}(2n)^2 = \frac{g^2}{J^2} n^2. \tag{3.4}$$

Per Ref. [9], this agrees well with numerical simulations – see also Fig. 3.1.

It should be noted that the total population in the steady-state subradiant solution is not simply given by $\left|C_-^{(\infty)}\right|^2$, but should also include the 16 peaks of the BIC visible on the bottom right of Fig. 3.1, i.e.

$$\left|C_{\text{tot}}^{(\infty)}\right|^2 = \left|C_-^{(\infty)}\right|^2 + 16 \cdot 5.854 \cdot 10^{-4} \approx 0.9897. \tag{3.5}$$

In other words, only $\sim 1.03\,\%$ of the initial population has been truly lost to the bath as external emissions, while $\sim 0.94\,\%$ has gone into the BIC.

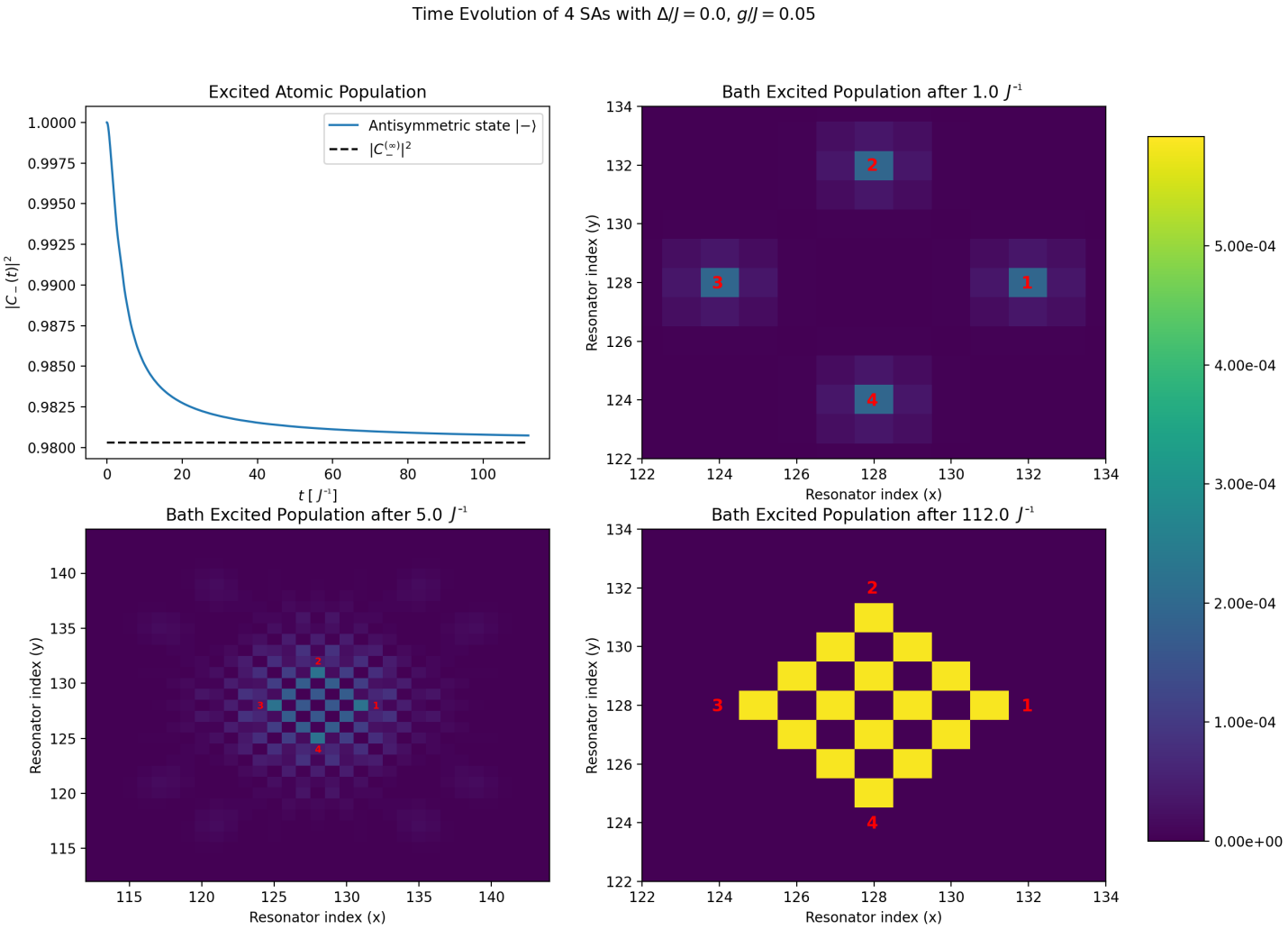

Figure 3.1: Time evolution of the antisymmetric state $|-\rangle = \frac{1}{2}(|1\rangle - |2\rangle + |3\rangle - |4\rangle)$ for four identical small atoms in a diamond configuration with radius $2n = 4$. The coupling points of the four atoms are marked with their respective indices (1-4) in red in the plots of the bath. The simulation was performed with a bath size of 256×256 and a time step of $\Delta t = 10^{-2} J^{-1}$, using atom detuning $\Delta = 0$ and coupling strength $g = 0.05\,\mathrm{J}$. *Top left*: Population in $|-\rangle$, converging towards the theoretically predicted steady-state value $\left|C_-^{(\infty)}\right|^2 \approx 0.9803$. *Top right*: Bath population after $1J^{-1}$. As we can see, the four small atoms are all emitting energy into the bath at the coupling points, but interference effects are yet to establish themselves. *Bottom left*: Bath population after $5J^{-1}$. Interference effects are just starting to establish themselves, while earlier emissions can be seen escaping from the diamond. *Bottom right*: Bath population after $112J^{-1}$. A standing wave interference pattern with population peaks of $5.854 \cdot 10^{-4}$ is visible between the atoms, while all emissions outside the diamond cancel out.

Based on our intuition from 1D and the reasoning in section 2.5, we expect subradiance for the symmetric eigenstate $|+\rangle = \frac{1}{2}(|1\rangle + |2\rangle + |3\rangle + |4\rangle)$ if the diamond "radius" is changed to an odd integer $2n + 1$. Let us verify this numerically in the case $2n + 1 = 3$.

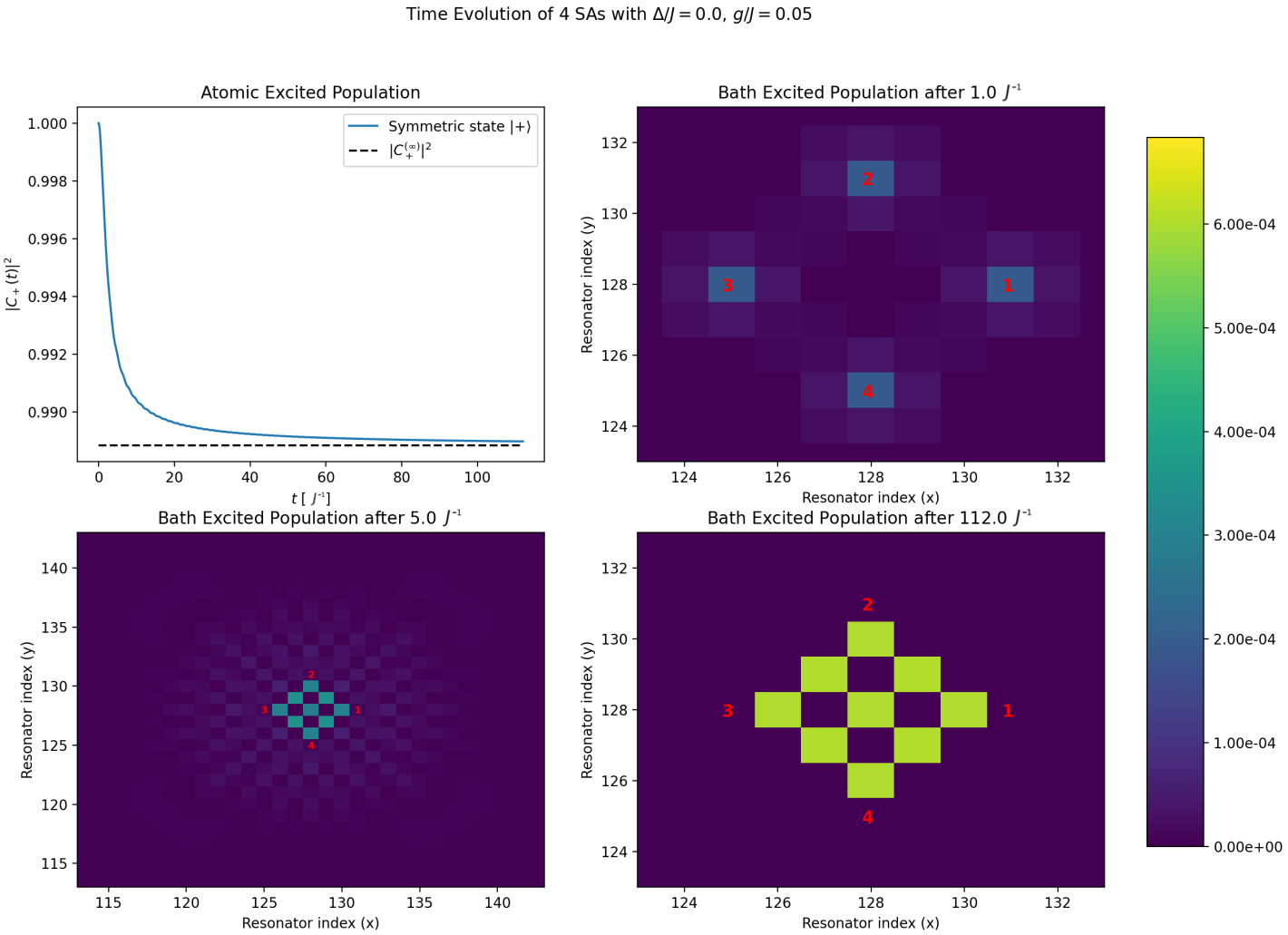

Figure 3.2: Time evolution of the symmetric state $|+\rangle = \frac{1}{2}(|1\rangle + |2\rangle + |3\rangle + |4\rangle)$ for four identical small atoms in a diamond configuration with radius $2n+1 = 3$. The simulation was again performed with a bath size of 256×256 and a time step of $\Delta t = 10^{-2} J^{-1}$, using atom detuning $\Delta = 0$ and coupling strength $g = 0.05\,\mathrm{J}$. *Top left*: Population in $|+\rangle$, converging towards $\left|C_+^{(\infty)}\right|^2 \approx 0.9888$. *Top right*: Bath population after $1J^{-1}$. Like in the even-radius case, the atoms are all emitting energy into the bath at the coupling points, and interference effects are yet to establish themselves. *Bottom left*: Bath population after $5J^{-1}$. Interference effects are slightly further along towards fully establishing themselves than in the previous case, since the radius is now 3 instead of 4. However, earlier emissions can still be seen escaping from the diamond. *Bottom right*: Bath population after $112J^{-1}$. A BIC with population peaks of roughly $6.0 \cdot 10^{-4}$ is visible between the atoms, while all external emissions cancel out.

As we see in Fig. 3.2, using the same values for g and Δ as we did in the antisymmetric case with even radius yields nigh-identical behaviour, with the steady-state population in $|+\rangle$ being

$$\left|C_+^{(\infty)}\right|^2 = \left(\frac{1}{1+S(g,n)}\right)^2, \tag{3.6}$$

now with

$$S(g,n) = \frac{g^2}{4J^2}(2n+1)^2 = \frac{g^2}{J^2}\left(n+\frac{1}{2}\right)^2. \tag{3.7}$$

Showing this is entirely analogous to the antisymmetric case with radius $2n$ discussed in Ref. [9].

Because our configuration now has an odd radius, there is a small but noticeable oscillation over time still remaining in the BIC at $t = 112J^{-1}$. These oscillations correspond to a wavefront of emissions going back and front between the atoms, periodically being reabsorbed and then reemitted, gradually dissipating as it is slowly released – partly as external emissions, partly into the BIC. At $t = 112J^{-1}$ specifically, the total population in the not-quite-standing wave is $5 \cdot 6.008 \cdot 10^{-4} + 4 \cdot 6.041 \cdot 10^{-4} \approx 5.420 \cdot 10^{-3}$. Since the $|+\rangle$ population at that time is ~ 0.9890, the total retained population at $t = 112J^{-1}$ is

$$|C_{\text{tot}}|^2 = |C_+|^2 + 5.420 \cdot 10^{-3} \approx 0.9944. \tag{3.8}$$

Thus, only $\sim 0.56\,\%$ of the initial population has been lost to the bath as external emissions, while $\sim 0.54\,\%$ has gone into the BIC. In other words, we yet again find an approximately 50-50 split between external emissions and BIC population, with a slight bias towards external emissions.

It makes intuitive sense that this should hold in general, since each atom should give off approximately half of its emissions in the direction of another atom's coupling point, and half along the diagonals pointing outward. The reason that the split is slightly biased towards external emissions is likely that the analysis of the group velocity is based on the approximation that $\vec{k}$ is continuous. This does not hold in reality, which means that a small fraction of emissions actually propagate away from the main diagonals. For this fraction of emissions, there are clearly roughly 3 times as many directions leading away from the atoms as there are directions towards the interior. It should be noted that some of the population remaining at $t = 112J^{-1}$ will eventually end up being emitted into the environment. Thus, $0.56\,\%$ is a slight underestimate of the total population lost to external emissions as $t \to \infty$.

These diamond configurations are not the only ones that yield subradiant symmetric states. Based on the discussion in section 2.5, we know that two small atoms with coupling points displaced by $\Delta\vec{x}_+ = (2n+1)[1,1]$ for some integer n has a symmetric eigenstate that is "subradiant" along the $[1,1]$ diagonal. However, it is not fully subradiant, because it is still able to decay via emissions along the other diagonal in the $[1,-1]$ direction. To achieve full subradiance, we need to add another two coupling points, spaced just like the first two but displaced by $\Delta\vec{x}_- = (2m+1)[1,-1]$ for some integer m (which is not necessarily equal to n). For this more general class of symmetric subradiant configurations, the same expressions for $C_+^{(\infty)}$ hold as before, but with

$$S(g,n,m) = \frac{g^2}{J^2}\left(n+\frac{1}{2}\right)\left(m+\frac{1}{2}\right). \tag{3.9}$$

The results of a simulation of one of these more general configurations with $n = 1$ and $m = 0$ can be seen in Fig. 3.3. It should be noted that the small oscillations visible in the $|+\rangle$ state population come from the emission and reabsorption of the wavefront causing the oscillations in the BIC discussed above.

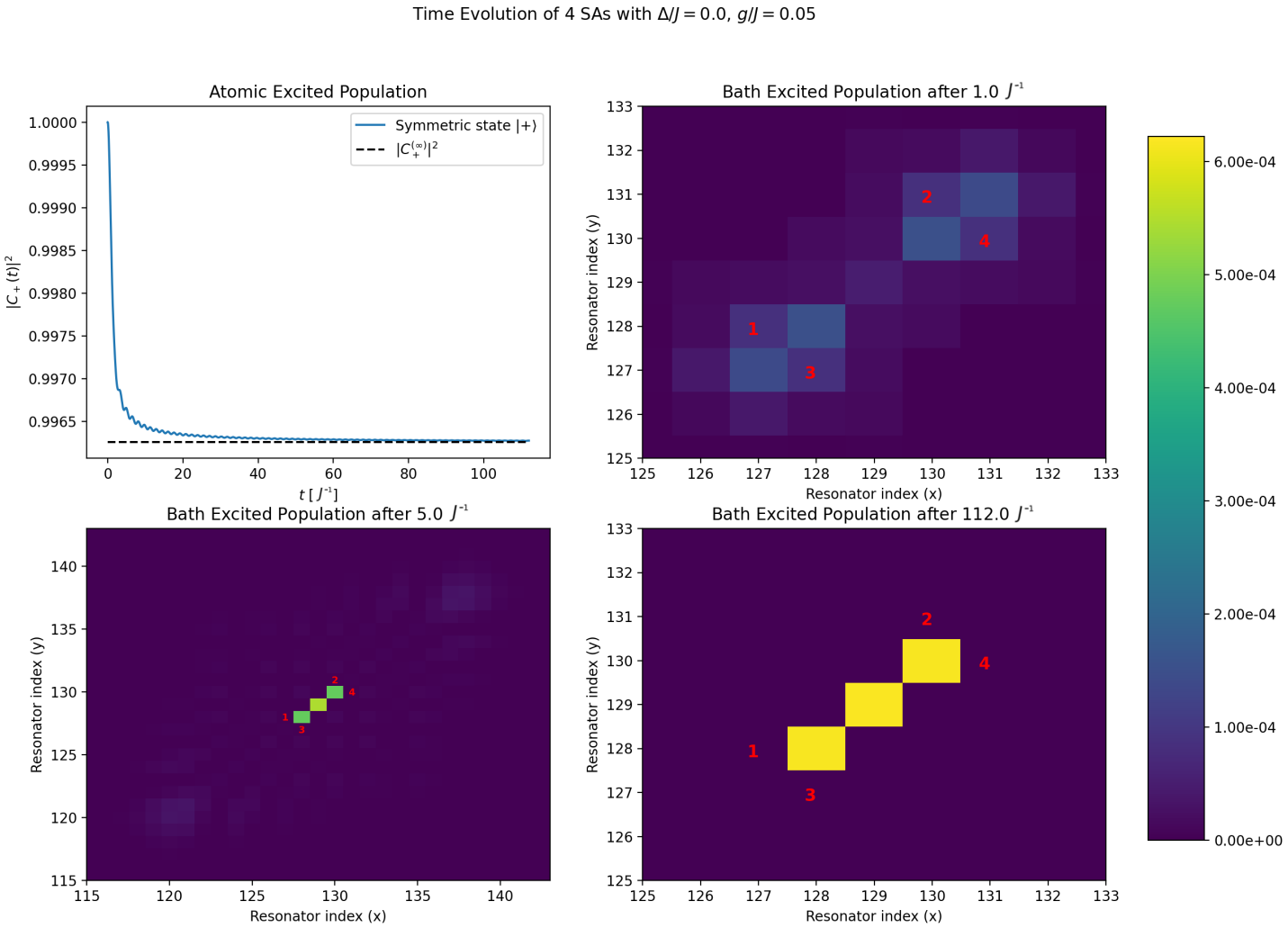

Figure 3.3: Time evolution of the symmetric state $|+\rangle = \frac{1}{2}(|1\rangle + |2\rangle + |3\rangle + |4\rangle)$ for four identical small atoms in a stretched diamond configuration with spacings $2n+1=3$ and $2m+1=1$. The simulation was again performed with a bath size of 256×256 and a time step of $\Delta t = 10^{-2} J^{-1}$, using atom detuning $\Delta = 0$ and coupling strength $g = 0.05\,\mathrm{J}$. *Top left*: Population in $|+\rangle$, converging towards $\left|C_+^{(\infty)}\right|^2 \approx 0.9963$. *Top right*: Bath population after $1J^{-1}$. The atoms are emitting energy at the coupling points, and no interference effects are established yet. *Bottom left*: Bath population after $5J^{-1}$. Interference effects are almost completely established, since the spacings are now only 3 and 1. Earlier emissions – mostly along the $[1,1]$ diagonal (having the larger spacing) – can be seen escaping. *Bottom right*: Bath population after $112J^{-1}$. A standing wave interference pattern with two low peaks at $\sim 6.157 \cdot 10^{-4}$ and one high peak at $\sim 6.190 \cdot 10^{-4}$ is visible.

The fact that the expression in Eq. (3.9) holds for arbitrary m, n and g can be seen in Fig. 3.4, where we examine the remaining population after $112J^{-1}$ for several different combinations of m, n and g.

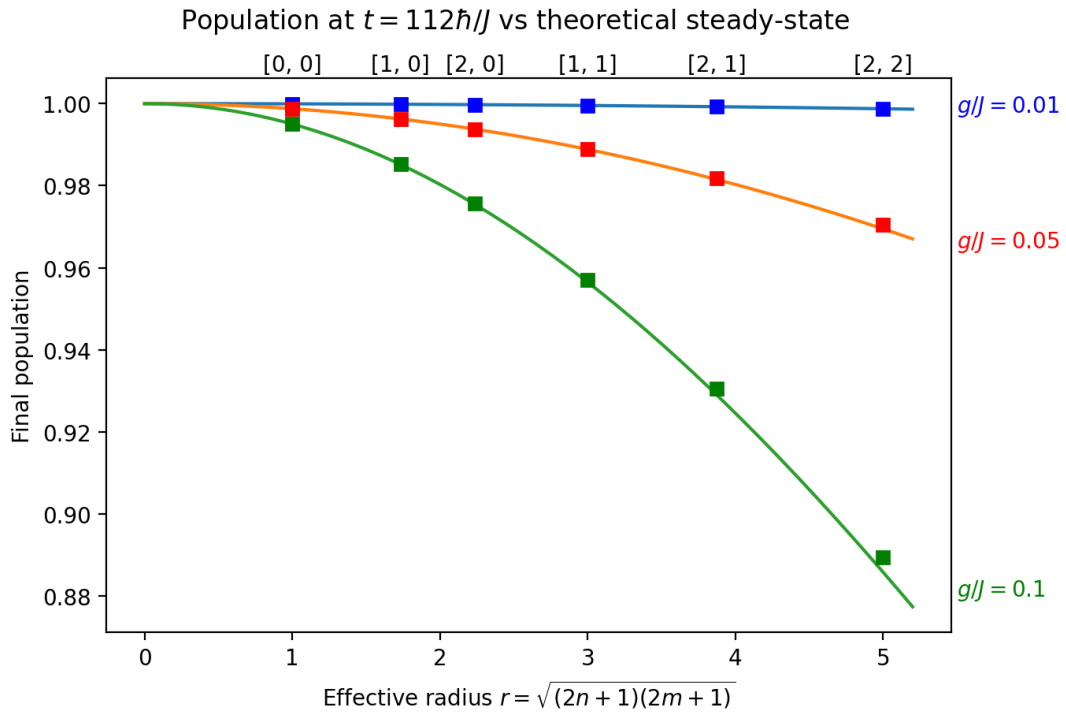

Figure 3.4: Theoretical steady-state population $\left|C_+^{(\infty)}\right|^2$ in the $|+\rangle$ state (solid lines) compared to the actual population after $112J^{-1}$ (squares), plotted in blue for $g/J = 0.01$, orange/red for $g/J = 0.05$ and green for $g/J = 0.1$. Above each set of data points is the combination of integers $[n, m]$ they correspond to. As we can see, the agreement is very good. For larger effective radius r and coupling strength g, there is a larger discrepancy. This is because the atoms in those cases are further from reaching equilibrium, due to the increased propagation time between the coupling points and larger overall decay, respectively.

3.3 Subradiant Giant Atoms in 2D environments

Just like for 1D lattices, any 4-atom configuration with a subradiant symmetric state $|+\rangle$ should be translatable into a subradiant giant atom coupled to the same points. This is precisely what one finds if one performs numerical simulations [10], see also Fig. 3.5.

It should be noted that in the giant atom case, the steady state population is still given by

$$\left|C_1^{(\infty)}\right|^2 = \left(\frac{1}{1 + S(g, n, m)}\right)^2, \tag{3.10}$$

but the S function now uses the effective coupling strength $G = \sqrt{N_c}g$ instead of the plain coupling strength g:

$$S(g, n, m) = \frac{N_c g^2}{4J^2}(2n+1)(2m+1) = \{N_c = 4\} = \frac{g^2}{J^2}(2n+1)(2m+1). \tag{3.11}$$

In fact, it can be shown that the self-energy (and thus the time-evolution) of a giant atom with coupling strength $g = g_0/\sqrt{N_c}$ is exactly the same as that of the $|+\rangle$ state of a set of small atoms with coupling strength g_0 coupled to the same points.

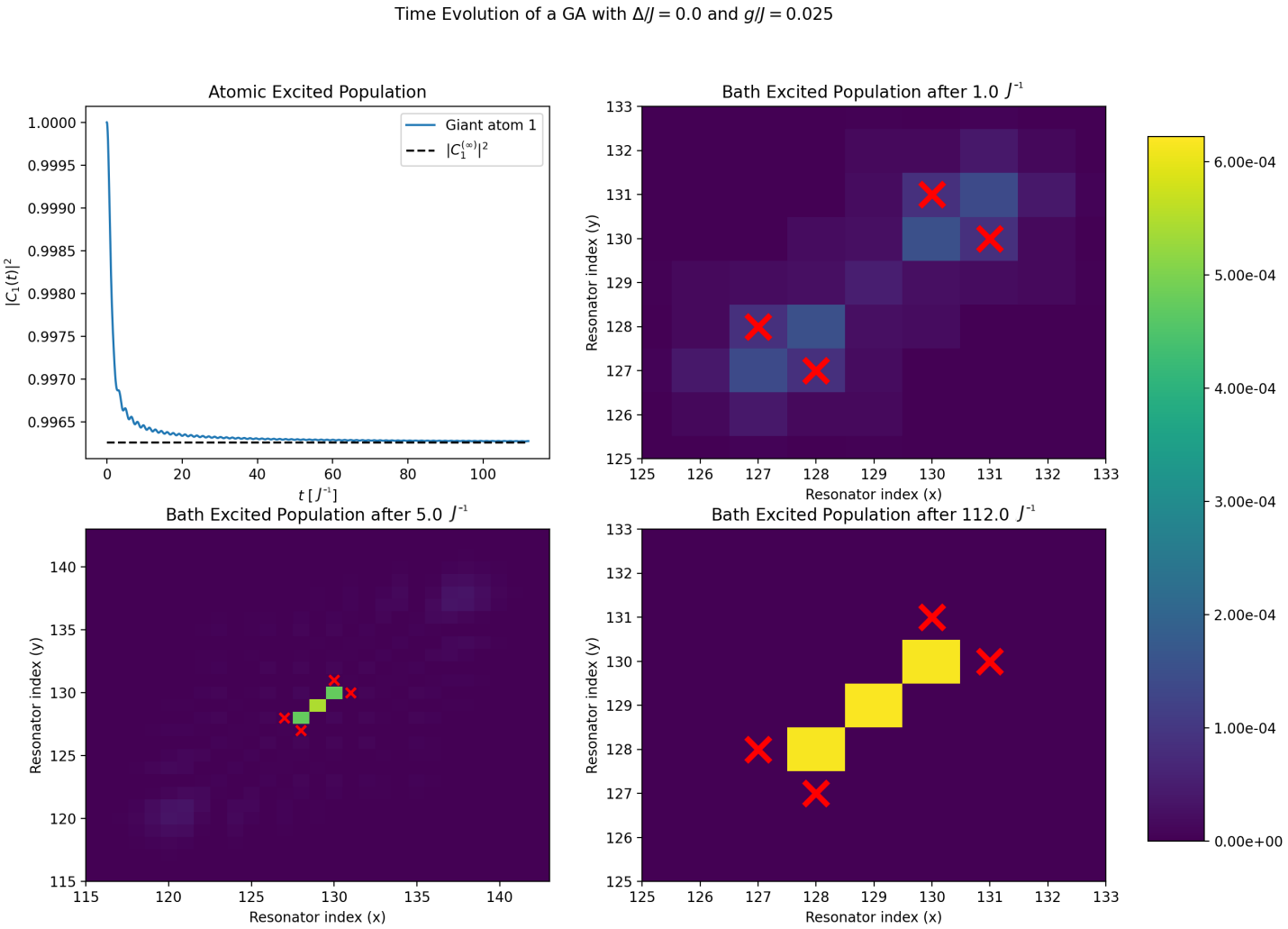

Figure 3.5: Time evolution of a giant atom with coupling points in a stretched diamond configuration, spaced at $2n+1=3$ and $2m+1=1$. The simulation was again performed with a bath size of 256×256 and a time step of $\Delta t = 10^{-2}J^{-1}$, but this time using atom detuning $\Delta = 0$ and coupling strength $g = 0.025\,\mathrm{J}$. As we can see, the result is identical to the result in Fig. 3.3, since the effective coupling strength $G=\sqrt{N_c}g$ is the same. *Top left*: Atomic excited population, converging towards $\left|C_1^{(\infty)}\right|^2 \approx 0.9963$. *Top right*: Bath population after $1J^{-1}$. The atoms are emitting energy at the coupling points (marked with x's), and no interference effects are established yet. *Bottom left*: Bath population after $5J^{-1}$. Interference effects are almost completely established, and earlier emissions – mostly along the $[1,1]$ diagonal – can be seen escaping. *Bottom right*: Bath population after $112J^{-1}$. A standing wave interference pattern with two low peaks at $\sim 6.157\cdot10^{-4}$ and one high peak at $\sim 6.190\cdot10^{-4}$ is visible.

Now, consider a giant atom with equal coupling of strength g to eight coupling points, where the coupling points can be split into two subsets of four such that both subsets would give rise to subradiance on their own. Let us use our previously established notation with $n_{1,2}$ and $m_{1,2}$ determining the spacings for the two subsets along the $[1,1]$ and $[1,-1]$ diagonals, respectively. As we found in the theory section, the self-energy for such a giant

atom can be written as a sum

$$\Sigma_{\text{tot}}(z) = \sum_{\Delta\vec{x}} \iint_{-\pi}^{\pi} \frac{\mathrm{d}^2\vec{k}}{(2\pi)^2} \frac{g^2 \cos\left(\vec{k}\cdot\Delta\vec{x}\right)}{z + 2J(\cos k_1 + \cos k_2)}, \tag{3.12}$$

where the sum goes over the differences in position between any two coupling points. Notably, this includes $N_c = 8$ cases with displacement $[0, 0]$, corresponding to the difference in position between any coupling point and itself. In our case, using our split into subsets we can write this as

$$\Sigma_{\text{tot}}(z) = \Sigma_1(z) + \Sigma_2(z) + \Sigma_{\text{int}}(z), \tag{3.13}$$

where $\Sigma_i(z)$ contains all the terms coming from pairs of points both in subset i and $\Sigma_{\text{int}}(z)$ contains all the terms corresponding to choosing one point from each subset. Since $\Sigma_i(z)$ is the same as that of a giant atom coupling with strength g to just the points in subset i, we already know that

$$\Sigma_i(0) = 0, \quad -\partial_z \Sigma_i(z)\Big|_{z=0} = S(g, n_i, m_i) = \frac{g^2}{J^2}(2n_i + 1)(2m_i + 1). \tag{3.14}$$

It can be shown that $\Sigma_{\text{int}}(0) = 0$ also holds, and that the pole of the projected resolvent at $z = 0$ is still the only contributor to the population at $t \to \infty$. As for the contribution of the interaction self-energy to the final population, it can be shown that

$$-\partial_z \Sigma_{\text{int}}(z)\Big|_{z=0} = \xi \frac{2g^2}{J^2} \delta_{[1,1]} \delta_{[1,-1]}, \tag{3.15}$$

where $\xi \in \{-1, 1\}$ and $\delta_{[1,\pm1]}$ is the width of the overlap between the BICs generated by the two subsets along the $[1, \pm1]$ diagonals. The value of ξ depends on the relative displacements of the two subsets from one another, and on the values of $n_{1,2}$ and $m_{1,2}$. This sign determines whether the unperturbed population reduction encoded in $S_0 = S(g, n_1, m_1) + S(g, n_2, m_2)$ is increased or decreased by the interaction term.

To understand why the expression for this perturbation to S_0 coming from $\Sigma_{\text{int}}(z)$ looks the way it does, let us examine the weak-coupling limit. In this limit, S_0 is small, so that the unperturbed final atomic population is

$$\left|C_1^{(\infty)}\right|^2 = (1 + S_0)^{-2} \approx 1 - 2S_0. \tag{3.16}$$

But we know from simulations that the population in the BIC is always approximately half of the atomic population loss. In other words, S_0 must be roughly equal to the total population in the BIC! Looking at the expression for S_i in (3.14), this makes a lot of sense, since the BIC resulting from subset i populates precisely a $(2n_i + 1) \times (2m_i + 1)$ grid of resonators, which by this logic should have a population of approximately g^2/J^2 each. Looking back at our earlier results, we see that this indeed holds. For example, for the 3×1 grid of standing wave peaks in Fig. 3.5, the peaks at $t = 112J^{-1}$ lie at 6.16–$6.19 \cdot 10^{-4}$, which is only slightly less than $g^2/J^2 = 6.25 \cdot 10^{-4}$.

Thus, $\xi = +1$ corresponds to constructive interference between the standing waves generated by the two subsets in the area of overlap, $\xi = -1$ corresponds to destructive interference. When the overlap is zero, there is no interference, which means that the interaction term does not affect S_0.

To see this more clearly, let us examine some examples. If both subsets are centred on the same point in the bath, the size of the BIC overlap is given by

$$\delta_{[1,1]} = 2\min(n_1, n_2) + 1, \quad \delta_{[1,-1]} = 2\min(m_1, m_2) + 1, \tag{3.17}$$

and

$$\xi = (-1)^{n_1+n_2+m_1+m_2}. \tag{3.18}$$

This can be seen in Fig. 3.6, where $n_1 + m_1 + n_2 + m_2 = 1 + 2 + 2 + 0 = 5$ is odd, causing destructive interference in the overlap. On the other hand, in Fig. 3.7, $n_1+m_1+n_2+m_2 = 1 + 2 + 2 + 1 = 6$ is even, causing constructive interference.

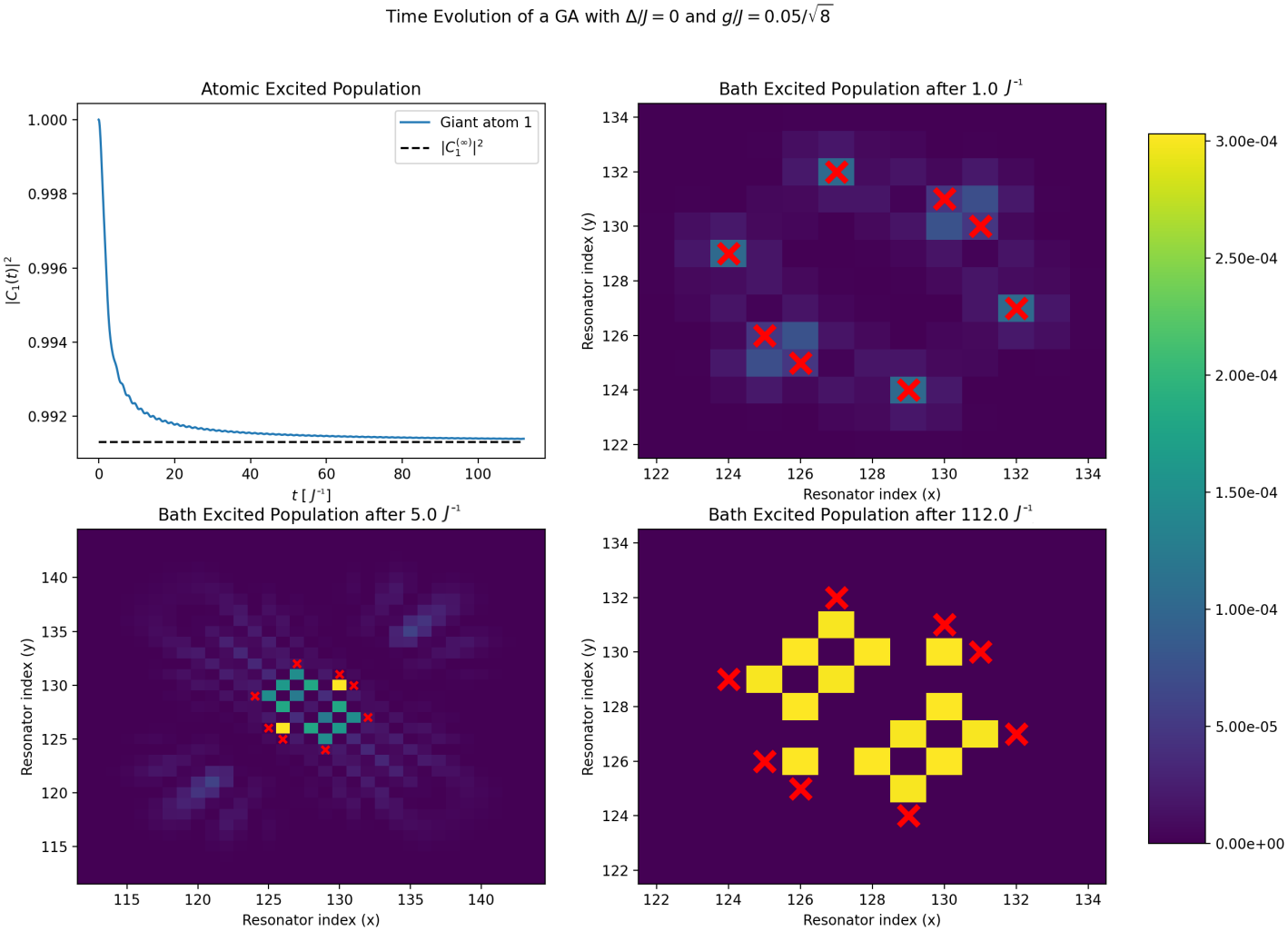

Figure 3.6: Time evolution of a giant atom with 8 coupling points spaced so that $n_1 = 1$, $m_1 = 2$, $n_2 = 2$ and $m_2 = 0$. The simulation was again performed with a bath size of 256×256 and a time step of $\Delta t = 10^{-2}J^{-1}$, using atom detuning $\Delta = 0$ and coupling strength $g = 0.05/\sqrt{8}\,\mathrm{J}$. *Top left*: Atomic excited population, converging towards $\left|C_1^{(\infty)}\right|^2 \approx 0.9913$. *Top right*: Bath population after $1J^{-1}$. The atoms are emitting energy at the coupling points (marked with x's), and no interference effects are established yet. *Bottom left*: Bath population after $5J^{-1}$. Interference effects are mostly established, and earlier emissions can be seen escaping. *Bottom right*: Bath population after $112J^{-1}$. A standing wave interference pattern with peaks of $2.994 \cdot 10^{-4}$ and $3.027 \cdot 10^{-4}$ is visible. As expected, this is just slightly less than $g^2/J^2 = 3.125 \cdot 10^{-4}$. In the centre, we can see a gap in the BIC caused by destructive interference.

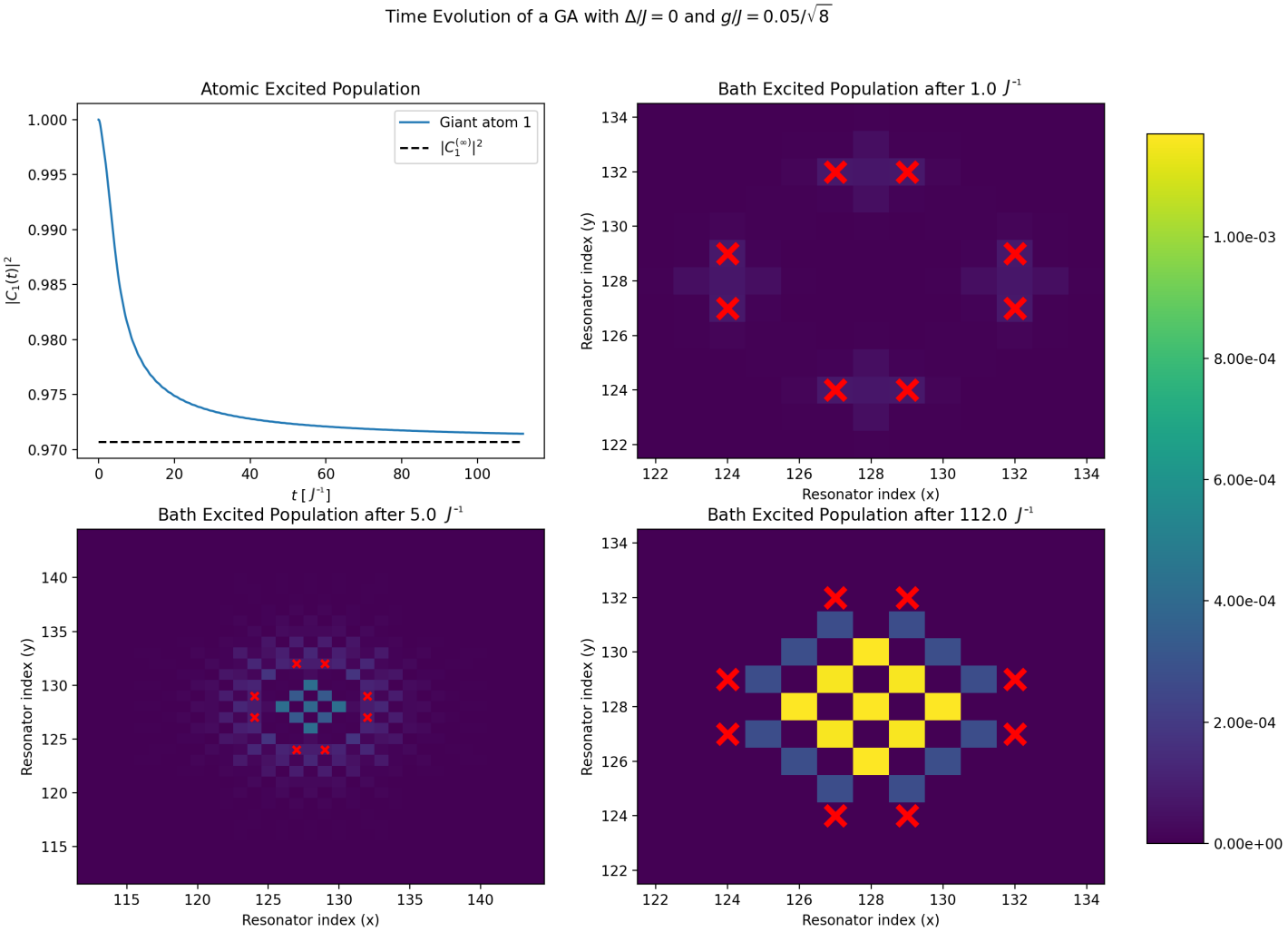

Figure 3.7: Time evolution of a giant atom with 8 coupling points spaced so that $n_1 = 1$, $m_1 = 2$, $n_2 = 2$ and $m_2 = 1$. Apart from this, all parameters are exactly the same as in Fig. 3.6. *Top left*: Atomic excited population, converging towards $\left|C_1^{(\infty)}\right|^2 \approx 0.9707$. *Top right*: Bath population after $1J^{-1}$. The atoms are emitting energy at the coupling points (marked with x's), and no interference effects are established yet. *Bottom left*: Bath population after $5J^{-1}$. Interference effects are mostly established, and earlier emissions can be seen escaping. *Bottom right*: Bath population after $112J^{-1}$. Because of constructive interference, the standing wave interference pattern has peaks of $\sim 1.2 \cdot 10^{-3}$ in the overlap, while the peaks outside of the overlap lie at $\sim 2.8 \cdot 10^{-4}$. These values are slightly further from the steady-state values than before, because it takes a longer time to fully populate the bound state when the total steady-state population is higher.

For completeness, let us also examine a case where there is no overlap between the BICs generated by the two subsets. One way to achieve this would be to move the two subsets so that they are far away from each other. This is not necessary, however. As can be seen in Fig. 3.8 below, it is sufficient to e.g. displace one of the subsets in Fig. 3.6 by $[0, 1]$.

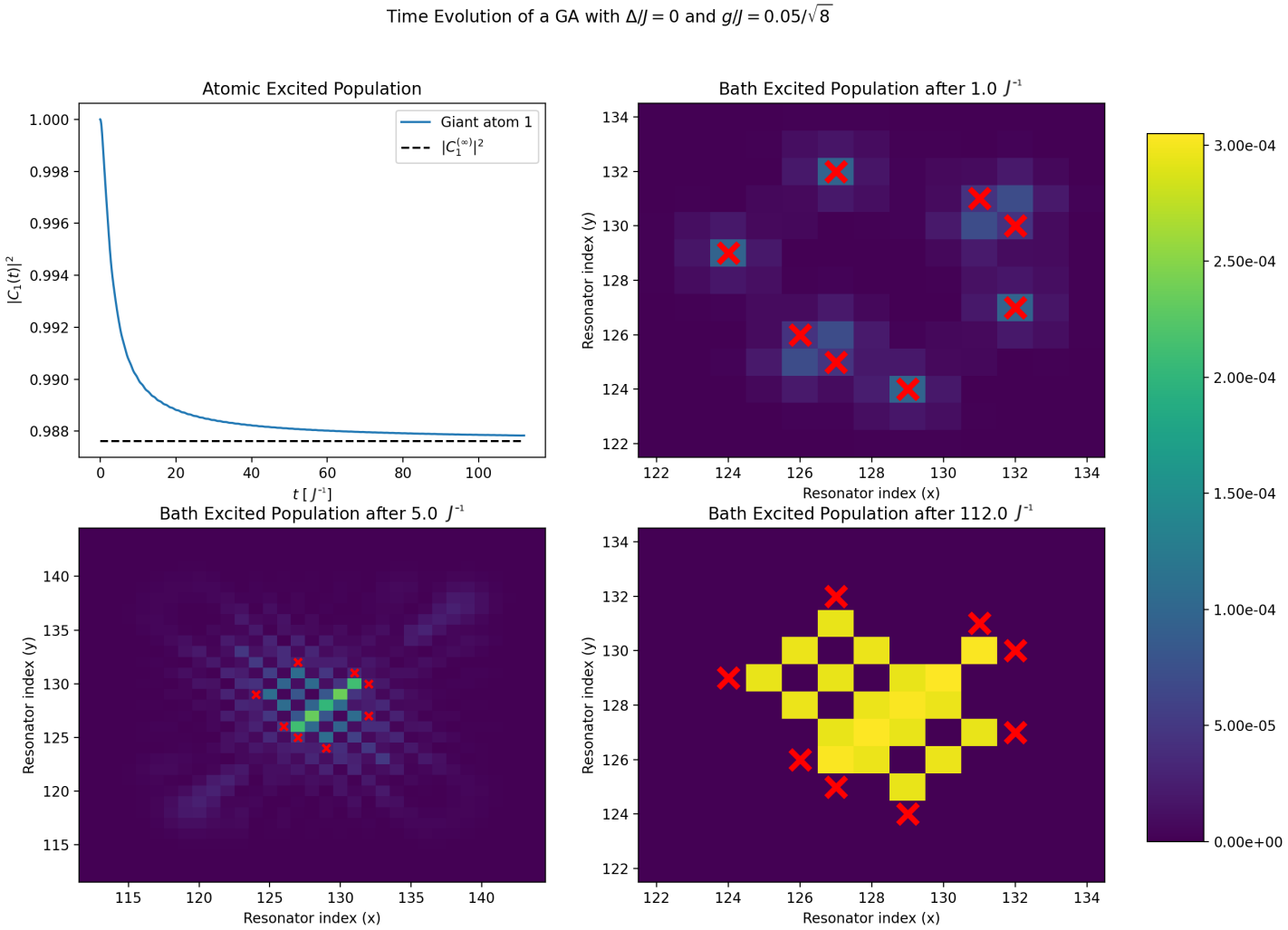

Figure 3.8: Time evolution of a giant atom with 8 coupling points spaced so that $n_1 = 1$, $m_1 = 2$, $n_2 = 2$ and $m_2 = 0$, displaced by $[0, 1]$ from being centred on the same point. All other parameters are the same as in Fig. 3.6. *Top left*: Atomic excited population, converging towards $\left|C_1^{(\infty)}\right|^2 \approx 0.9876$. *Top right*: Bath population after $1J^{-1}$. The atoms are emitting energy at the coupling points (marked with x's), and no interference effects are established yet. *Bottom left*: Bath population after $5J^{-1}$. Interference effects are mostly established, and earlier emissions can be seen escaping. *Bottom right*: Bath population after $112J^{-1}$. There is no interference between the standing wave bound states generated by the two subsets, so every peak has roughly the same population ($\sim 3 \cdot 10^{-4}$). It should be noted that because one of the subsets has more closely spaced atoms, it is slightly closer to reaching the steady state population of $\sim g^2/J^2$, which can be seen as a slightly brighter yellow colour.

3.4 DFI in 2D structured environments

Just like in 1D, two subradiant giant atoms coupled to a 2D structured environment exhibit DFI if at least one coupling point of each atom lies on top of an *interaction point* of the other. These interaction points are precisely the points where the BICs have a peak, and as we will see, the interaction strength is proportional to the steady-state population of the peaks involved.

To start with, let us examine the simplest possible case, where the two atoms with $\Delta = 0$ and equal coupling strength g have four coupling points each, spaced so that $m = n = 0$ for both atoms. As we see in Fig. 3.9, the behaviour in this configuration is very similar to the behaviour found in Ref. [5] for two giant atoms exhibiting DFI in 1D.

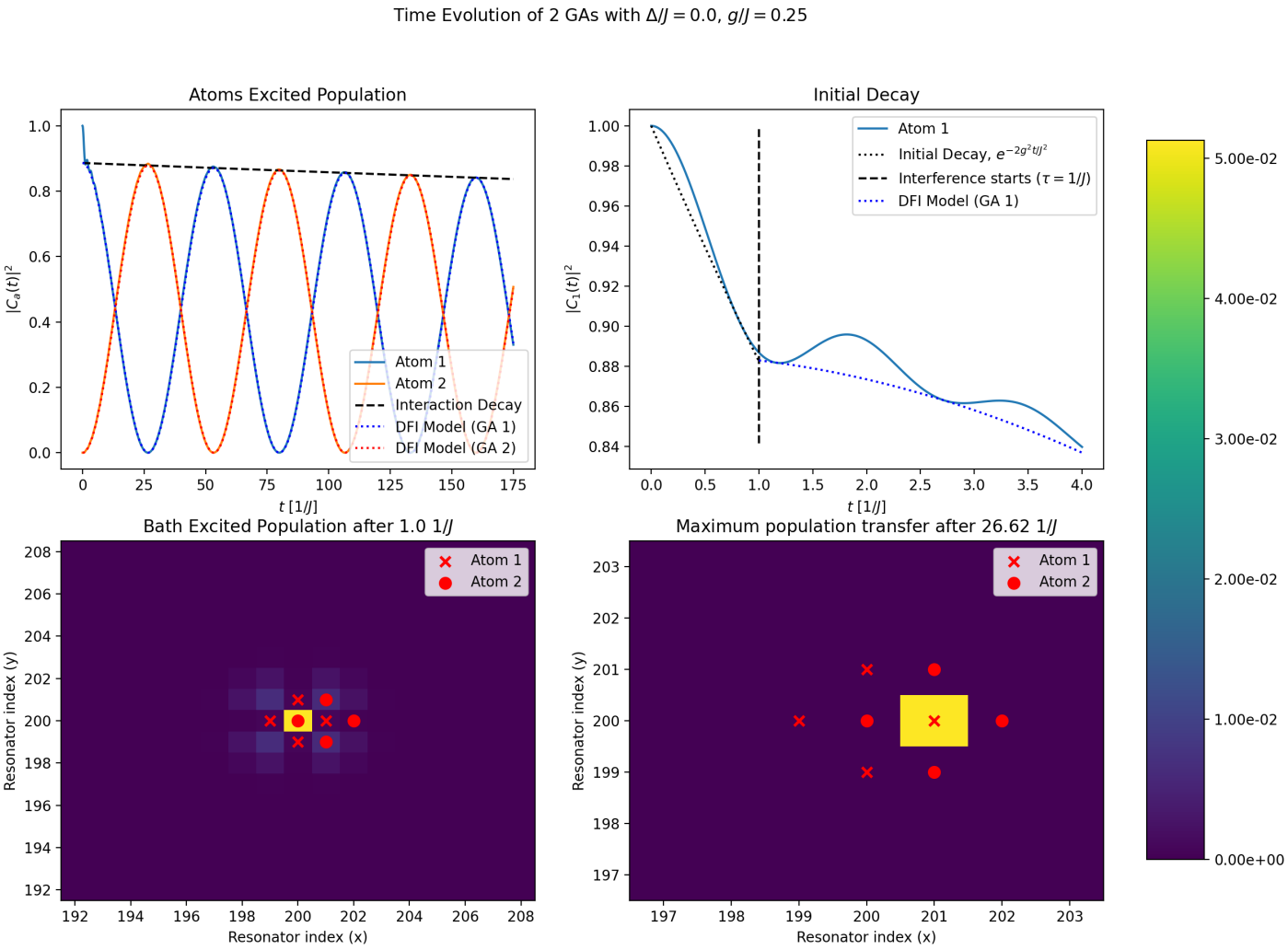

Figure 3.9: Time evolution of two identical giant atoms with 4 coupling points spaced so that $n = m = 0$. The simulation was performed with a bath size of 400×400 and a time step of $\Delta t = 10^{-2}J^{-1}$, using atom detuning $\Delta = 0$ and coupling strength $g = 0.25\,J$. *Top left*: Atomic excited population, going back and forth between the two atoms with period $2\tau_{\text{int}} \approx 53.25$. There is a decay in the amplitude of the oscillations $\sim e^{-2z_I t}$ with $z_I \approx 1.635 \cdot 10^{-4}$. *Top right*: Initial decay $\sim e^{-2g^2 t}$ caused by time delay, lasting until interference establishes itself at $\tau = 1/J$. *Bottom left*: Bath population after $1/J$. Interference effects are established, and some earlier emissions can be seen escaping. *Bottom right*: Bath population after $26.62J^{-1}$, when maximum population transfer is achieved. At this time, the population in the second atom is ~ 0.8841, and the population in its sole standing wave peak is $\sim 5.13 \cdot 10^{-2}$.

The population in the atoms is very well described as the sum of a small oscillating transient population which is gradually lost to the bath and the DFI model outlined in Ref. [5]. In this model, there is an initial period before interference effects establish themselves at $\tau = 1/J$ where the excited atom decays according to $|C_1(t)|^2 = e^{-2g^2 t/J^2}$.

After $\tau = 1/J$, the atom populations are modelled as

$$\begin{cases} |C_1(t)|^2 = \cos(z_R t)^2 e^{-2z_I t}, \\ |C_2(t)|^2 = \sin(z_R t)^2 e^{-2z_I t}, \end{cases} \tag{3.19}$$

where $z_{R,I}$ are related to the poles of the resolvent projected onto the two eigenstates $|\pm\rangle = \frac{1}{2}(|1\rangle \pm |2\rangle)$ of the 2-atom system. Specifically, in terms of the dominant unstable poles $z_\pm$ of $G_\pm(z) = \langle \pm | G(z) | \pm \rangle$, $z_{R,I}$ are defined [5] as

$$z_R = \left| \frac{\mathrm{Re}[z_+] - \mathrm{Re}[z_-]}{2} \right| \tag{3.20}$$

and

$$z_I = \left| \frac{\mathrm{Im}[z_+] + \mathrm{Im}[z_-]}{2} \right|. \tag{3.21}$$

If we examine the values of these parameters for different values of g by running simulations and fitting a model of this type roughly, we find the results in Fig. 3.10 below. As we can see, if we perform a power law fit $z_{R,I} \approx k(g/J)^r$ to get a sense of how $z_{R,I}$ are depend on g/J, we find that $z_R \approx 0.835(g/J)^{1.92}$ increases slightly slower than g^2/J^2, and $z_I \approx 0.436(g/J)^{5.72}$ increases significantly faster. If we use $\frac{z_R}{z_I} \approx 1.92(g/J)^{-3.80}$ as a measure of the quality of the DFI, it is clear – see also Fig. 3.11 – that the best DFI is achieved in the weak coupling limit. Of course, depending on the application, one might value interaction speed more highly than the metric $\frac{z_R}{z_I}$ does, in which case there will be some optimal $g/J > 0$.

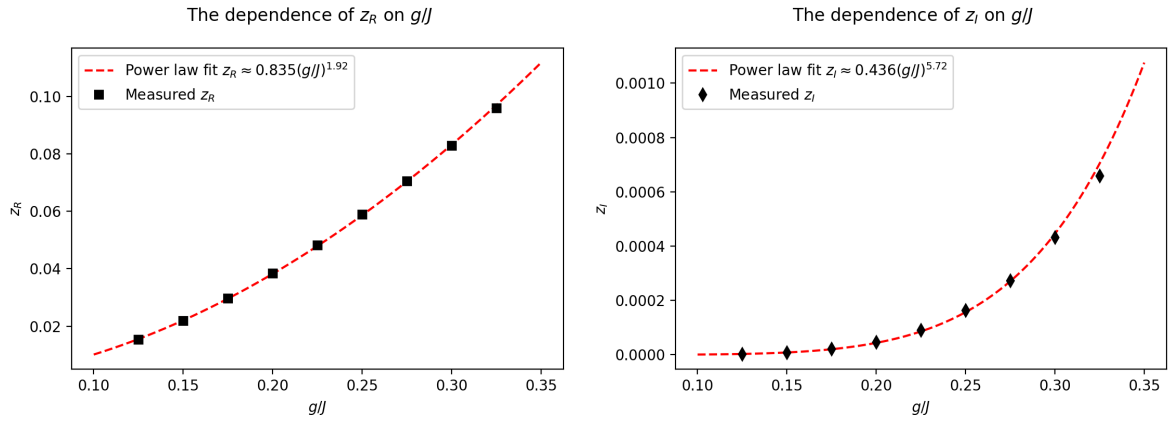

Figure 3.10: The dependence of z_R (top) and z_I (bottom) on the coupling strength g, expressed as a fraction of J. As we can see, z_R increases slower than $(g/J)^2$, while z_I increases almost as $(g/J)^6$.

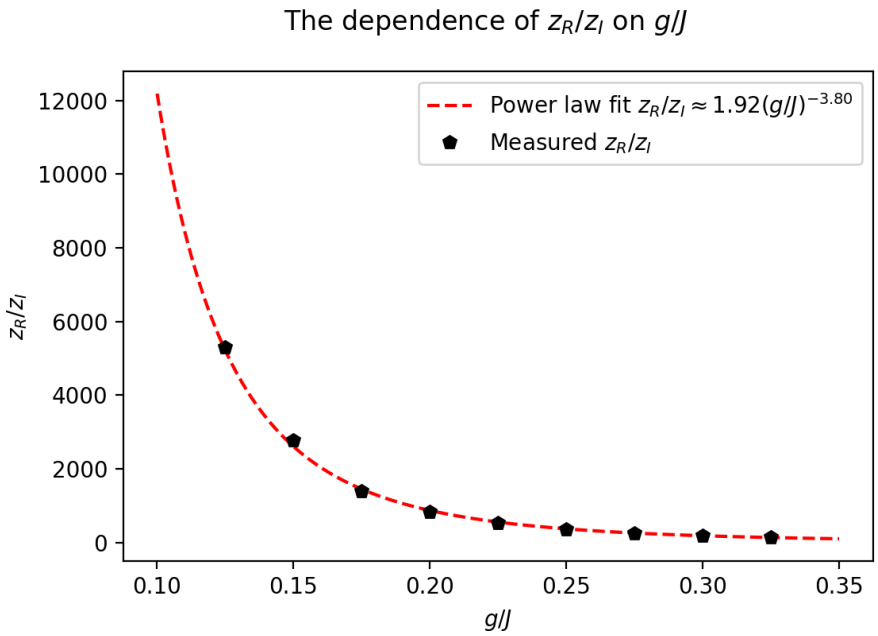

Figure 3.11: The dependence of the ratio z_R/z_I on the coupling strength g, expressed as a fraction of J. As one could surmise from Fig. 3.10, this ratio is roughly proportional to $(g/J)^{-4}$.

Similar behaviour to this simplest case is gotten for any pair of subradiant giant atoms at $\Delta = 0$, as long as they each have at least one coupling point on one of the interaction points of the other atom. If this is not fulfilled, however, there is no DFI – see e.g. figures 3.12 and 3.13. These two examples (and other similar configurations not exhibiting DFI) can be thought of as the 2D analogues of the separate and nested topologies from section 2.4.2.

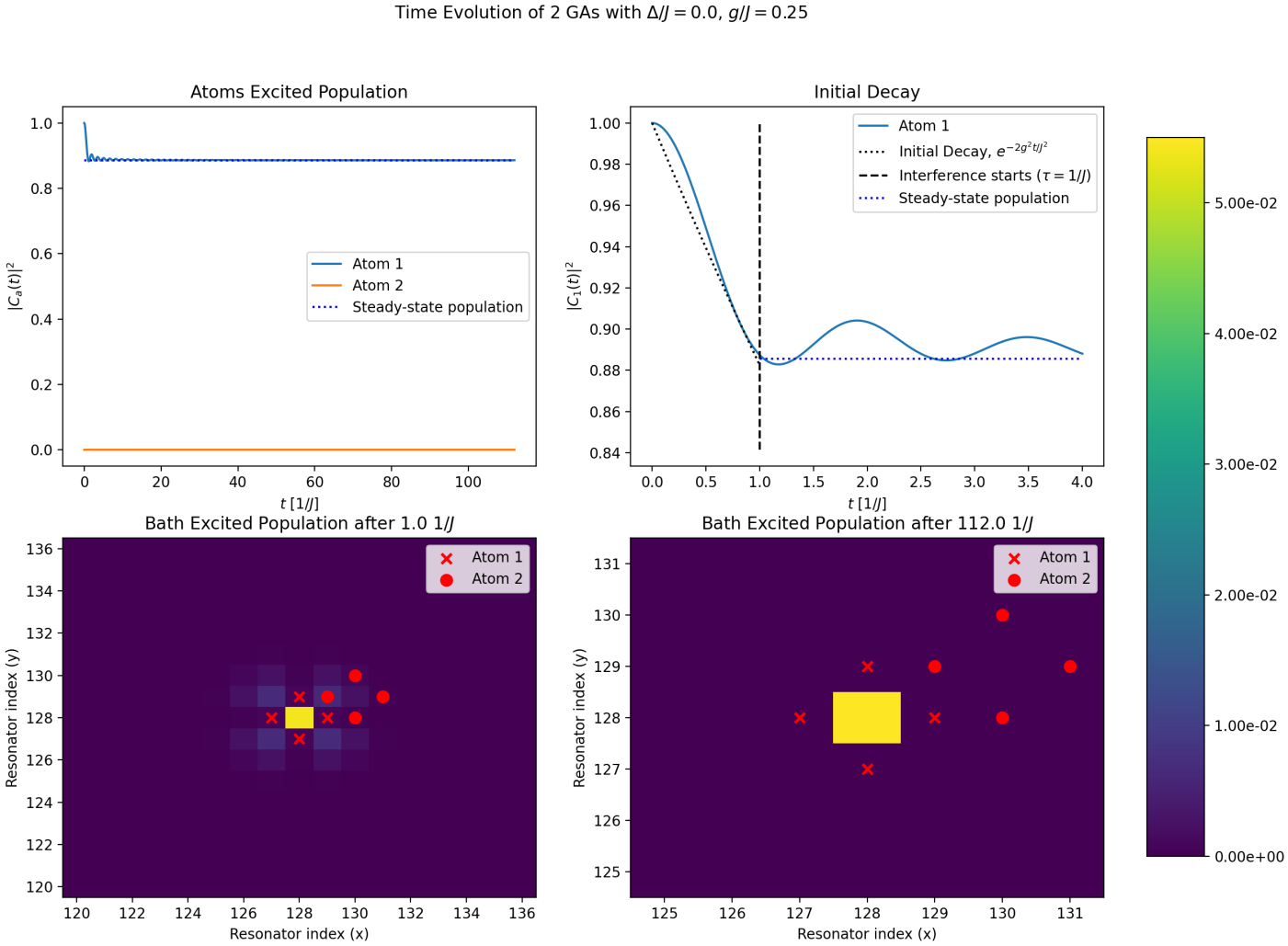

Figure 3.12: Time evolution of two identical giant atoms with 4 coupling points spaced so that $n = m = 0$, displaced so that no DFI is possible. The simulation was performed with a bath size of 256×256 and a time step of $\Delta t = 10^{-2}/J$, using atom detuning $\Delta = 0$ and coupling strength $g = 0.25\,J$. *Top left*: Atomic excited population, behaving largely as though the atoms were invisible to one another. *Top right*: Initial decay $\sim e^{-2g^2t/J^2}$ caused by time delay, lasting until interference establishes itself at $\tau = 1/J$. *Bottom left*: Bath population after $1/J$. Interference effects are established, and some earlier emissions can be seen escaping. *Bottom right*: Bath population after $112/J$, when he system has largely reached its steady state solution.

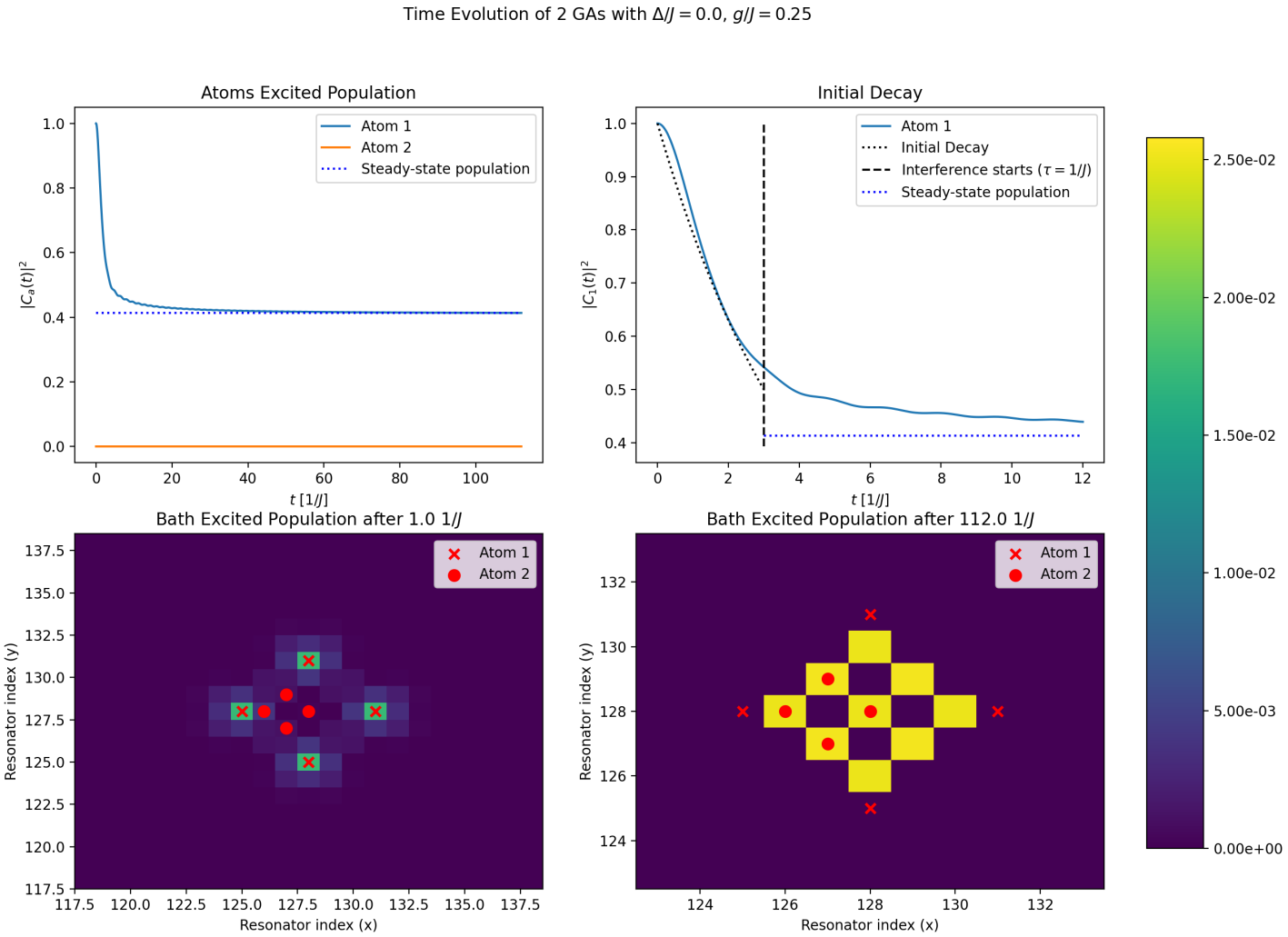

Figure 3.13: Time evolution of two giant atoms with 4 coupling points each. This time, atom one has $n_1 = m_1 = 1$ while atom 2 still has $n_2 = m_2 = 0$, displaced so that one atom is entirely enclosed between the coupling points of the other. Other than this, all parameters are exactly the same as in Fig. 3.12. *Top left*: Atomic excited population, behaving largely as though the atoms were invisible to one another. *Top right*: Initial decay caused by time delay, lasting until interference establishes itself at $\tau \approx 3/J$. Because of dispersive effects, the line between before and after the establishment of interference is less clear than with $m_1 = n_1 = 0$. Note that the initial decay rate is also no longer approximately proportional to $2g^2/J^2$ because of this. *Bottom left*: Bath population after $3/J$. Interference effects are mostly established, and earlier emissions can be seen escaping. *Bottom right*: Bath population after $112/J$, when the system has largely reached its steady state solution.

To conclude the results chapter, let us briefly look at some more complicated configurations exhibiting DFI. For example, we could consider a single giant atom with $n = m = 1$, where each of its coupling points is surrounded by the four coupling points of a giant atom with $n = m = 0$. As can be seen in Fig. 3.14, an initial excitation in the larger atom will spread out among the four smaller ones, then gather back in the large atom, and so on.

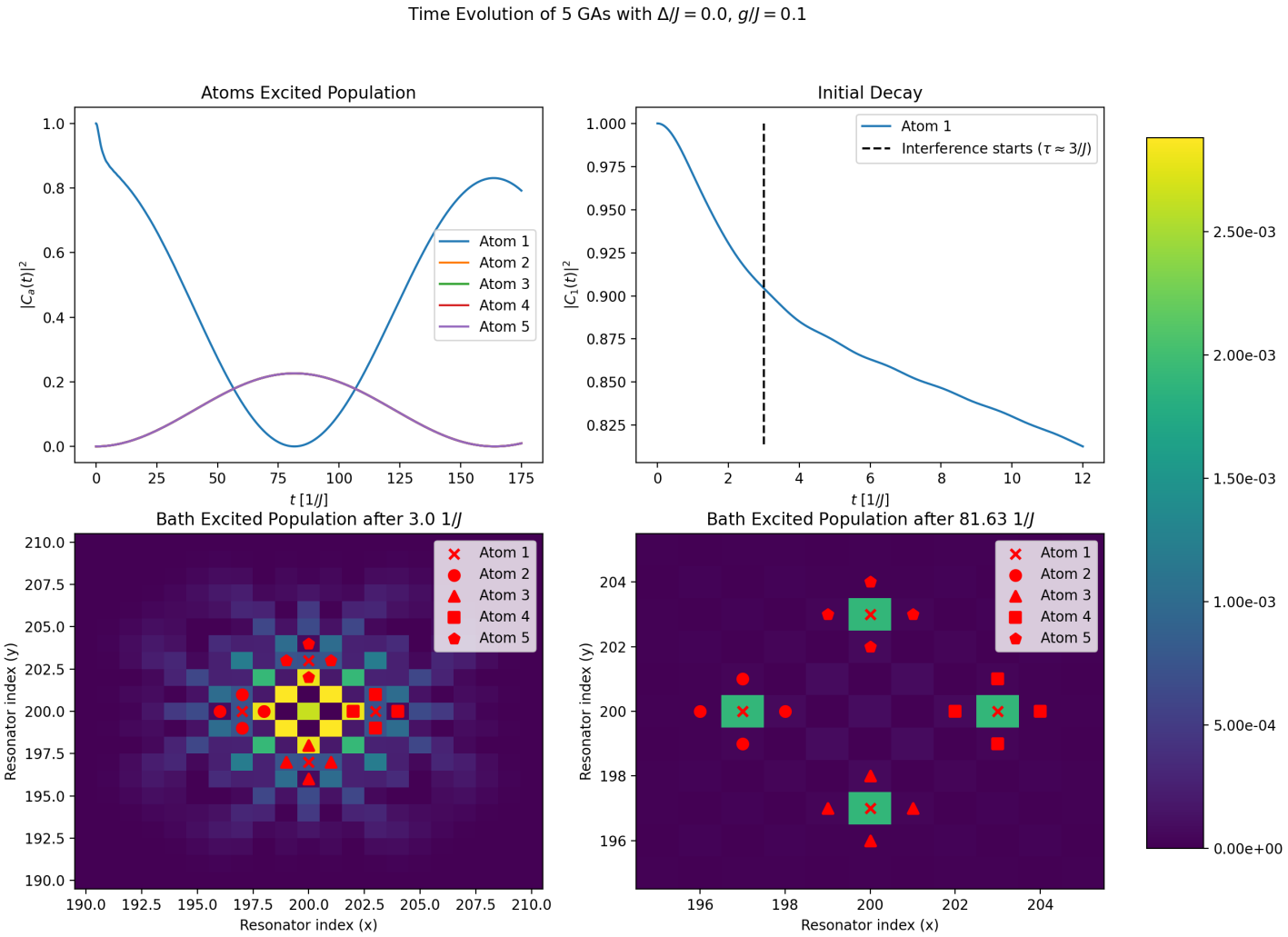

Figure 3.14: Time evolution of five giant atoms with 4 coupling points each. Atom 1 has $n = m = 1$ while atoms 2–5 have $n = m = 0$. The simulation was performed with a bath size of 400×400 and a time step of $\Delta t = 10^{-2}/J$, using atom detuning $\Delta = 0$ and coupling strength $g = 0.1\,J$. *Top left*: The atomic excited population, moving back and forth between atom 1 and the four other atoms. It should be noted that the curves for atoms 2–5 are directly on top of one another. *Top right*: Initial decay caused by time delay, lasting until interference establishes itself at $\tau \approx 3/J$. *Bottom left*: Bath population after $3/J$. Interference effects are mostly established, and earlier emissions can be seen escaping. *Bottom right*: Bath population after $81.63/J$, when all of the initial population has left atom 1 and the remaining atomic population is evenly spread out among atoms 2–5.

If we make atoms 2–5 bigger, so that they too have $n = m = 1$, we get a very similar result, as can be seen in Fig. 3.15 below. In this case, all the giant atoms are identical, but displaced by $[5, 0]$ or $[0, 5]$ with respect to one another. Notably, this configuration can be extended into a grid of arbitrary size, where every atom couples to its four neighbours – just like the resonators in the bath. In fact, the same can be accomplished using a more compact configuration with displacements $[2, 1]$ and $[1, -2]$, as shown in Fig. 3.16. In both of these figures, the initial excitation was placed in a central atom surrounded by four others. In Fig. 3.17, we see what happens if we instead place the initial excitation in one corner of a "square", which can interact along the edges of the square but not along

the diagonal.

It should be noted that just like in 1D structured environments, but unlike in 1D continuous waveguides [2], all-to-all coupling between three or more giant atoms is impossible if all the atoms have detuning $\Delta = 0$. This can be shown to follow from the strict restrictions on the spacing between coupling points necessary for DFI between a pair of such giant atoms.

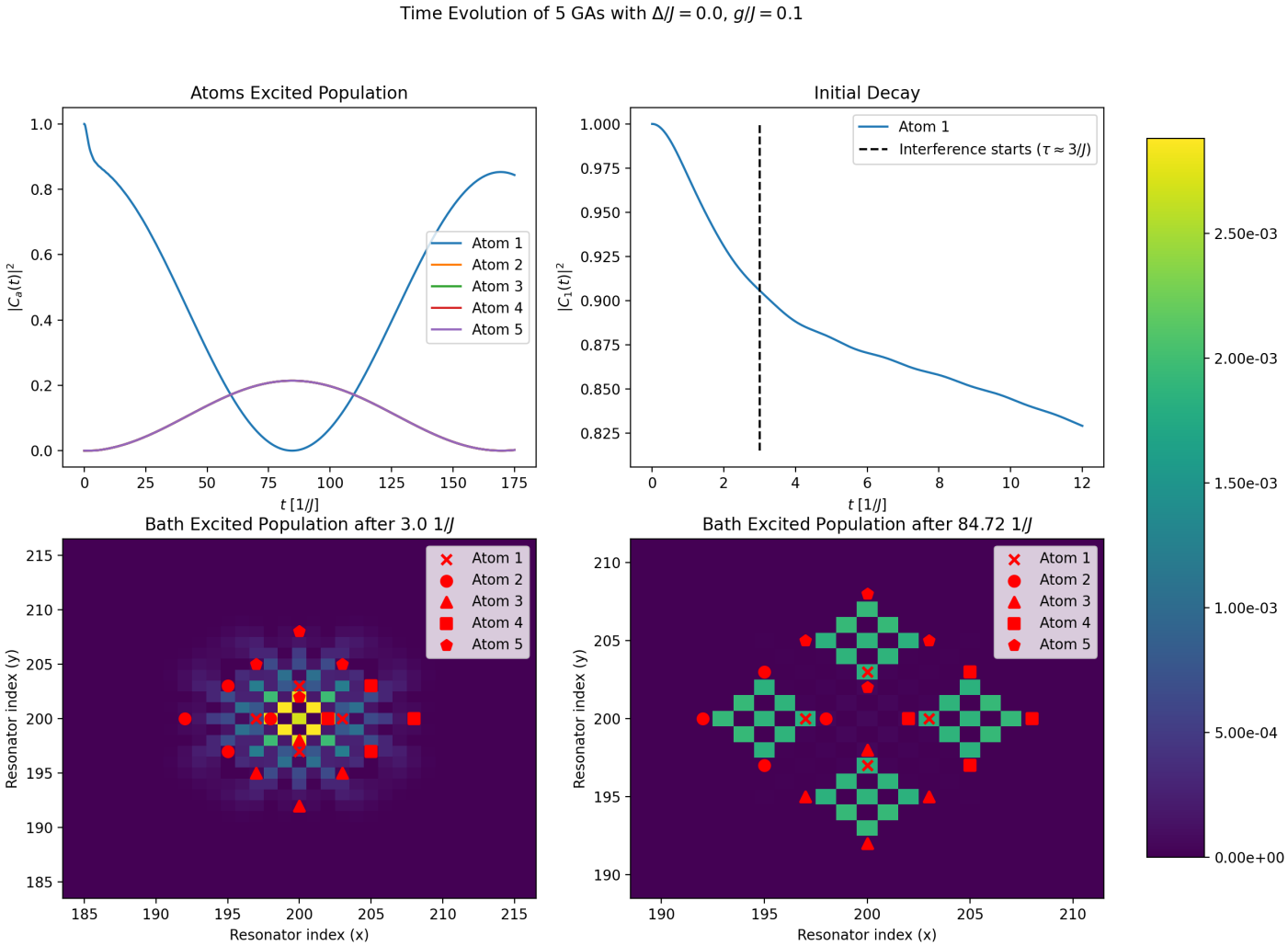

Figure 3.15: Time evolution of five identical giant atoms with 4 coupling points each, spaced so that $n = m = 1$. The atoms are displaced by $[0, 5]$ or $[5, 0]$ with respect to each other, and the excitation starts in atom 1. All other parameters are the same as in Fig. 3.14. *Top left*: The atomic excited population, moving back and forth between atom 1 and the four other atoms. Again, the curves for atoms 2–5 are directly on top of one another. *Top right*: Initial decay caused by time delay, lasting until interference establishes itself at $\tau \approx 3/J$. *Bottom left*: Bath population after $3/J$. Interference effects are mostly established, and earlier emissions can be seen escaping. *Bottom right*: Bath population after $84.72/J$, when all of the initial population has left atom 1 and the remaining atomic population is evenly spread out among atoms 2–5.

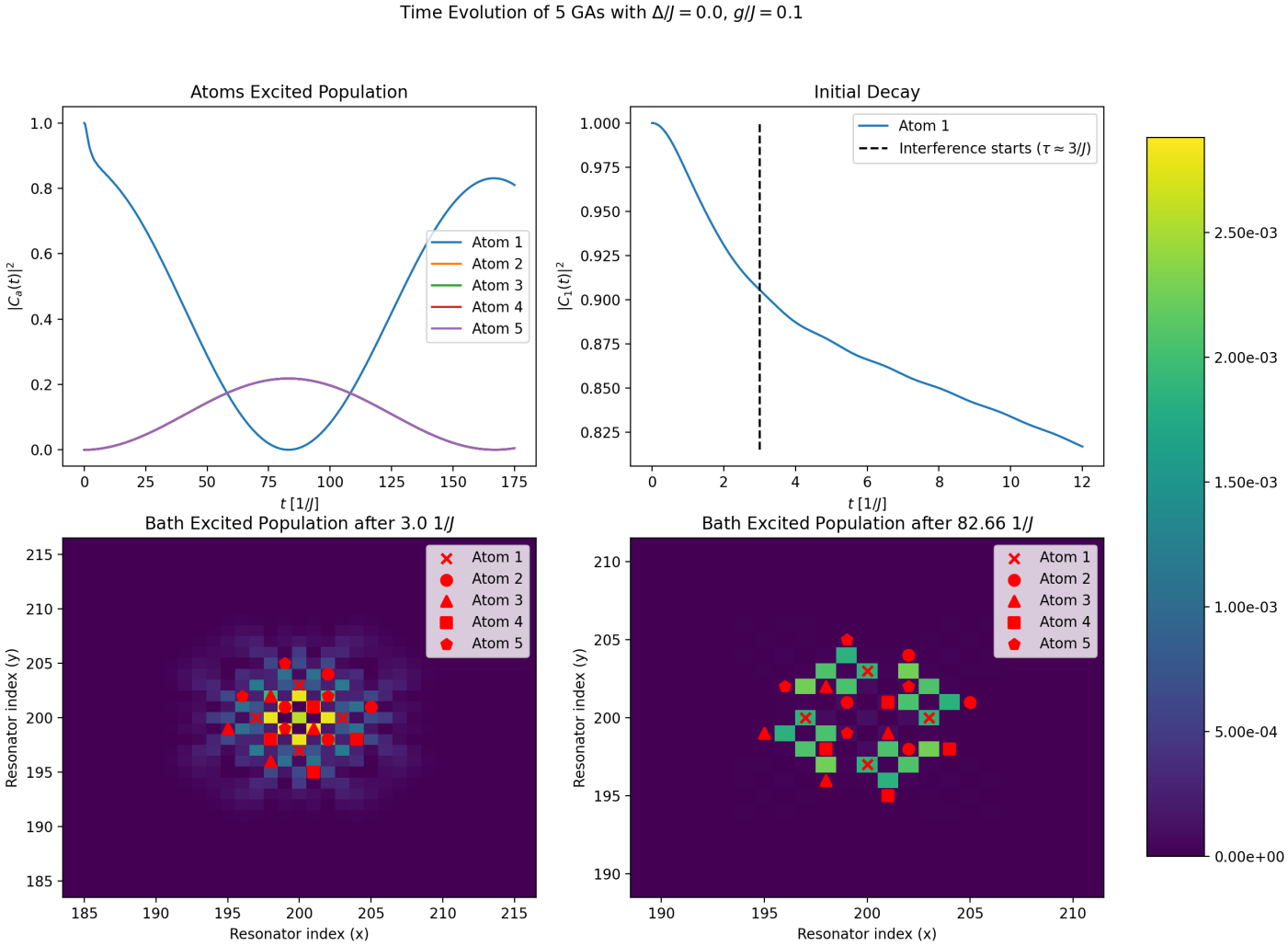

Figure 3.16: Time evolution of a 5-atom system identical to the one in Fig. 3.15, except that the displacement between the atoms are changed to $[2, 1]$ and $[1, -2]$ to make the configuration more compact. Again, the curves for atoms 2–5 are directly on top of one another. *Top left*: The atomic excited population, moving back and forth between atom 1 and the four other atoms. *Top right*: Initial decay caused by time delay, lasting until interference establishes itself at $\tau \approx 3/J$. *Bottom left*: Bath population after $3/J$. Interference effects are mostly established, and earlier emissions can be seen escaping. *Bottom right*: Bath population after $82.66/J$, when all of the initial population has left atom 1 and the remaining atomic population is evenly spread out among atoms 2–5.

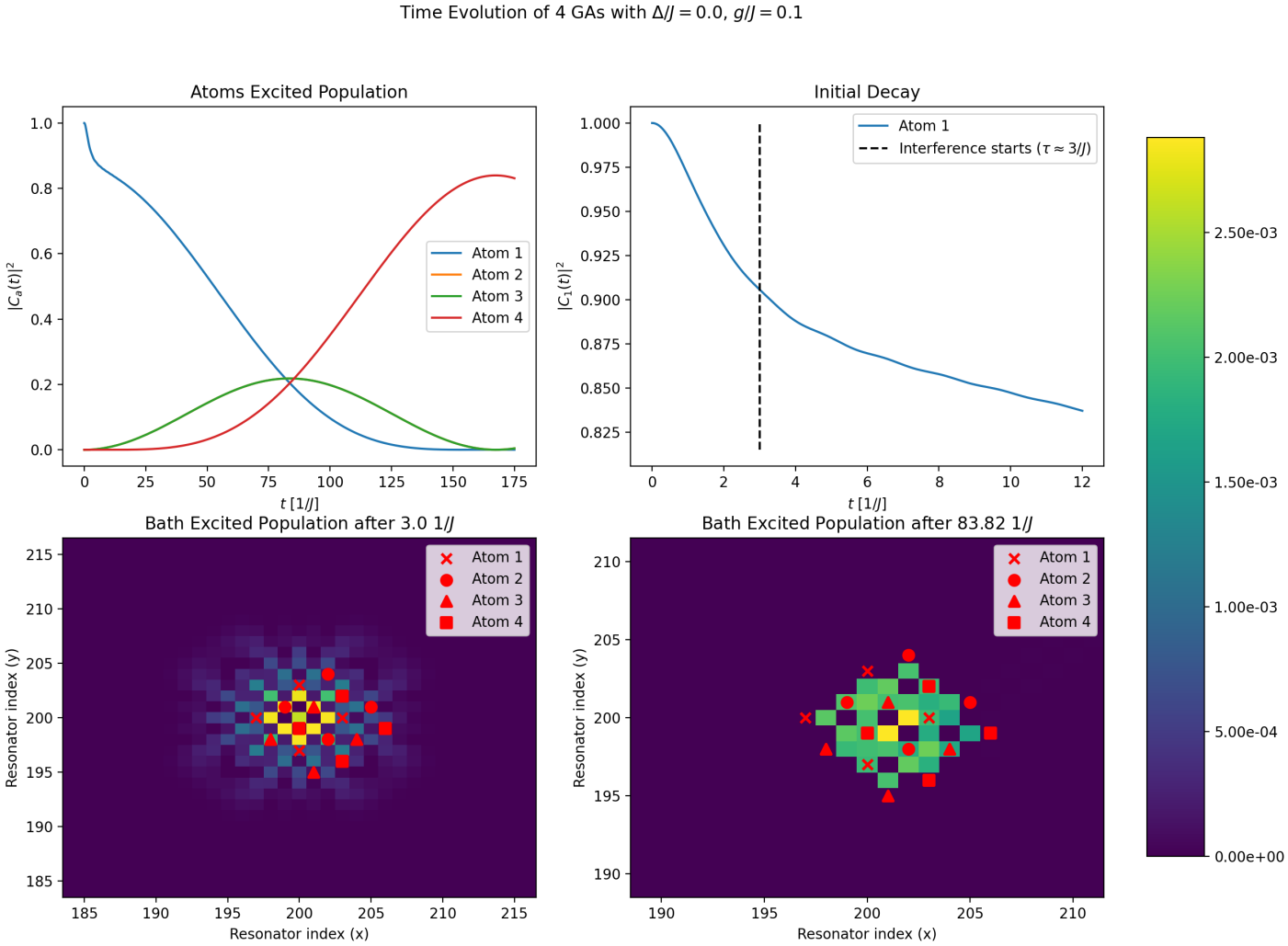

Figure 3.17: Time evolution of a 4-atom system identical to the one in Fig. 3.16, except that the two leftmost atoms have been replaced with an additional atom on the right, displaced by $[2, 1]$ and $[1, -2]$ from the two rightmost atoms in Fig. 3.16. *Top left*: The atomic excited population, moving from atom 1 through the two atoms to its immediate right to the atom on the far right, and then back again. *Top right*: Initial decay caused by time delay, lasting until interference establishes itself at $\tau \approx 3/J$. *Bottom left*: Bath population after $3/J$. Interference effects are mostly established, and earlier emissions can be seen escaping. *Bottom right*: Bath population after $82.66/J$, when all of the initial population has left atom 1 and the remaining atomic population is evenly spread out among atoms 2–5.

One could of course go on to examine ever wilder configurations based on the effects we found in section 3.3, but we will leave this for future research and move on to a discussion of the results we have described in this chapter.

4

Discussion, Conclusions and Outlook

As we have seen, the possibilities when it comes to DFI in 2D are limited mostly by one's imagination. It should be noted that all of the giant atom configurations described in the **Results** chapter above use $\Delta = 0$, and are thus restricted to have coupling points at odd spacings along 45° diagonals. Preliminary examinations suggest that other values of Δ inside the band also allow for at least imperfect DFI, with other spacings between coupling points being necessary for subradiance. This is similar to what has been found previously in 1D [5].

Apart from detunings within the band, it should also be mentioned that although we did not examine it here, preliminary studies also suggest that it is possible to achieve DFI for $|\Delta| > 4J$ in 2D environments by leveraging the overlap of bound states outside the band. Just like in 1D environments (cf. Ref. [5]), this is possible for both small and giant atoms. There are two major disadvantages of using this method for DFI. The first is that the bound state population decays exponentially with distance from the coupling points, which limits this kind of DFI to operating over very short distances. The other major disadvantage is that the interaction is quite slow in comparison to the DFI found in the middle of the band. On the other hand, there is also one major advantage to this kind of DFI, namely that the interaction can be easily turned on and off by shifting the detuning towards or away from the band gap. This is much harder to accomplish with DFI in the middle of the band, since any small perturbation away from zero detuning will tend to cause significant energy emissions.

Something else that should be discussed is the validity of the approximations we have made use of. As briefly outlined in section 2.3, the RWA is a good approximation when the detuning is relatively small and the coupling is weak compared to ω_a and ω_B, which holds without issues when dealing with optical light and microwaves. It is also the regime we are most interested in anyway, since these conditions are those which yield the best DFI within the band. Furthermore, this is precisely the regime in which the Wigner-Weisskopf approximation is applicable. Even if our numerical models do not rely on this approximation, it is still nice to have, since a lot of our intuitive understanding is built on it.

One approximation that is slightly dubious, or at least restricts the applicability of the findings in this thesis is the truncation of our atoms to just two energy levels. While there are a fair few atom-like systems that can be approximated this way, it is likely a poor approximation for e.g. weakly anharmonic superconducting qubits. By definition, a weakly anharmonic system only has a small difference between the excitation energy $\omega_{01} = E_1 - E_0$ from the ground state to the first excited state $|0\rangle \to |1\rangle$ and the excitation

energy $\omega_{12} = E_2 - E_1$ from the first to second excited state $|1\rangle \to |2\rangle$. This means that if some perturbation has a high probability of causing an excitation $|0\rangle \to |1\rangle$, then it also has a high probability of exciting $|1\rangle \to |2\rangle$, which is a problem for our model, since we are ignoring the existence of the $|2\rangle$ state altogether. For this reason, it would be very much of interest to study giant atoms with three, four or even more relevant energy levels, which has not been done before to any significant extent [23]. Taking more energy levels into account would also enable more accurate modelling of the multiple excitation regime, which we have ignored by truncating to the single-excitation subspace. In short, there are many opportunities for future research.

In fact, even if one keeps all of our approximations, there is still a multitude of avenues warranting further research. For example, one could dive even deeper into how the strength and quality of DFI between two giant atoms look for giant atoms with eight coupling points like we examined in section 3.3. Alternatively, one could take a closer look at subradiance and DFI at other values of Δ – both inside and outside of the band. This could also be combined with the methods of *reverse design* discussed in Ref. [10] based on guessing the Fourier space couplings necessary for subradiance, DFI or other effects rather than the real-space couplings. One could also perform a more detailed study of the origins of different contributions to the time evolution using numerical computations in resolvent formalism, akin to that performed for single giant atoms in 2D in Ref. [9] and for multiple giant atoms in 1D in Ref. [5].

Apart from this, one could look into the effects of having complex coupling strengths in 2D environments. These have previously been shown to be able to induce chiral emissions in 1D environments [4]. Another thing to consider is environments with different lattice structures, e.g. triangular and hexagonal lattices. Furthermore, efforts should be made towards combining the algorithm for efficient simulation of giant atoms developed in this thesis (see section 3.1 and appendix B) with the methods used in Refs. [9, 10] for speeding up the computation of the Fourier transforms at each time step. In the algorithm used in this thesis, the Fourier transforms are the main remaining bottleneck when it comes to the time cost of the algorithm.

Summing up, there is still much to be done in the field of giant atoms, even specifically in the context of 2D structured environments. However, the results of this thesis should be able to serve as a good basis for this future research. Of course, this includes further theoretical studies, but also experimental ones – experiments are, after all, the only true arbiters of whether or not a model is useful. Since the models used in this thesis have been useful in previous experiments performed in 1D environments [33, 37], we have every reason to think that the same will hold for the results of this thesis – with the possible exception of systems with very low anharmonicity, as outlined above. Furthermore, the algorithms developed in this thesis for efficient simulation of giant atoms should hopefully prove useful for further numerical studies of giant atoms – in environments of arbitrary dimensionality.

References

[1] A. F. Kockum, "Quantum optics with giant atoms—the first five years," in *International Symposium on Mathematics, Quantum Theory, and Cryptography*, T. T. et al, Ed., 2021, pp. 125–146. [Online]. Available: https://doi.org/10.1007/978-981-15-5191-8_12.

[2] A. F. Kockum, G. Johansson, and F. Nori, "Decoherence-free interaction between giant atoms in waveguide quantum electrodynamics," *Phys. Rev. Lett.*, vol. 120, p. 140 404, 14 2018. DOI: 10.1103/PhysRevLett.120.140404. [Online]. Available: https://link.aps.org/doi/10.1103/PhysRevLett.120.140404.

[3] B. Kannan, M. Ruckriegel, and D. e. a. Campbell, "Waveguide quantum electrodynamics with superconducting artificial giant atoms," *Nature*, 775–779, 583 2020. [Online]. Available: https://doi.org/10.1038/s41586-020-2529-9.

[4] A. Soro and A. F. Kockum, "Chiral quantum optics with giant atoms," *Physical Review A*, vol. 105, no. 2, 2022. DOI: 10.1103/physreva.105.023712. [Online]. Available: https://doi.org/10.1103%2Fphysreva.105.023712.

[5] A. Soro, C. S. Muñoz, and A. F. Kockum, "Interaction between giant atoms in a one-dimensional structured environment," *Physical Review A*, vol. 107, no. 1, 2023. DOI: 10.1103/physreva.107.013710. [Online]. Available: https://doi.org/10.1103%2Fphysreva.107.013710.

[6] T. Scheidsteger, R. Haunschild, and C. Ettl, "Historical Roots and Seminal Papers of Quantum Technology 2.0," *Nanoethics*, pp. 271–296, 16 2022. [Online]. Available: https://doi.org/10.1007/s11569-022-00424-z.

[7] P Krantz, M Kjaergaard, F Yan, T P. Orlando, S Gustavsson, and W D. Oliver, "A quantum engineer's guide to superconducting qubits," *Phys. Rev. Applied*, vol. 6, 2 Jun. 2019.

[8] M. V. Gustafsson, T. Aref, A. F. Kockum, M. K. Ekström, G. Johansson, and P. Delsing, "Propagating phonons coupled to an artificial atom," *Science*, vol. 346, no. 6206, pp. 207–211, 2014. DOI: 10.1126/science.1257219. [Online]. Available: https://www.science.org/doi/abs/10.1126/science.1257219.

[9] A. González-Tudela and J. I. Cirac, "Markovian and non-markovian dynamics of quantum emitters coupled to two-dimensional structured reservoirs," *Phys. Rev. A*, vol. 96, p. 043 811, 4 2017. DOI: 10.1103/PhysRevA.96.043811. [Online]. Available: https://link.aps.org/doi/10.1103/PhysRevA.96.043811.

[10] A. González-Tudela, C. S. Muñoz, and J. I. Cirac, "Engineering and harnessing giant atoms in high-dimensional baths: A proposal for implementation with cold atoms," *Phys. Rev. Lett.*, vol. 122, p. 203 603, 20 2019. DOI: 10.1103/PhysRevLett.122.203603. [Online]. Available: https://link.aps.org/doi/10.1103/PhysRevLett.122.203603.

[11] C. Cohen-Tannoudji, J. Dupont-Roc, and G. Grynberg, *Atom-Photon Interactions*. Wiley-VCH Verlag GmbH & Co., 2004, ch. III: Nonperturbative Calculation of Transition Amplitudes, pp. 165–256.

[12] D. J. Griffiths and D. F. Schroeter, 3rd ed. Cambridge, UK: Cambridge University Press, 2018, ISBN: 9781107189638.

[13] P. Virtanen *et al.*, "Scipy 1.0: Fundamental algorithms for scientific computing in python," *Nature Methods*, vol. 17, pp. 261–272, 2020. DOI: 10.1038/s41592-019-0686-2.

[14] A. Al-Mohy and N. Higham, "A new scaling and squaring algorithm for the matrix exponential," *SIAM Journal on Matrix Analysis and Applications*, vol. 31, Jan. 2009. DOI: 10.1137/09074721X.

[15] C. Moler and C. Loan, "Nineteen dubious ways to compute the exponential of a matrix, twenty-five years later," *Society for Industrial and Applied Mathematics*, vol. 45, pp. 3–49, Mar. 2003. DOI: 10.1137/S00361445024180.

[16] T. Hahn, *Routines for the diagonalization of complex matrices*, 2006. DOI: 10.48550/ARXIV.PHYSICS/0607103. [Online]. Available: https://arxiv.org/abs/physics/0607103.

[17] W. H. Press, S. A. Teukolsky, W. T. Vettering, and B. P. Flannery, *Numerical Recipes: The Art of Scientific Computing*, 3rd ed. Cambridge, UK: Cambridge University Press, 2007.

[18] W. Rossmann, *Lie Groups – An Introduction Through Linear Groups*, 1st ed. New York, USA: Oxford University Press, Inc., 2002.

[19] J. W. Cooley and J. W. Tukey, "An algorithm for the machine calculation of complex fourier series," *Mathematics of Computation*, vol. 19, no. 90, pp. 297–301, 1965, ISSN: 00255718, 10886842. [Online]. Available: http://www.jstor.org/stable/2003354 (visited on 05/24/2023).

[20] M. E. Peskin and D. V. Schroeder, *An Introduction to Quantum Field Theory*. Boca Raton, USA: CRC Press, 2018, ISBN: 9780201503975.

[21] J. W. Brown and R. V. Churchill, *Complex Variables and Applications*, 7th ed. New York, USA: McGraw-Hill, Inc., 2004, 262–265.

[22] L. V. Ahlfors, *Complex Analysis*, 3rd ed. New York, USA: McGraw-Hill, Inc., 1979, ch. 4: Complex Integration, pp. 101–172.

[23] A. S. Álvarez, "Theoretical quantum optics with giant atoms," Licentiate thesis, Chalmers University of Technology, Gothenburg, Sweden, 2023.

[24] J. D. Hood *et al.*, "Atom-atom interactions around the band edge of a photonic crystal waveguide," *Proceedings of the National Academy of Sciences of the United States of America*, vol. 113, no. 38, pp. 10 507–10 512, 2016, ISSN: 10916490. DOI: 10.1073/pnas.1603788113.

[25] L. Krinner, M. Stewart, A. Pazmiño, J. Kwon, and D. Schneble, "Spontaneous emission of matter waves from a tunable open quantum system," *Nature*, vol. 559, no. 7715, pp. 589–592, 2018, ISSN: 14764687. DOI: 10.1038/s41586-018-0348-z.

[26] M. Stewart, J. Kwon, A. Lanuza, and D. Schneble, "Dynamics of matter-wave quantum emitters in a structured vacuum," *Physical Review Research*, vol. 2, no. 4, p. 043 307, 2020, ISSN: 2643-1564. DOI: 10.1103/physrevresearch.2.043307.

[27] Y. Liu and A. A. Houck, "Quantum electrodynamics near a photonic bandgap," *Nature Physics*, vol. 13, no. 1, pp. 48–52, 2017, ISSN: 17452481. DOI: 10.1038/nphys3834.

[28] M. Mirhosseini *et al.*, "Superconducting metamaterials for waveguide quantum electrodynamics," *Nature Communications*, vol. 9, no. 1, p. 3706, 2018, ISSN: 20411723. [Online]. Available: http://dx.doi.org/10.1038/s41467-018-06142-z.

[29] A. F. Kockum, "Quantum optics with artificial atoms," Available at https://publications.lib.chalmers.se/records/fulltext/206197/206197.pdf, PhD thesis, Chalmers University of Technology, Gothenburg, Sweden, 2014.

[30] R. H. Dicke, "Coherence in spontaneous radiation processes," *Phys. Rev.*, vol. 93, pp. 99–110, 1 1954. DOI: 10.1103/PhysRev.93.99. [Online]. Available: https://link.aps.org/doi/10.1103/PhysRev.93.99.

[31] K. Lalumière, B. C. Sanders, A. F. van Loo, A. Fedorov, A. Wallraff, and A. Blais, "Input-output theory for waveguide qed with an ensemble of inhomogeneous atoms," *Phys. Rev. A*, vol. 88, p. 043 806, 4 2013. DOI: 10.1103/PhysRevA.88.043806. [Online]. Available: https://link.aps.org/doi/10.1103/PhysRevA.88.043806.

[32] G. Calajó, F. Ciccarello, D. Chang, and P. Rabl, "Atom-field dressed states in slow-light waveguide QED," *Physical Review A*, vol. 93, no. 3, p. 033 833, 2016, ISSN: 24699934. DOI: 10.1103/PhysRevA.93.033833.

[33] M. Scigliuzzo *et al.*, "Controlling atom-photon bound states in an array of josephson-junction resonators," *Phys. Rev. X*, vol. 12, p. 031 036, 3 2022. DOI: 10.1103/PhysRevX.12.031036. [Online]. Available: https://link.aps.org/doi/10.1103/PhysRevX.12.031036.

[34] X. Wang, T. Liu, A. F. Kockum, H.-R. Li, and F. Nori, "Tunable Chiral Bound States with Giant Atoms," *Physical Review Letters*, vol. 126, no. 4, p. 43 602, 2021. DOI: 10.1103/PhysRevLett.126.043602. [Online]. Available: https://link.aps.org/doi/10.1103/PhysRevLett.126.043602.

[35] X. Wang and H.-R. Li, "Chiral quantum network with giant atoms," *Quantum Science and Technology*, vol. 7, no. 3, p. 035 007, 2022. DOI: 10.1088/2058-9565/ac6a04. [Online]. Available: https://dx.doi.org/10.1088/2058-9565/ac6a04.

[36] T. Morita, "Useful Procedure for Computing the Lattice Green's Function-Square, Tetragonal, and bcc Lattices," *Journal of Mathematical Physics*, vol. 12, no. 8, pp. 1744–1747, Oct. 2003, ISSN: 0022-2488. DOI: 10.1063/1.1665800. eprint: https://pubs.aip.org/aip/jmp/article-pdf/12/8/1744/11285553/1744_1_online.pdf. [Online]. Available: https://doi.org/10.1063/1.1665800.

[37] V. S. Ferreira *et al.*, "Collapse and revival of an artificial atom coupled to a structured photonic reservoir," *Phys. Rev. X*, vol. 11, p. 041 043, 4 2021. DOI: 10.1103/PhysRevX.11.041043. [Online]. Available: https://link.aps.org/doi/10.1103/PhysRevX.11.041043.

A

The Residue of an Operator

The formal definition of residues is somewhat unwieldy, but let us give it anyway for completeness: For a meromorphic complex-valued function $A(z)$, the residue at an isolated singularity λ is defined [22] as the unique number $R \in \mathbb{C}$ such that the function

$$f(z) \equiv A(z) - \frac{R}{z - \lambda} \tag{A.1}$$

is the derivative of some single-valued analytic function in an annulus $0 < |z - \lambda| < \delta$.

For most practical purposes, it is sufficient to know how to calculate the residue of a function f with a *pole of order n at λ*, i.e. a function which can be expressed as

$$f(z) = g(z) + \sum_{k=1}^{n} \frac{c_k}{(z - \lambda)^k}, \tag{A.2}$$

for some $g(z)$ analytic in a neighbourhood of $z = \lambda$ and $c_k \in \mathbb{C}$ for all k. For such a function f, its residue at the pole λ, denoted $\operatorname{Res}_{z=\lambda}[f(z)]$ is simply the value c_1. It is possible to show [21] that for any function f with a pole of order n at λ,

$$\operatorname*{Res}_{z=\lambda}[f(z)] = c_1 = \lim_{z \to \lambda} \frac{1}{(n-1)!} \frac{\mathrm{d}^{n-1}}{\mathrm{d}z^{n-1}} [(z - \lambda)^n f(z)]. \tag{A.3}$$

If the pole is *simple*, i.e. if $n = 1$, this reduces to

$$\operatorname*{Res}_{z=\lambda}[f(z)] = \lim_{z \to \lambda} (z - \lambda) f(z). \tag{A.4}$$

While one could try to generalise either the formal definition in Eq. (A.1) or the order-n pole residue formula in Eq. A.3 to handle operator-valued functions, this will not actually be necessary for our purposes. It will suffice to have a definition that can handle simple operator-valued poles. In other words, we only need a definition of

$$\operatorname*{Res}_{z=\hat{H}} \left[\hat{A}(z)\right] \tag{A.5}$$

that works in the case when the operator-valued function $\hat{A}(z)$ can be written as

$$\hat{A}(z) = \frac{\alpha(z)}{z - \hat{H}}. \tag{A.6}$$

Here, $\alpha(z)$ is some complex-valued function that is analytic and nonzero everywhere (or at least "in a neighbourhood of $z = \hat{H}$", which we have not yet defined the meaning of).

The only hard demand we have for our new definition is that it should still allow us to use the residue theorem, i.e. we demand

$$\operatorname*{Res}_{z=\hat{H}}\left[\hat{A}(z)\right] = \frac{1}{2\pi i}\oint_\gamma \mathrm{d}z\,\hat{A}(z) \tag{A.7}$$

for any positively oriented simple closed curve γ that encloses "$z = \hat{H}$" (which we have yet to define properly). Note that we have here implicitly assumed that the winding number of γ around "$z = \hat{H}$" is one, since the full residue theorem [22] states that

$$\sum_k I(\gamma, \lambda_k) \operatorname*{Res}_{z=\lambda_k}\left[A(z)\right] = \frac{1}{2\pi i}\oint_\gamma \mathrm{d}z\,A(z). \tag{A.8}$$

Here, $\{\lambda_k\}$ are the poles of $A(z)$ enclosed within γ, and the winding number $I(\gamma, \lambda_k)$ is the number of times the path γ winds around the pole λ_k counterclockwise (every clockwise winding subtracting one from the total). Because the exact meaning of "$z = \hat{H}$" is unclear, let us simply provisionally define the operator residue enclosed within a curve γ for a function $\hat{A}(z)$ with a simple operator valued pole as

$$\operatorname*{Res}_{\gamma}\left[\hat{A}(z)\right] \equiv \frac{1}{2\pi i}\oint_\gamma \mathrm{d}z\,\hat{A}(z). \tag{A.9}$$

Inserting a resolution of the identity in the eigenbasis $\{|\lambda_k\rangle\}$ of $\hat{H}$ (which we for simplicity assume to be discrete), we see that

$$\begin{aligned}
\operatorname*{Res}_{\gamma}\left[\hat{A}(z)\right] &= \frac{1}{2\pi i}\oint_\gamma \mathrm{d}z\,\frac{\alpha(z)}{z-\hat{H}}\sum_k |\lambda_k\rangle\langle\lambda_k| = \\
&= \frac{1}{2\pi i}\sum_k \oint_\gamma \mathrm{d}z\,\frac{\alpha(z)}{z-\lambda_k}\,|\lambda_k\rangle\langle\lambda_k| = \{\text{residue theorem}\} = \\
&= \sum_{\lambda_k\in\mathrm{Int}(\gamma)} \operatorname*{Res}_{z=\lambda_k}\left[\frac{\alpha(z)}{z-\lambda_k}\right]|\lambda_k\rangle\langle\lambda_k| = \sum_{\lambda_k\in\mathrm{Int}(\gamma)} \alpha(\lambda_k)\,|\lambda_k\rangle\langle\lambda_k|\,,
\end{aligned} \tag{A.10}$$

where $\mathrm{Int}(\gamma)$ is the region of $\mathbb{C}$ enclosed by γ. In other words, if γ "encloses $z = \hat{H}$ with winding number 1" in the sense that it encloses all eigenvalues of $\hat{H}$ with winding number 1, we get that

$$\operatorname*{Res}_{\gamma}\left[\hat{A}(z)\right] = \sum_k \alpha(\lambda_k)\,|\lambda_k\rangle\langle\lambda_k| = \alpha(\hat{H})\sum_k |\lambda_k\rangle\langle\lambda_k| = \alpha(\hat{H}). \tag{A.11}$$

This means that one reasonable definition of the total residue of a function $\hat{A}(z)$ which is of the form in Eq. (A.6) is

$$\operatorname*{Res}_{z=\hat{H}}\left[\hat{A}(z)\right] \equiv \lim_{z\to\hat{H}}(z-\hat{H})\hat{A}(z) = \alpha(\hat{H}), \tag{A.12}$$

where the operator limit is also defined using resolution of the identity in the $\hat{H}$ eigenbasis:

$$\lim_{z\to\hat{H}}\hat{f}(z) \equiv \sum_k \lim_{z\to\lambda_k}\hat{f}(z)\,|\lambda_k\rangle\langle\lambda_k|\,. \tag{A.13}$$

Note that this definition of the total residue yields the same results as one would get by just pretending $\hat{H}$ is a complex number and blindly applying the usual formula for the

residue of a function with a simple pole. With this definition, the residue theorem holds as-is, i.e.

$$\operatorname*{Res}_{z=\hat{H}} \left[\hat{A}(z)\right] = \frac{1}{2\pi i} \oint_\gamma \mathrm{d}z\, \hat{A}(z) \tag{A.14}$$

for any positively oriented simple closed curve γ that "encloses $z = \hat{H}$ with winding number 1" in the sense that it encloses all eigenvalues of $\hat{H}$ with winding number 1.

As discussed in section 2.2, if the eigenbasis of $\hat{H}$ is continuous, the resolvent $\hat{G}(z) = (z - \hat{H})^{-1}$ has a branch cut along the eigenvalue spectrum instead of discrete poles. The original definition of the residue theorem does not handle branch cuts in the region enclosed by the integration contour, because "the residue of a branch cut" is not defined a priori. Thus, we will not attempt to define the residue of an operator with a continuous eigenvalue spectrum, though it could conceivably be done – at least for functions with simple operator-valued poles.

B

Efficient Computation of the Time Evolution Operator

As outlined in sections 2.1.1 and 2.3.1, the method we use to compute the time evolution of a set of atoms (small or giant) coupled to a structured bath is based on repeated application of the operator

$$\tilde{U}(\Delta t) \equiv \mathcal{F}^{-1} U_K(\Delta t) \mathcal{F} U_V(\Delta t), \tag{B.1}$$

where $\mathcal{F}$ denotes the FFT. While $U_K(\Delta t) = \exp[-iH_B\Delta t]$ is easy to compute, since H_B is diagonal in the momentum basis, computing $U_V(\Delta t) = \exp[-i(H_A + H_{\text{int}})\Delta t]$ is less straightforward, since H_{int} is off-diagonal. In this appendix, we will show that U_V can nonetheless be efficiently computed – both for small and giant atoms, provided that no bath resonator couples to multiple atoms. Notably, the methods described below work the same regardless of the dimensionality of the bath.

B.1 Small atoms

In a d-dimensional simple cubic lattice with side length N (an N by N square lattice in the 2D case), there are N^d resonators. Thus, looking at the definitions of H_A and H_{int} in equations (2.47) and (2.48), we see that the position basis matrix representation of $H = H_A + H_{\text{int}}$ for small atoms can be written as a block matrix

$$H = \begin{bmatrix} D & \Gamma \\ \Gamma^T & \mathbb{0} \end{bmatrix}. \tag{B.2}$$

Note that this H is denoted by V in the **Theory** section, where we reserve H for the total Hamiltonian $H_A + H_B + H_{\text{int}}$. Since we will not need the total Hamiltonian in this appendix, we can use H for $H_A + H_{\text{int}}$ with little risk of confusion. In this block matrix, D is a diagonal $M \times M$ matrix with matrix elements

$$[D]_{ij} = \Delta_i \delta_{ij}, \tag{B.3}$$

where δ_{ij} is the Kronecker delta, Γ is an $M \times N^d$ matrix with elements

$$[\Gamma]_{in} = \begin{cases} g_i & \text{if atom } i \text{ couples to resonator } n, \\ 0 & \text{otherwise,} \end{cases} \tag{B.4}$$

and $\mathbb{0}$ is the $N^d \times N^d$ zero matrix. Since by definition

$$U_V(\Delta t) = \exp[-iH\Delta t] = \sum_{k=0}^{\infty} \frac{(-i\Delta t)^k}{k!} H^k, \tag{B.5}$$

let us examine how H^k looks for different values of k.

The cases $k = 0$ and $k = 1$ are trivial: $k = 0$ simply yields the $(M + N^d) \times (M + N^d)$ identity matrix and $k = 1$ yields H itself. Looking at the first non-trivial case, $k = 2$, we see that

$$H^2 = \begin{bmatrix} D^2 + \Gamma\Gamma^T & D\Gamma \\ \Gamma^T D & \Gamma^T\Gamma \end{bmatrix}. \tag{B.6}$$

Since D is diagonal, so is D^2. Specifically, its matrix elements are

$$\left[D^2\right]_{ij} = \Delta_i^2 \delta_{ij}. \tag{B.7}$$

Looking closely at the definition of Γ, we can see that $\Gamma\Gamma^T$ is also diagonal, since

$$\begin{aligned} \left[\Gamma\Gamma^T\right]_{ij} &= \sum_{n=1}^{N^d} \Gamma_{in}\Gamma_{jn} = \{\text{Small atoms, no resonator couples to multiple atoms}\} = \\ &= g_i^2 \delta_{ij}. \end{aligned} \tag{B.8}$$

In other words, the upper-left block, which we can call $H^2_{(1,1)}$, is still an $M \times M$ diagonal matrix, with matrix elements

$$\left[H^2_{(1,1)}\right]_{ij} = (\Delta_i^2 + g_i^2)\delta_{ij}. \tag{B.9}$$

Turning our attention to the upper-right block, which we can call $H^2_{(1,2)}$, the fact that D is diagonal also implies that

$$[D\Gamma]_{in} = \Delta_i \Gamma_{in} = \begin{cases} \Delta_i g_i & \text{if atom } i \text{ couples to resonator } n, \\ 0 & \text{otherwise.} \end{cases} \tag{B.10}$$

Thus, the upper-right block also has unchanged structure – the only effect of squaring H is that the non-zero matrix elements change from g_i to $\Delta_i g_i$. Since H is symmetric, the lower-left block $H^2_{(2,1)}$ is simply the transpose of $H^2_{(1,2)}$.

As for the lower-right block, which we can call $H^2_{(2,2)}$, its matrix elements are

$$\begin{aligned} \left[\Gamma^T\Gamma\right]_{mn} &= \sum_{i=1}^{M} \Gamma_{im}\Gamma_{in} = \{\text{Small atoms}\} = \\ &= \begin{cases} g_{i_n}^2 \delta_{mn} & \text{if an atom couples to resonator } m = n, \\ 0 & \text{otherwise,} \end{cases} \end{aligned} \tag{B.11}$$

where i_n is the index for the atom coupling to resonator n. In other words, the lower-right block remains diagonal (like it is for both $k = 0$ and $k = 1$), but it is not identically zero like it is for $k = 1$. Notably, because of the fact that no resonator couples to multiple atoms, none of the blocks contain any elements with constants from a mix of different atoms.

If we examine the case $k = 3$, i.e.

$$H^3 = \begin{bmatrix} DH^2_{(1,1)} + \Gamma H^2_{(2,1)} & H^2_{(1,1)}\Gamma \\ \Gamma^T H^2_{(1,1)} & \Gamma^T H^2_{(1,2)} \end{bmatrix} = \begin{bmatrix} D^3 + 2D\Gamma\Gamma^T & \left(D^2 + \Gamma\Gamma^T\right)\Gamma \\ \Gamma^T\left(D^2 + \Gamma\Gamma^T\right) & \Gamma^T D\Gamma \end{bmatrix}, \tag{B.12}$$

we see a pattern start to emerge. Continuing to use the notation we just established for the different blocks, $H^3_{(1,1)}$ is clearly still diagonal, since it is a linear combination of products of the diagonal matrices D and $\Gamma\Gamma^T$. Similarly, $H^3_{(1,2)}$ must have the same structure as Γ, since it is the product of a diagonal matrix and Γ, and $H^3_{(2,1)}$ is still the transpose of $H^3_{(1,2)}$. As for the lower-right block, since $D\Gamma$ has the same structure as Γ but with $g_i \to \Delta_i g_i$, it must be that $\Gamma^T D\Gamma$ has the same structure as $\Gamma^T\Gamma$, but with $g_i^2 \to \Delta_i g_i^2$.

This leads us to conjecture the following structure for H^k with $k \geq 1$:

$$H^k = \begin{bmatrix} \Lambda_k & \Lambda_{k-1}\Gamma \\ \Gamma^T\Lambda_{k-1} & \Gamma^T\Lambda_{k-2}\Gamma \end{bmatrix}, \tag{B.13}$$

with $\{\Lambda_k\}_{k=-1}^{\infty}$ being the sequence of diagonal matrices defined by the recursive formula

$$\Lambda_{k+1} = D\Lambda_k + \Gamma\Gamma^T\Lambda_{k-1} \tag{B.14}$$

and the seed values

$$\Lambda_{-1} = \mathbb{0}_M, \quad \Lambda_0 = \mathbb{1}_M, \tag{B.15}$$

where $\mathbb{0}_M$ and $\mathbb{1}_M$ are the $M \times M$ zero and identity matrices, respectively. To prove that Eq. (B.13) indeed holds for all $k \geq 1$, we can use induction. First, we note that it holds for $k = 1$, because

$$H^1 = H = \begin{bmatrix} D & \Gamma \\ \Gamma^T & \mathbb{0} \end{bmatrix}, \tag{B.16}$$

which is precisely the expression in (B.13) with $k = 1$, since $\Lambda_1 = D\Lambda_0 + \Gamma\Gamma^T\Lambda_{-1} = D$.

Now we only need to perform the inductive step, i.e. prove that Eq. (B.13) holds in case $k+1$ given that it holds in case k. Let us therefore assume that the equation does hold in case k. If so, we have

$$\begin{aligned} H^{k+1} = HH^k = \{\text{inductive assumption}\} = \begin{bmatrix} D & \Gamma \\ \Gamma^T & \mathbb{0} \end{bmatrix} \begin{bmatrix} \Lambda_k & \Lambda_{k-1}\Gamma \\ \Gamma^T\Lambda_{k-1} & \Gamma^T\Lambda_{k-2}\Gamma \end{bmatrix} = \\ = \begin{bmatrix} D\Lambda_k + \Gamma\Gamma^T\Lambda_{k-1} & \Big(D\Lambda_{k-1} + \Gamma\Gamma^T\Lambda_{k-2}\Big)\Gamma \\ \Gamma^T\Lambda_k & \Gamma^T\Lambda_{k-1}\Gamma \end{bmatrix} = \{\text{equation (B.14)}\} = \\ = \begin{bmatrix} \Lambda_{k+1} & \Lambda_k\Gamma \\ \Gamma^T\Lambda_k & \Gamma^T\Lambda_{k-1}\Gamma \end{bmatrix}, \end{aligned} \tag{B.17}$$

which is indeed the expression given by Eq. (B.13) with $k \to k+1$. Thus, Eq. (B.13) must hold for all $k \geq 1$.

Inserting this expression into Eq. (B.5) gives us that

$$U_V(\Delta t) = \mathbb{1} + \begin{bmatrix} D_0 & D_1\Gamma \\ \Gamma^T D_1 & \Gamma^T D_2\Gamma \end{bmatrix} = \begin{bmatrix} \mathbb{1}_M + D_0 & D_1\Gamma \\ \Gamma^T D_1 & \mathbb{1}_{N^d} + \Gamma^T D_2\Gamma \end{bmatrix}, \tag{B.18}$$

where $\mathbb{1}$ is the $(M + N^d) \times (M + N^d)$ identity matrix and $D_{0,1,2}$ are the diagonal matrices

$$\begin{cases} D_0 \equiv \sum_{k=1}^{\infty} \frac{(-i\Delta t)^k}{k!}\Lambda_k, \\ D_1 \equiv \sum_{k=1}^{\infty} \frac{(-i\Delta t)^k}{k!}\Lambda_{k-1}, \\ D_2 \equiv \sum_{k=1}^{\infty} \frac{(-i\Delta t)^k}{k!}\Lambda_{k-2}. \end{cases} \tag{B.19}$$

From these definitions, we see that element i along the diagonal of D_l can be computed as

$$d_l^{(i)} \equiv [D_l]_{ii} = \sum_{k=1}^{\infty} \frac{(-i\Delta t)^k}{k!} \lambda_{k-l}^{(i)}, \tag{B.20}$$

where $\lambda_k^{(i)} \equiv [\Lambda_k]_{ii}$ is element i along the diagonal of Λ_k. By Eq. (B.14), these satisfy the recursive formula

$$\lambda_{k+1}^{(i)} = \Delta_i \lambda_k^{(i)} + g_i^2 \lambda_{k-1}^{(i)}, \tag{B.21}$$

with the seed values

$$\lambda_{-1}^{(i)} = 0, \quad \lambda_0^{(i)} = 1. \tag{B.22}$$

In terms of these constants, we can express the matrix elements of the four blocks making up $U_V(\Delta t)$ as follows:

$$\begin{cases} [\mathbb{1}_M + D_0]_{ij} = \delta_{ij}\left(1 + d_0^{(i)}\right) \\ [D_1\Gamma]_{in} = \left[\Gamma^T D_1\right]_{ni} = \begin{cases} g_i d_1^{(i)} & \text{if atom } i \text{ couples to resonator } n \\ 0 & \text{otherwise} \end{cases} \\ \left[\mathbb{1}_{N^d} + \Gamma^T D_2 \Gamma\right]_{mn} = \begin{cases} \delta_{mn}\left(1 + g_{i_n}^2 d_2^{(i_n)}\right) & \text{if atom } i_n \text{ couples to resonator } m = n \\ \delta_{mn} & \text{otherwise.} \end{cases} \end{cases} \tag{B.23}$$

Now, consider the 2×2 Hamiltonian

$$H_i = \begin{bmatrix} \Delta_i & g_i \\ g_i & 0 \end{bmatrix}. \tag{B.24}$$

By virtually the exact same logic we used above, we can show that

$$H_i^k = \begin{bmatrix} \lambda_k^{(i)} & g_i \lambda_{k-1}^{(i)} \\ g_i \lambda_{k-1}^{(i)} & g_i^2 \lambda_{k-2}^{(i)} \end{bmatrix} \tag{B.25}$$

for all $k \geq 1$, which means that the time evolution operator associated with H_i is

$$U_i = \exp(-iH_i\Delta t) = \mathbb{1}_2 + \begin{bmatrix} d_0^{(i)} & g_i d_1^{(i)} \\ g_i d_1^{(i)} & g_i^2 d_2^{(i)} \end{bmatrix} = \begin{bmatrix} 1 + d_0^{(i)} & g_i d_1^{(i)} \\ g_i d_1^{(i)} & 1 + g_i^2 d_2^{(i)} \end{bmatrix}. \tag{B.26}$$

Comparing this with the expressions in Eq. (B.23), we see that every single element in $U_V(\Delta t)$ that is not trivially equal to 0 or 1 can be found in U_i for some value of i. Specifically, looking back at at the matrix elements of the four blocks of $U_V(\Delta t)$, defined as before, we see that

$$\begin{cases} [\mathbb{1}_M + D_0]_{ij} = \delta_{ij}[U_i]_{11} \\ [D_1\Gamma]_{in} = \left[\Gamma^T D_1\right]_{ni} = \begin{cases} [U_i]_{12} & \text{if atom } i \text{ couples to resonator } n \\ 0 & \text{otherwise} \end{cases} \\ \left[\mathbb{1}_{N^d} + \Gamma^T D_2 \Gamma\right]_{mn} = \begin{cases} \delta_{mn}[U_{i_n}]_{22} & \text{if atom } i_n \text{ couples to resonator } m = n \\ \delta_{mn} & \text{otherwise} \end{cases} \end{cases} \tag{B.27}$$

In other words, instead of calculating $U_V(\Delta t)$ naively as an $(M + N^d) \times (M + N^d)$ matrix exponential (with complexity $\mathcal{O}\left[(M + N^d)^3\right]$ [14, 15]), it suffices to compute $\{U_i\}_{i=1}^M$,

which amounts to M different 2×2 matrix exponentials (which is $\mathcal{O}[M]$), provided that one separately takes into account which resonators the different atoms couple to (which is $\mathcal{O}\Big[M + N^d\Big]$). For large N, this results in a very significant speedup – especially with bath dimensionality $d > 1$.

B.2 Giant atoms

For giant atoms, the position basis matrix representation of $H_A + H_{\text{int}}$ is still

$$H = \begin{bmatrix} D & \Gamma \\ \Gamma^T & \mathbb{0} \end{bmatrix}, \tag{B.28}$$

with all the same definitions as before. The only difference from the case with small atoms is the fact that each atom couples to multiple points, which means that Γ now has multiple non-zero elements in each row. Indeed, it is still the case for all $k \geq 1$ that

$$H^k = \begin{bmatrix} \Lambda_k & \Lambda_{k-1}\Gamma \\ \Gamma^T\Lambda_{k-1} & \Gamma^T\Lambda_{k-2}\Gamma \end{bmatrix}, \tag{B.29}$$

with $\{\Lambda_k\}_{k=-1}^{\infty}$ defined in the exact same way as before. This implies that

$$U_V(\Delta t) = \mathbb{1} + \begin{bmatrix} D_0 & D_1\Gamma \\ \Gamma^T D_1 & \Gamma^T D_2 \Gamma \end{bmatrix} = \begin{bmatrix} \mathbb{1}_M + D_0 & D_1\Gamma \\ \Gamma^T D_1 & \mathbb{1}_{N^d} + \Gamma^T D_2 \Gamma \end{bmatrix} \tag{B.30}$$

still holds, with $D_{0,1,2}$ defined like before. The only difference comes from the more complicated structure of Γ.

B.2.1 Giant Atoms with Even Coupling Strength

In particular, assuming for simplicity that atom i couples to each coupled resonator with the same coupling strength g_i,

$$\begin{aligned} \Big[\Gamma\Gamma^T\Big]_{ij} &= \sum_{n=1}^{N^d} \Gamma_{in}\Gamma_{jn} = \Big\{\text{Atom } i \text{ couples to } N_c^{(i)} \text{ resonators}\Big\} = \\ &= N_c^{(i)} g_i^2 \delta_{ij}, \end{aligned} \tag{B.31}$$

where we've also (like before) made the assumption that no resonator couples to multiple atoms. We also find that

$$\begin{aligned} \Big[\Gamma^T\Gamma\Big]_{mn} &= \sum_{i=1}^{M} \Gamma_{im}\Gamma_{in} = \\ &= \begin{cases} g_{i_{mn}}^2 & \text{if an atom couples to resonators } m \text{ and } n, \\ 0 & \text{otherwise,} \end{cases} \end{aligned} \tag{B.32}$$

with i_{mn} being the index for the atom coupling to both resonator m and resonator n. This means that $\Gamma^T D_2 \Gamma$ is no longer diagonal. Note however that $D\Gamma$ still has the same structure as Γ for any diagonal D – this is the reason that Eq. (B.13) still holds. The change to the matrix elements of $\Gamma\Gamma^T$ also means that the matrix elements $\bar{\lambda}_k^{(i)} \equiv [\Lambda_k]_{ii}$ are different for giant atoms. While their seed values are still

$$\bar{\lambda}_{-1}^{(i)} = 0, \quad \bar{\lambda}_0^{(i)} = 1, \tag{B.33}$$

their recursive formula is different:

$$\bar{\lambda}_{k+1}^{(i)} = \Delta_i \bar{\lambda}_k^{(i)} + N_c^{(i)} g_i^2 \bar{\lambda}_{k-1}^{(i)}. \tag{B.34}$$

But this is precisely the recursive formula for $\lambda_k^{(i)}$ with $g_i^2 \to N_c^{(i)} g_i^2$! In other words, as far as the Λ_k matrices are concerned, a giant atom with $N_c^{(i)}$ coupling points, coupled to each of them with strength g_i, behaves exactly like a small atom with coupling strength $\sqrt{N_c^{(i)}} g_i$. This also propagates through to the matrix elements $\bar{d}_l^{(i)} \equiv [D_l]_{ii}$, since they are still, by definition, equal to

$$\bar{d}_l^{(i)} = \sum_{k=1}^{\infty} \frac{(-i\Delta t)^k}{k!} \bar{\lambda}_{k-l}^{(i)}, \tag{B.35}$$

Examining the matrix elements of the four blocks making up $U_V(\Delta t)$, we see that they now look like

$$\begin{cases} [\mathbb{1}_M + D_0]_{ij} = \delta_{ij}\left(1 + \bar{d}_0^{(i)}\right) \\ [D_1\Gamma]_{in} = \left[\Gamma^T D_1\right]_{ni} = \begin{cases} g_i \bar{d}_1^{(i)} & \text{if atom } i \text{ couples to resonator } n \\ 0 & \text{otherwise} \end{cases} \\ \left[\mathbb{1}_{N^d} + \Gamma^T D_2 \Gamma\right]_{mn} = \begin{cases} \delta_{mn} + g_{i_{mn}}^2 \bar{d}_2^{(i_{mn})} & \text{if atom } i_{mn} \text{ couples to resonators } m \text{ and } n \\ \delta_{mn} & \text{otherwise} \end{cases} \end{cases} \tag{B.36}$$

All the terms here except for $\bar{d}_{0,1,2}^{(i)}$ are known, and just like for small atoms we would like to calculate their values by evaluating M different 2×2 matrix exponentials. The effective Hamiltonian we need to use for atom i to accomplish this is

$$\bar{H}_i \equiv \begin{bmatrix} \Delta_i & \sqrt{N_c^{(i)}} g_i \\ \sqrt{N_c^{(i)}} g_i & 0 \end{bmatrix}, \tag{B.37}$$

because by the same logic we used previously, taking powers of this yields our desired $\bar{\lambda}_k^{(i)}$:

$$\bar{H}_i^k = \begin{bmatrix} \bar{\lambda}_k^{(i)} & \sqrt{N_c^{(i)}} g_i \bar{\lambda}_{k-1}^{(i)} \\ \sqrt{N_c^{(i)}} g_i \bar{\lambda}_{k-1}^{(i)} & N_c^{(i)} g_i^2 \bar{\lambda}_{k-2}^{(i)} \end{bmatrix}. \tag{B.38}$$

Its associated time evolution operator then becomes

$$\begin{aligned} \bar{U}_i \equiv \exp\left(-i\bar{H}_i \Delta t\right) &= \mathbb{1}_2 + \begin{bmatrix} \bar{d}_0^{(i)} & \sqrt{N_c^{(i)}} g_i \bar{d}_1^{(i)} \\ \sqrt{N_c^{(i)}} g_i \bar{d}_1^{(i)} & N_c^{(i)} g_i^2 \bar{d}_2^{(i)} \end{bmatrix} = \\ &= \begin{bmatrix} 1 + \bar{d}_0^{(i)} & \sqrt{N_c^{(i)}} g_i \bar{d}_1^{(i)} \\ \sqrt{N_c^{(i)}} g_i \bar{d}_1^{(i)} & 1 + N_c^{(i)} g_i^2 \bar{d}_2^{(i)} \end{bmatrix}. \end{aligned} \tag{B.39}$$

We do have some extra factors involving $N_c^{(i)}$ here compared to our desired matrix elements in Eq. (B.36), but those can easily be corrected for.

All in all, we find that we can reconstruct $U_V(\Delta t)$ from $\left\{\bar{U}_i\right\}$ in the following way:

$$\begin{cases} \left[\mathbb{1}_M + D_0\right]_{ij} = \delta_{ij}\left[\bar{U}_i\right]_{11} \\ \left[D_1\Gamma\right]_{in} = \left[\Gamma^T D_1\right]_{ni} = \begin{cases} \frac{1}{\sqrt{N_c^{(i)}}}\left[\bar{U}_i\right]_{12} & \text{if atom } i \text{ couples to resonator } n \\ 0 & \text{otherwise} \end{cases} \\ \left[\mathbb{1}_{N^d} + \Gamma^T D_2 \Gamma\right]_{mn} = \begin{cases} \delta_{mn} + \frac{\left[\bar{U}_{i_{mn}}\right]_{22} - 1}{N_c^{(i_{mn})}} & \text{if atom } i_{mn} \text{ couples to resonators } m \text{ and } n \\ \delta_{mn} & \text{otherwise.} \end{cases} \end{cases} \tag{B.40}$$

B.2.2 Giant Atoms with Uneven Coupling Strength

In the most general case, atom i couples to resonator n with coupling strength g_{ip_n}, with p being an index running from 1 to $N_c^{(i)}$. This means that

$$\begin{aligned} \left[\Gamma\Gamma^T\right]_{ij} &= \sum_{n=1}^{N^d} \Gamma_{in}\Gamma_{jn} = \{\text{no resonator couples to multiple atoms}\} \\ &= \sum_{p=1}^{N_c^{(i)}} g_{ip}^2 \delta_{ij}, \end{aligned} \tag{B.41}$$

and

$$\begin{aligned} \left[\Gamma^T\Gamma\right]_{mn} &= \sum_{i=1}^{M} \Gamma_{im}\Gamma_{in} = \\ &= \begin{cases} g_{ip_m} g_{ip_n} & \text{if resonators } m, n \text{ lie at coupling points } p_{m,n} \text{ of atom } i, \\ 0 & \text{otherwise.} \end{cases} \end{aligned} \tag{B.42}$$

Since the recursive formula for the Λ_k matrices is still

$$\Lambda_{k+1} = D\Lambda_k + \Gamma\Gamma^T\Lambda_{k-1}, \tag{B.43}$$

the matrix elements $\tilde{\lambda}_k^{(i)} \equiv [\Lambda_k]_{ii}$ use the same formula as for small atoms, except for the fact that the effective coupling strength is changed according to $g_i \to G_i$, where

$$G_i \equiv \sqrt{\sum_{p=1}^{N_c^{(i)}} g_{ip}^2}. \tag{B.44}$$

If we also define $\tilde{d}_l^{(i)} \equiv [D_l]_{ii}$, the matrix elements of the four blocks making up $U_V(\Delta t)$ now look like

$$\begin{cases} \left[\mathbb{1}_M + D_0\right]_{ij} = \delta_{ij}\left(1 + \tilde{d}_0^{(i)}\right) \\ \left[D_1\Gamma\right]_{in} = \left[\Gamma^T D_1\right]_{ni} = \begin{cases} g_{ip_n}\tilde{d}_1^{(i)} & \text{if resonator } n \text{ couples to atom } i \text{ at point } p_n \\ 0 & \text{otherwise} \end{cases} \\ \left[\mathbb{1}_{N^d} + \Gamma^T D_2 \Gamma\right]_{mn} = \begin{cases} \delta_{mn} + g_{ip_m} g_{ip_n}\tilde{d}_2^{(i)} & \text{if resonators } m, n \text{ couple to atom } i \text{ at } p_{m,n} \\ \delta_{mn} & \text{otherwise} \end{cases} \end{cases} \tag{B.45}$$

Using the effective Hamiltonian

$$\tilde{H}_i = \begin{bmatrix} \Delta_i & G_i \\ G_i & 0 \end{bmatrix} \tag{B.46}$$

for atom i, we get a corresponding effective time-evolution operator

$$\tilde{U}_i \equiv \exp\left(-i\tilde{H}_i \Delta t\right) = \begin{bmatrix} 1 + \tilde{d}_0^{(i)} & G_i \tilde{d}_1^{(i)} \\ G_i \tilde{d}_1^{(i)} & 1 + G_i^2 \tilde{d}_2^{(i)} \end{bmatrix}. \tag{B.47}$$

This translates into being able to reconstruct the matrix elements of $U_V(\Delta t)$ in Eq. (B.45) from $\left\{\tilde{U}_i\right\}$ using

$$\begin{cases} \left[\mathbb{1}_M + D_0\right]_{ij} = \delta_{ij}\left[\tilde{U}_i\right]_{11} \\ \left[D_1\Gamma\right]_{in} = \left[\Gamma^T D_1\right]_{ni} = \begin{cases} \frac{g_{ip_n}}{G_i}\left[\tilde{U}_i\right]_{12} & \text{if resonator } n \text{ couples to atom } i \text{ at point } p_n \\ 0 & \text{otherwise} \end{cases} \\ \left[\mathbb{1}_{N^d} + \Gamma^T D_2 \Gamma\right]_{mn} = \begin{cases} \delta_{mn} + \frac{g_{ip_m} g_{ip_n}}{G_i^2}\left(\left[\tilde{U}_i\right]_{22} - 1\right) & \text{if resonators } m, n \text{ couple to atom } i \text{ at } p_{m,n} \\ \delta_{mn} & \text{otherwise.} \end{cases} \end{cases} \tag{B.48}$$

B.3 A Non-Recursive Formula for Λ_k

Although it is not of much importance for the purposes of this thesis, it should be noted that one can express Λ_k without recursion as

$$\Lambda_k = \sum_{j=0}^{\left\lfloor \frac{k}{2} \right\rfloor} \binom{k-j}{j} D^{k-2j} \left(\Gamma\Gamma^T\right)^j \tag{B.49}$$

for all $k \geq 0$.

This comes from the fact that matrix element ij of upper-left block of H^k, i.e. $H^k_{(1,1)} = \Lambda_k$, basically keeps track of all the ways to transfer energy between atoms i and j in k steps. Since we've assumed that no resonator couples to multiple atoms, the only allowed moves during a single step are either to stay put in the atom ($\sim D$), or to move to a coupled resonator ($\sim \Gamma^T$), which forces the next move to be back to the atom ($\sim \Gamma$). Thus, a path of length k staying put in the atoms corresponds to D^k, and the other possible paths of length k can be gotten by exchanging any number of D^2s for $\Gamma\Gamma^T$s. Therefore, an arbitrary path of length k is made up of j copies of $\Gamma\Gamma^T$ and $k - 2j$ copies of D. The number of distinct orderings of such an array of copies is

$$\frac{(k-2j+j)!}{(k-2j)!j!} = \binom{k-j}{j}. \tag{B.50}$$

Together with the fact that j can be at most $\left\lfloor \frac{k}{2} \right\rfloor$, since we only have k copies of D to start with and need to be able to remove $2j$ of them, this gives us Eq. (B.49). Proving rigorously that it works can be done in a fairly straightforward (though somewhat tedious) manner using induction.

In terms of the matrix elements $\tilde{\lambda}_k^{(i)}$ for arbitrary giant atoms, Eq. (B.49) translates into

$$\tilde{\lambda}_k^{(i)} = \sum_{j=0}^{\lfloor \frac{k}{2} \rfloor} \binom{k-j}{j} \Delta_i^{k-2j} G_i^{2j}, \tag{B.51}$$

and of course the same holds for the special cases with even coupling strength (with $G_i \to \sqrt{N_c^{(i)}} g_i$) or a single coupling point (i.e. small atoms, with $G_i \to g_i$).

In fact, there is an even more compact way to write these matrix elements. By diagonalising the H_i matrix and noting that its eigenvalues are

$$\kappa_{i,\pm} \equiv \frac{\Delta_i}{2} \pm \sqrt{\frac{\Delta_i^2}{4} + G_i^2}, \tag{B.52}$$

it is possible to show (by examining the expression for $\left[H_i^k\right]_{11} = \tilde{\lambda}_k^{(i)}$ gotten from diagonalisation) that

$$\tilde{\lambda}_k^{(i)} = \frac{\kappa_{i,+}^{k+1} - \kappa_{i,-}^{k+1}}{\kappa_{i,+} - \kappa_{i,-}}. \tag{B.53}$$

This also means (suppressing the i index on $\kappa_{i,\pm}$) that

$$\tilde{d}_l^{(i)} = \frac{1}{\kappa_+ - \kappa_-} \sum_{k=1}^{\infty} \frac{(-i\Delta t)^k}{k!} \left(\kappa_+^{k-l+1} - \kappa_-^{k-l+1}\right), \tag{B.54}$$

and

$$\begin{aligned} U_i &= \frac{1}{\kappa_+ - \kappa_-} \begin{bmatrix} \kappa_+ e^{-i\Delta t\kappa_+} - \kappa_- e^{-i\Delta t\kappa_-} & g\left(e^{-i\Delta t\kappa_+} - e^{-i\Delta t\kappa_-}\right) \\ g\left(e^{-i\Delta t\kappa_+} - e^{-i\Delta t\kappa_-}\right) & g^2\left(\frac{1}{\kappa_+} e^{-i\Delta t\kappa_+} - \frac{1}{\kappa_-} e^{-i\Delta t\kappa_-}\right) \end{bmatrix} = \\ &= \frac{1}{\kappa_+ - \kappa_-} \begin{bmatrix} \kappa_+ e^{-i\Delta t\kappa_+} - \kappa_- e^{-i\Delta t\kappa_-} & g\left(e^{-i\Delta t\kappa_+} - e^{-i\Delta t\kappa_-}\right) \\ g\left(e^{-i\Delta t\kappa_+} - e^{-i\Delta t\kappa_-}\right) & \kappa_+ e^{-i\Delta t\kappa_-} - \kappa_- e^{-i\Delta t\kappa_+} \end{bmatrix}. \end{aligned} \tag{B.55}$$

Calculating $\tilde{d}_l^{(i)}$ and U_i this way is slightly faster than evaluating the 2×2 matrix exponential $\exp(-iH_i\Delta t)$, but the effect of doing so on the speed of the overall time evolution algorithm is negligible, since the vast majority of the time cost lies in the FFT and iFFT performed every time step. However, cursory examinations of this method do suggest that it tends to have better unitarity than matrix exponentiation of $-iH_i\Delta t$ via SciPy's `linalg.expm()`.

DEPARTMENT OF MICROTECHNOLOGY AND NANOSCIENCE
CHALMERS UNIVERSITY OF TECHNOLOGY
Gothenburg, Sweden
www.chalmers.se

CHALMERS
UNIVERSITY OF TECHNOLOGY